People's Democratic Republic Of Algeria
Ministry Of Higher Education and Scientific Research
University Amar Telidji Of Laghouat

**FACULTY: TECHNOLOGY**

**DEPARTMENT: MECHANICAL ENGINEERING**

**MASTER DISSERTATION**

**By:**

**Rezgallah Boulanouar Nadhir** **Fernane Louennas**

**DOMAIN: Sciences and Technology**

**FIELD: Mechanical Engineering**

**OPTION: Energetic**

***Theme***

# Effect of cooled approach length on heat transfer in regenerative water-cooled nozzle

**Jury Members:**

| Name | Grade | Quality |
|---|---|---|
| Mr. HAMDI Nacer eddine | MAA | President |
| Mr. MECHIKEL Mohamed | MAA | Examiner |
| Mr. BENSAYAH Khaled | MCA | Supervisor |

2021\2022

# ACKNOWLEDGEMENTS

نشكر الله أولا على التوفيق في كامل مشوار دراسي اللهم لك الحمد والصلاة والسلام على سيدنا محمد وعلى آله وصحبه وسلم

We would like to express our deep gratitude to:

Mr BENSAYAH Khaled our supervisor we thank him for his support, guiding, helping, advising us, and for his patience.

All those who have contributed directly or indirectly for helping us to complete this project.

We sincerely thank our dear parents, for their moral and material support during the realization of our project, without forgetting our brothers and sisters.

# Dedication

I dedicate this modest work to my dear Mother and my dear Father to those who have always encouraged me to succeed in my studies...

To my brother Mustapha and my sister and khalti Nora

The day has come to say thank you…

To my grandmother to my uncles el hadj Mohammed and Rabah

To the whole Rezgallah and Khelifi family

To all the teachers who played a role in my arrival at this level Merah, Bougrine Bensnouci, Bachiri, Bensayah …. etc.

To all the mechanics department teachers

To my partner Fernane Louennas

To all my friends Top of the list Mohamed, Abde-elhadi, Mustapha, Taha … etc.

REZGALLAH BOULANOUAR NADHIR

I dedicate this work

To my parents who supported and encouraged me during these years of study.

To my brothers, my friends (tahar imad, aissa moulai, lakhdar djoumeikh) and those who shared with me all the emotional moments during the realization of this work. They warmly supported and encouraged me throughout my career.

May they find here the testimony of my deep gratitude.

FRNANE LOUENNAS

## Abstract

ever since the development of liquid rocket engine, there has been a need to predict the peak heat flux that affects the engine material and thus to control the wall thermal behavior of rocket engine. To prevent thermal failure, the engine is generally cooled by means of a coolant that flows in passages that line the hottest part of the engine (i.e., combustion chamber and nozzle wall). This is the fluid-cooling system. If the coolant is one of the propellants, once it passes through the cooling circuit, it can be injected into the combustion chamber or it can be dumped overboard. The former case is referred to as Regenerative cooling system while the latter as dump cooling system. In case of high-performance cryogenic rocket engine (such as LO2/hydrogen and LO2/methane engines) the coolant working pressure is supercritical and thus it behaves far from a liquid or a perfect gas. The fluid-cooling system (often referred to regenerative cooling because of the limited application of the dump cooling) of cryogenic rocket engines, is the technological background of this MASTER thesis.

## Résumé

Depuis le développement du moteur de fusée liquide, il est nécessaire de prévoir le flux thermique maximal qui affecte le matériau du moteur et donc de contrôler le comportement thermique de la paroi du moteur de fusée. Pour éviter les défaillances thermiques, le moteur est généralement refroidi au moyen d'un liquide de refroidissement qui circule dans des passages qui bordent la partie la plus chaude du moteur (c'est-à-dire la chambre de combustion et la paroi de la tuyère). Il s'agit du système de refroidissement par fluide. Si le liquide de refroidissement est l'un des propergols, une fois qu'il a traversé le circuit de refroidissement, il peut être injecté dans la chambre de combustion ou être déchargé à l'extérieur. Dans le premier cas, on parle de système de refroidissement régénératif et dans le second de système de refroidissement par immersion. Dans le cas des moteurs-fusées cryogéniques à haute performance (tels que les moteurs LO2/hydrogène et LO2/méthane), la pression de travail du liquide de refroidissement est supercritique et son comportement est donc loin d'être celui d'un liquide ou d'un gaz parfait. Le système de refroidissement par fluide (souvent appelé refroidissement régénératif en raison de l'application limitée du refroidissement par décharge) des moteurs-fusées cryogéniques constitue le contexte technologique de ce mémoire de maîtrise.

# NOMENCLATURE

| Symbol | Description |
|---|---|
| $a$ | Speed of sound (also $c$) |
| $\alpha$ | Kinetic energy of the average quantities |
| $c^*$ | Speed of turbulent sound |
| $c_p$ | Spesific heat at constant pressure |
| $c_v$ | Spesific heat at constant volume |
| $C_f$ | friction coefficient |
| $\delta$ | Thickness of the boundary layer |
| $\Delta U$ | Explicit increase in vector $U$ |
| $\delta U$ | Implicit increase of the vector $U$ |
| $\delta_{i,j}$ | Kronecker symbol |
| $\Delta t$ | Time increase |
| $e$ | Internal energy per unit of mass |
| $e_t$ | Total energy per unit mass |
| $\varepsilon$ | Rate of dissipation of turbulent kinetic energy |
| $\varepsilon^*$ | Isotropic dissipation rate |
| $F$ | Eulerian flow in the direction $x$ |
| $F_v$ | Viscous flow in the direction $x$ |
| $F_\xi$ | Eulerian flow in the direction $\xi$ |
| $F_{v\xi}$ | Viscous flow in the direction $\xi$ |
| $G$ | Eulerian flow in the direction $y$ |
| $G_v$ | Viscous flow in the direction $y$ |
| $G_\eta$ | Eulerian flow in the direction $\eta$ |
| $G_{v\eta}$ | Viscous flow in the direction $\eta$ |
| $\gamma$ | Specific Heat Report ($\gamma = c_p/c_v$) |
| $h$ | Heat transfer coefficient |
| $h_t$ | Total enthalpy per unit mass |
| $k$ | Kinetic energy of turbulent |
| $\omega$ | Specific dissipation rate |
| $l$ | Spatial scale of turbulence |
| $l_m$ | Mixing length |
| $\lambda_c$ | coefficient of thermal conductivity |
| $M_e$ | Number of Mach outside the boundary layer (also $M_\infty$) |
| $M_t$ | Turbulent Mach number ($M_t = \sqrt{2k}/c$) |
| $\mathscr{H}$ | Heaviside function |
| $\mathscr{C}_{\mathcal{NS}}(u_i)$ | Navier-Stokes operator |
| $q_j$ | Heat flow per unit area and unit time in the direction $x_j$ |
| $q_w$ | Parietal heat flow |
| $\mu$ | Molecular viscosity |
| $\nu$ | Kinematic viscosity |
| $\mu_t$ | Turbulent viscosity |
| $\mu_{ef}$ | Effective diffusion coefficient of momentum |
| $\mu_{kef}$ | Effective diffusion coefficient of $k$ |
| $\mu_{\omega ef}$ | Effective diffusion coefficient of $\omega$ |
| $Pr$ | Prandtl number |
| $Pr_t$ | Prandtl turbulent number |
| $p$ | hydrostatic pressure |
| $p^*$ | Effective pressure $p^* = p + \frac{2}{3}\rho k$ |

| | |
|---|---|
| $p_0$ | Generator or chamber pressure (also $p_c$) |
| $p_w$ | Static wall pressure |
| $Re$ | Reynolds number |
| $Re_t$ | Reynolds turbulent number |
| $\rho$ | density |
| $S_0$ | Vector of source terms |
| $\vec{S}_{i+\frac{1}{2}}$ | Vector surface between meshes $(i, j)$ et $(i+1, j)$ |
| $\vec{S}_{j+\frac{1}{2}}$ | Vector surface between meshes $(i, j)$ et $(i, j+1)$ |
| $\begin{pmatrix} m_x \\ m_y \end{pmatrix}$ | Module 1 surface vector components between $(i, j)$ et $(i+1, j)$ |
| $\begin{pmatrix} n_x \\ n_y \end{pmatrix}$ | Module 1 surface vector components between $(i, j)$ et $(i, j+1)$ |
| $\sigma_{ij}$ | Tenseur des contraintes visqueuses |
| $t$ | Time |
| $T$ | Temperature |
| $T_0$ | Generator temperature |
| $T_w$ | Parietal temperature |
| $T_{aw}$ | Adiabatic temperature |
| $\tau$ | Kolmogorov time |
| $\eta$ | Kolmogorov ladder |
| $\tau_w$ | Parietal friction |
| $U$ | Vector of conservative quantities |
| $u$ | speed in the direction $x$ |
| $u_i$ | speed in the direction $x_i$ |
| $V$ | Vector of non-conservative quantities |
| $v$ | speed in the direction $y$ |
| $\mathcal{V}_{i,j}$ | Mesh volume $(i, j)$ |
| $S_{ij}$ | Strain tensor |
| $\Omega_{ij}$ | Vorticity Tensor |

| | |
|---|---|
| $\bar{f}$ | Overall average of quantity $f$ |
| $f'$ | Fluctuation of quantity $f$ for the overall average |
| $\tilde{f}$ | Quantity Favre Average $f$ |
| $f''$ | Fluctuation of quantity $f$ for the average of Favre |

| | |
|---|---|
| $(x, y)$ | Axes of the Cartesian landmark |

**Abréviations**

| | |
|---|---|
| $RANS$ | Reynolds Averaged Navier-Stokes |
| $SST$ | Shear Stress Tensor |
| $JPL$ | Jet Propulsion Laboratory |
| $CFD$ | computational fluid dynamics |

# Contents

# List of Figures

# List of Tables

# 1 INTRODUCTION

## 1.1 Rocket Engines Cooling

Gases inside an engines combustion chamber can reach 3,500 K which is about half as hot as the surface of the Sun – certainly above the melting point of most materials. Engines need to reach this temperature in order to function correctly, but how can they survive this? In this section we will learn about engine cooling methods used to keep rocket engines from melting.

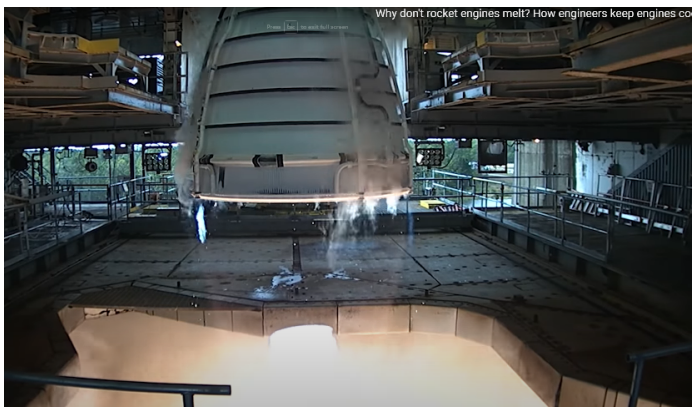


To design a high-performance rocket engine capable of long burn durations and reliable ignition, it is paramount to have precise predictions of the behavior of chemical kinetics, fluid mechanics, thermodynamics, heat transfer, and temperature-dependent material properties. Rocket engines are propelled by exhausting high-temperature gas from the combustion chamber through a supersonic nozzle. Propulsion can be achieved using a range of energy sources including chemical, nuclear, solar, and electrical; however, this research focused on chemical rocket propulsion.



**Figure 1.1:** A render of an injector face of an engine. Here propellants mix and combust in the main combustion chamber releasing incredible amounts of heat energy

Chemical propulsion can be further categorized by propellant type, liquid, solid, and hybrid fuel. Liquid fuel rocket engines require storage tanks, pumps, and injectors; however, they allow combustion cessation and re-ignition which facilitates steering and increases application potential.

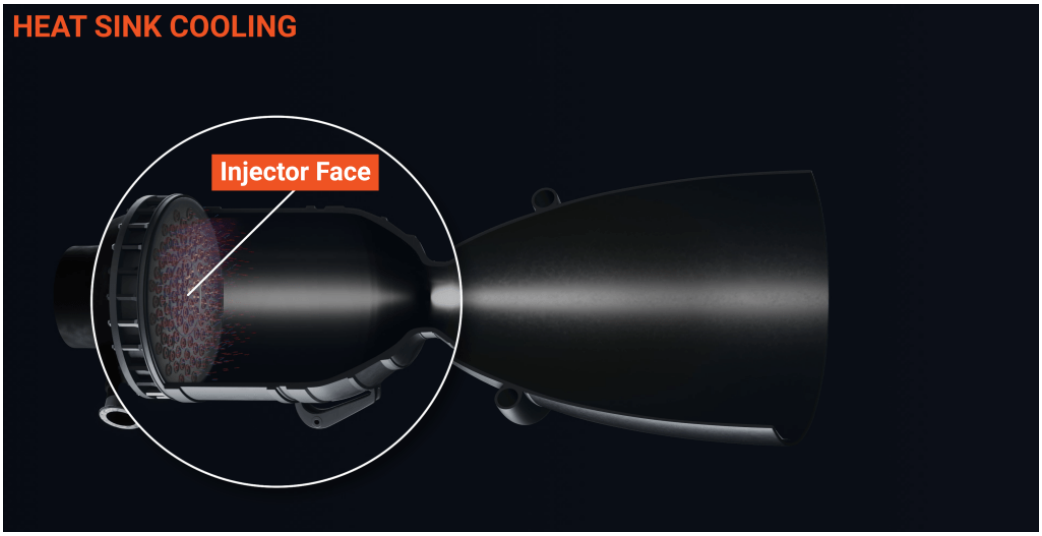


**Figure 1.2:** A render of an injector face of an engine. Here propellants mix and combust in the main combustion chamber releasing incredible amounts of heat energy

Solid fuel rocket engines do not require the complicated mechanics of liquid fuel, although once ignited the fuel burns until the charge has been exhausted. Hybrid fuel rocket engines typically use solid fuel and a liquid oxidizer, albeit, a variety of propellant combinations have been explored. Hybrid rocket engines assume the relative safety and simplicity of solid fuel as well as the start-stop capability of liquid fuel but tend to have decreased performance.

The extreme temperature gradients found in rocket engines and the upper atmosphere cause high heat transfer rates and significant material stress. Combustion temperatures in rocket engines typically range from 2700 K to 3600 K, which is substantially higher than the melting point of metals. This necessitates a sagacious cooling system to extend engine lifespans, despite enduring harsh conditions for prolonged burn times. There are numerous cooling methods for rocket nozzles, including dump, film, transpiration, radiation, ablative, and regenerative cooling. Ablative and regenerative cooling are two of the most commonly utilized methods

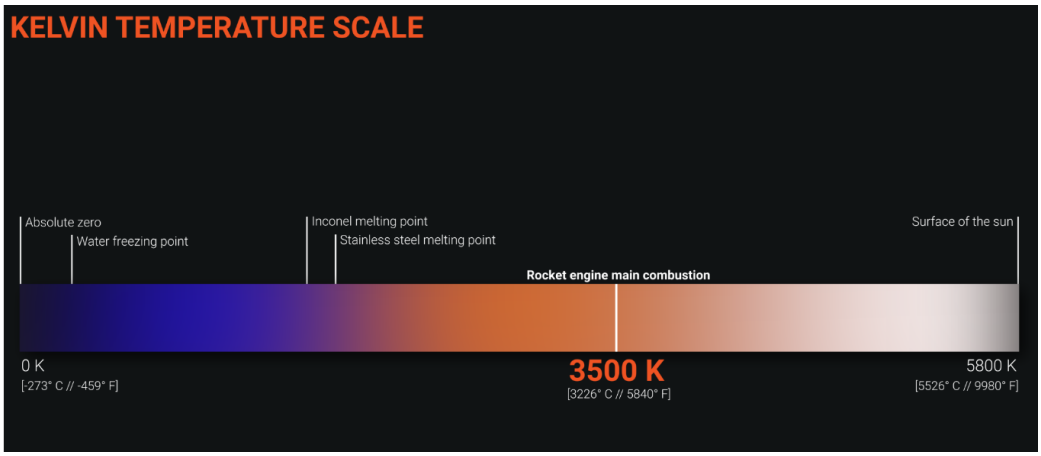


**Figure 1.3:** A render of an engine that only utilizes heat sink cooling

## 1.2 Fuel Oxidizer Ratio

Another option to keep an engine from melting is to run the engine in a fuel rich or oxidizer rich configuration, which will lower the temperature of the main exhaust. This ratio is known as the fuel to oxidizer mass ratio.If someone wanted to burn all of your propellant and have all of it react with each other, you need to burn it at their stoichiometric ratio. Stoichiometric ratio is where the complete amount of fuel and oxidizer perfectly react with each other so no propellant is left unburnt. This means that each atom of each molecule will react with one other atom for complete combustion. The result of this is that you release the maximum amount of heat from the chemical bonds as possible, which would be great in some situations, but not when dealing with rocket engines. The more heat a rocket engine produces, the more you will have to cool your engine so it doesn't melt, which is not ideal.

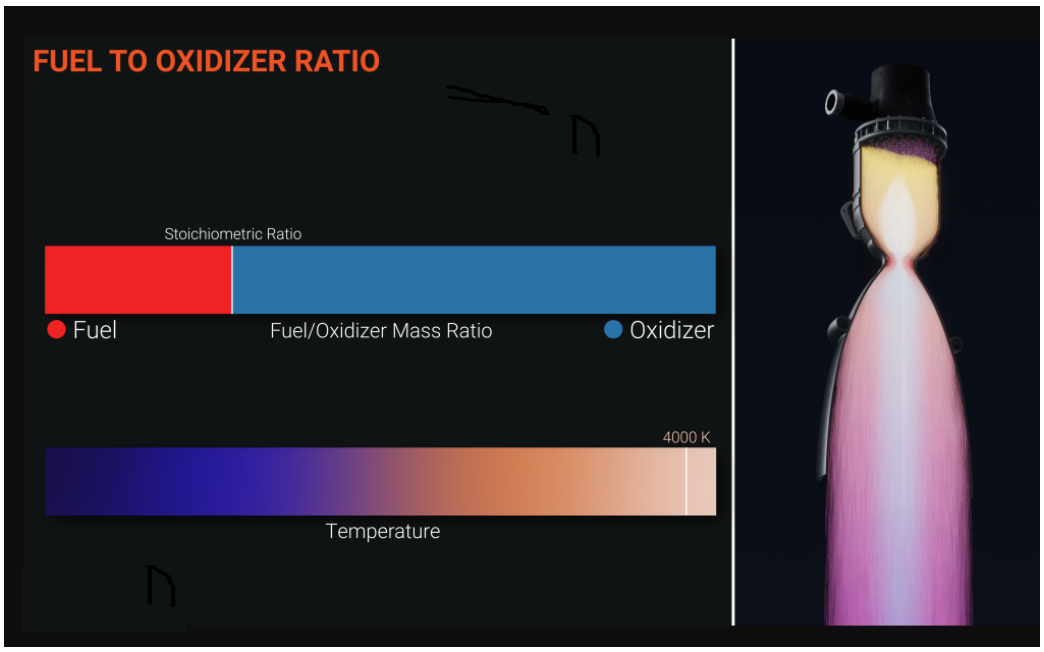


**Figure 1.4:** A graphic of the fuel to oxidizer mass ratio if fuel and oxidizer would be burnt at thestoichiometric ratio, resulting in extremely high temperatures that would destroy an engine

This means that rocket engines have a fuel to oxidizer ratio slightly off from stoichiometric. An engine's main combustion chamber will tend to run fuel rich as this will have a lower thermal load and have high efficiency.You could also run the pre-burner or gas generator fuel rich to keep it cool, which is important as it is extremely hard to cool a spinning turbine. The turbine will have a set amount of heat that it can take based on its materials, so the fuel oxidizer ratio needs to change to be suitable. Turbines can be designed to run fuel or oxidizer rich, like the Space Shuttle's RS-25 main engine, which ran fuel rich, or the soviet designed NK-33engine, which ran oxidizer rich propellant through their closed cycle pre-burners.

## 1.3 Cooling techniques for rocket engines

### 1.3.1 Heat sink cooling

The most direct way to limit the internal surface temperature is to provide a sufficiently thick chamber or nozzle wall with the necessary heat capacity to soak up the heat transferred during the prescribed firing duration. The thrust chamber does not reach a thermal equilibrium, and temperatures continue to increase with operating duration. The heat absorbing capacity of the hardware determines its maximum duration. The rocket combustion operation has to be stopped just before any of the exposed walls reaches a critical temperature at which it could fail. The most suitable materials for this type of cooling are those for which the product specific heat x thermal conductivity x density has high values. The best material from this standpoint is copper [1].

The foregoing criterion is not, however, a unique guide to motor construction, since considerations of strength and weight are frequently of greater importance. In any case, as the required operating duration for an uncooled motor is raised, the requisite motor weight becomes excessive for practical use. Consequently, even if heat-sink system has the advantages of simplicity and cheapness of manufacture, for durations greater than 10 to 20 seconds, it results in a weight penalty [2]. This method has mostly been used with low chamber pressures and low heat transfer rates since this type of motors weights more than rocket motors of equal thrust output that employ regenerative cooling.

### 1.3.2 Film cooling and transpiration cooling

Film cooling and transpiration cooling are supplementary techniques that are used occasionally with regenerative cooling method to locally augment its cooling capability. With film cooling method wall surfaces are protected from excessive heat by a thin film of coolant or propellant introduced through orifices around the injector periphery or through manifolded orifices in the chamber wall near the injector and sometimes in several more planes toward the throat [1]. Transpiration cooling method is essentially a special type of film cooling: a coolant (either gaseous or liquid propellant) is introduced through porous chamber walls at a rate sufficient to maintain the desired temperature of the combustion-gas-side chamber wall [1].

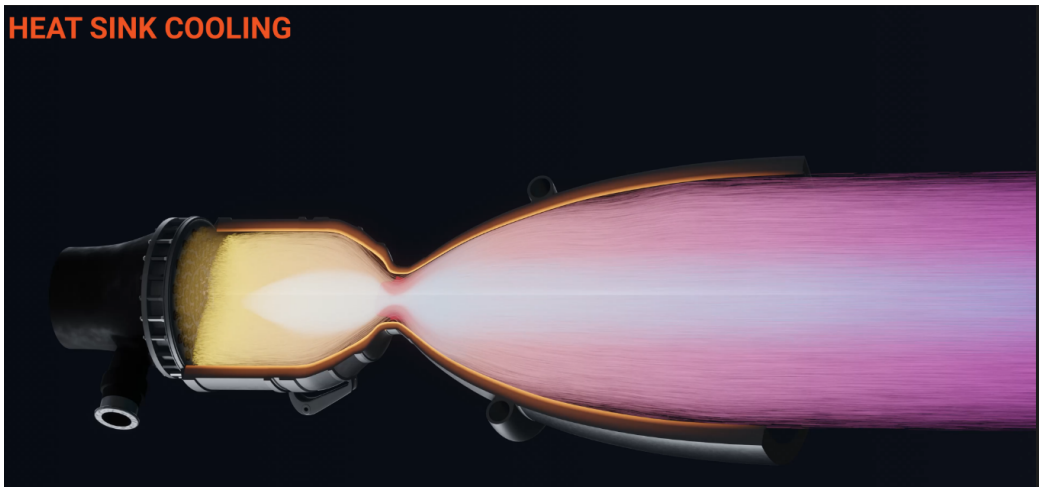


**Figure 1.5:** A render of an engine that only utilizes heat sink cooling

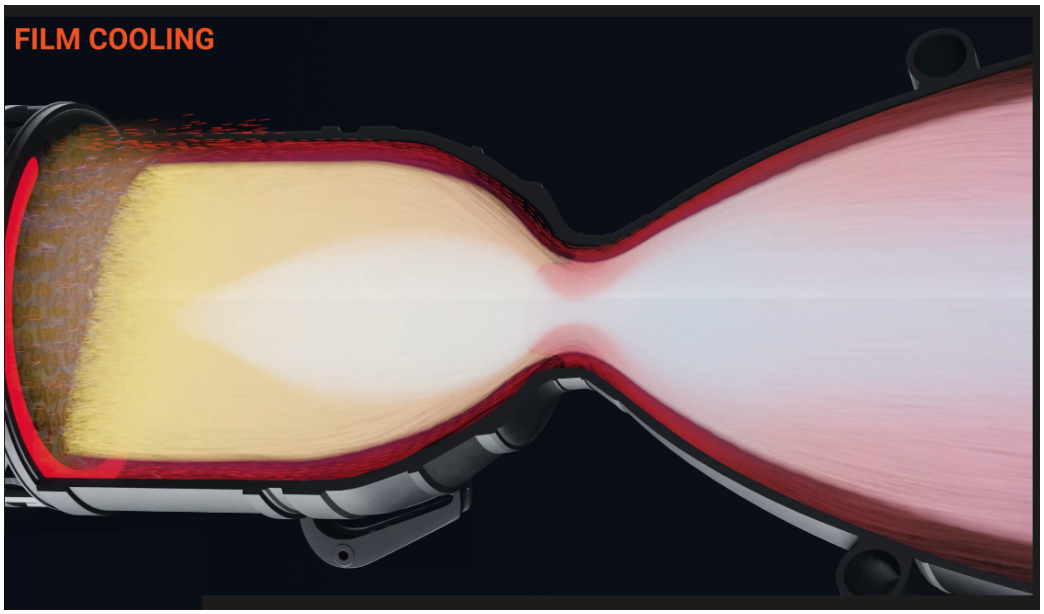


**Figure 1.6:** A film cooled engine in which more fuel rich propellants are injected into the outer perimeter of the injector face to create an insulating layer of unburnt fuel (lack of oxidizer) between the inner combustion chamber and the combustion chamber walls

## 1.4 Ablative Cooling

Ablative cooling is one of the most simple and effective ways of cooling an engine. This method uses a material which will vaporize and then get thrown away, taking the heat with it. This is usually made out of carbon composite which has an extremely high melting point. This is the same method that most spacecraft use for heat shields. When a spacecraft re-enters the atmosphere it gets very, very hot. The heat shield takes this heat, and when it's surface gets too hot, it melts a layer away, taking the heat with it. This stops the heat from penetrating deeper into the spacecraft.

This same principle can be applied to cooling a rocket engine. Inside the walls of the combustion chamber and nozzle is a layer of carbon composites. When the propellant is burning in the engine, this carbon layer will slowly be burnt off. This method has no moving parts and is

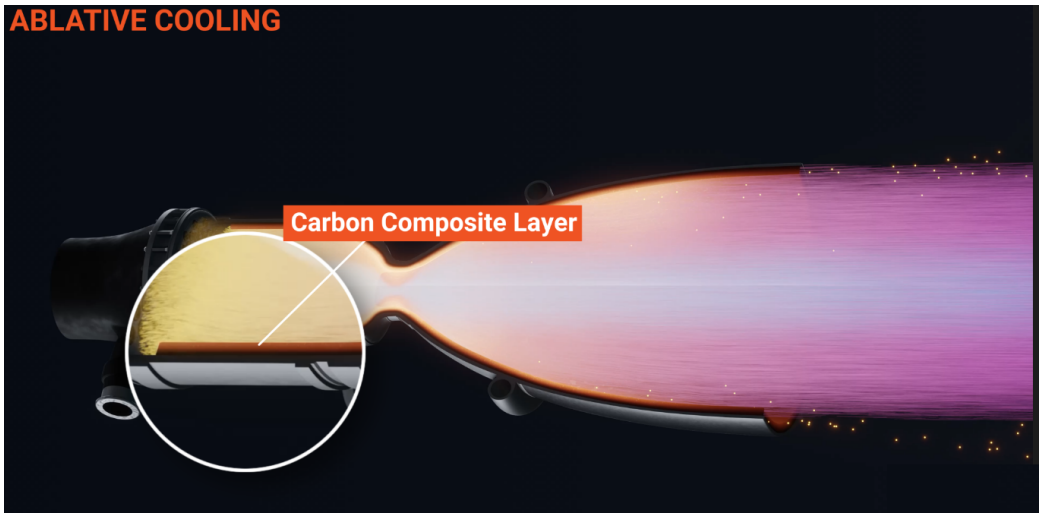


**Figure 1.7:** A carbon composite layer that acts as an ablative layer which insulates the metal walls of the main combustion chamber and absorbs heat when it sublimates away

self-regulating, which makes it an extremely efficient and reliable method for cooling engines. But there are some limitations, most obviously that an engine cooled this way can't be reused. Some engines won't even be able to go through full testing before being used as it wears down the ablative chamber walls. Most famously, the Apollo Lunar Ascent engine couldn't be test fired as a complete unit until it was fired on the surface of the moon to take the astronauts home

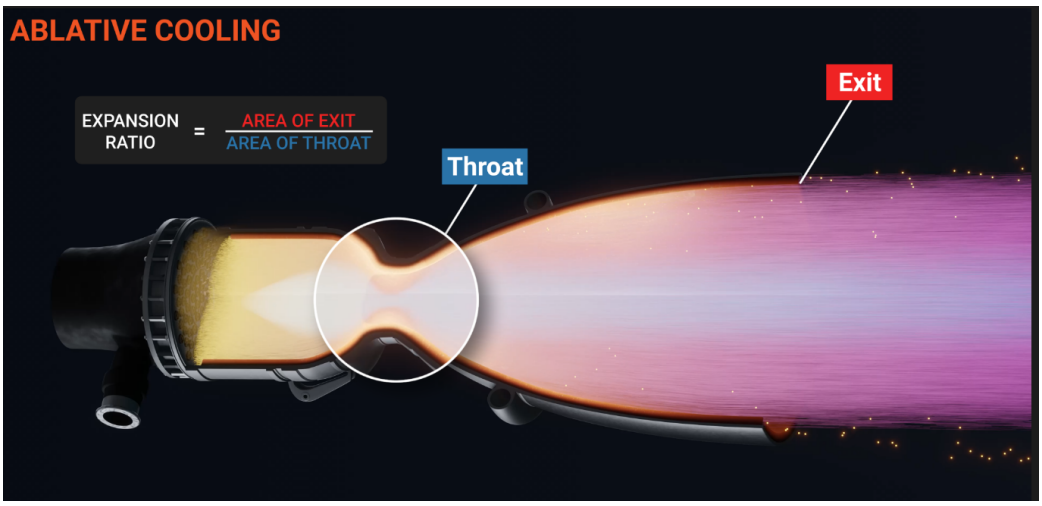


**Figure 1.8:** Ablatively cooled engines will over time open up the throat of the engine due to wearing away more and more of the ablative layer, resulting in lower performance over time

Another type of small engines, reaction control thrusters, can also use ablative chambers, as this type of engine is only used for a short duration and has a set amount of propellant it can burn through before running out. This means engineers can design the thickness of the wall to match the maximum use.

## 1.5 Radiation cooling

With this method, heat is radiated away from the surface of the outer thrust chamber wall. It has been successfully applied to very small, high-temperature material combustion chambers and to low-heat-flux regions, such as nozzle extensions (i.e., diverging nozzle exhaust sections beyond an area ratio of about 6 to 10) [3].

## 1.6 Regenerative cooling

To cool the walls of a regenerative rocket engine, the fuel (e.g., hydrogen, kerosene, methane) or the oxidizer (e.g., oxygen) is passed through cooling channels that are machined in the wall. Finally, the heated coolant is injected into the thrust chamber or goes to turbine. This cooling technique is used primarily with bi-propellant chambers pressure and high heat transfer rates.[1]

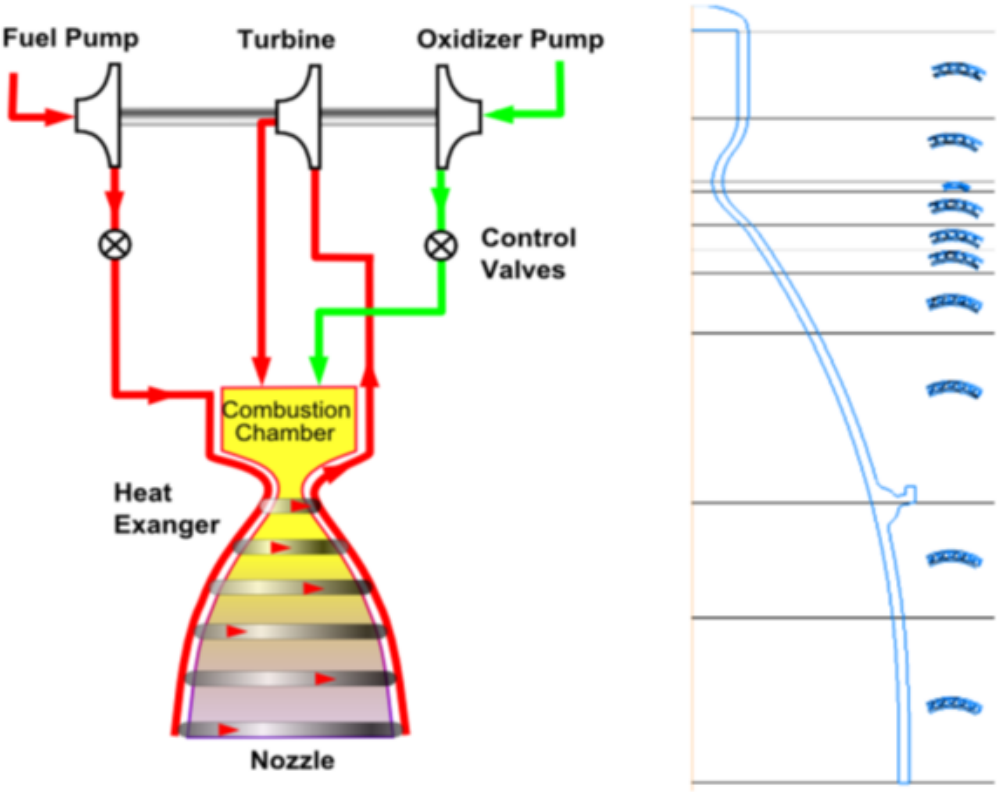


**Figure 1.9:** Ablatively cooled engines will over time open up the throat of the engine due to wearing away more and more of the ablative layer, resulting in lower performance over time

The term regenerative cooling is intended to convey the fact that the heat absorbed by the coolant propellant is not wasted but augments the initial temperature and the energy level of the propellant prior to injection; this increase in the internal energy of the liquid propellant can be calculated as a correction to the enthalpy of the propellant. However, the overall effect on rocket performance is usually very slight. With some propellants the specific impulse can be 1% larger if the propellants are preheated through a temperature differential of 100 to 200 K. [1]

This method is called regenerative cooling because of the similarity to steam regenerators. A large number of successful motors of this type have been built. Regenerative cooling, appears currently to be an efficient approach to the solution of the heat problem. It has the advantage that, once the cooling system has been developed correctly, the engine can be operated for long durations (several minutes at a time) without damage. Furthermore, these motors can be made extremely light in weight, the thrust-weight ratio markedly increasing with the larger thrusts. However, it has to be kept in mind that regenerative system permits only limited throttling with most coolants, has reduced reliability with some coolants (e.g., hydrazine) and requires increased pump power because of the large pressure drop at high heat-flux levels.

The trade-off among these aspects makes regenerative cooling interesting for large high-pressure, high heat flux thrust chambers and for expander (and expander-bleed) cycle engines. A typical value of the integrated heat flux over the entire surface is about 2 % of the heat of combustion for a small engine (thrust < 5000 N). This percentage is considerably smaller for larger thrust motors, because the combustor volume increases approximately in proportion to the mass flow, while the surface of combustor increases only as the two-thirds power for similar shapes.

The practicability of running a rocket engine continuously with only regenerative cooling, using either one or both propellants, is directly the results of this low percentage of heat transfer. None of the common propellants can absorb more than few per cent of the heat of combustion without vaporizing or decomposing and thus becoming unsuitable as coolants [2] Chemical changes in the liquid coolant can seriously influence the heat transfer from hot walls to coolant. Cracking of the coolant, with an attendant formation of insoluble gas, tends to reduce the maximum heat flux and thus promotes failure more readily. Hydrocarbon fuel coolants (methane, kerosene) can break down and form solid, sticky carbon deposits inside the cooling channel, impeding the heat transfer. Some propellants, such as hydrazine, can decompose spontaneously and explode in the cooling passages if they become too hot [1].

The choice of the material for the inner wall in the chamber and the throat region, which are the critical locations, is influenced by the hot-gas resulting from the propellant combination, the maximum wall temperature, the heat transfer, and the feed system. For high-performance and high heat transfer, regeneratively cooled thrust chambers, a material with high thermal conductivity and a thin wall design will reduce the thermal stresses. Copper is an excellent conductor and it will not really oxidize in fuel-rich non corrosive gas mixture, such as are produced by oxygen and hydrogen below a mixture ratio of 6:0. The inner walls are therefore usually made of a copper alloy (with small additions of zirconium, silver, or silicon), which has a conductivity not quite as good as pure (oxygen-free) copper but has improved high temperature strength[1].

The wall temperature on the hot side of the cooling channels in a regeneratively cooled combustion chamber can be reduced increasing the coolant side surface area relative to the hot-gas side surface by the use of extended surfaces or “fins”. An increase in the number of passages, and therefore the surface area of the passages that circumferentially line the

outer wall of a combustion chamber, necessarily increases their aspect ratio. In turn the material between them, known as rib, functionally becomes a fin. High aspect ratio cooling channels (HARCC) have shown a great potential of influencing positively both the temperature field and the pressure loss [4, 5]. Round tubes do not possess this interesting and convenient geometry.

## 1.7 Rocket & Principles properties

### 1.7.1 Propellants

The properties of the combustion products, such as temperature, specific heat, weight, viscosity, etc., have a direct influence on the heat-transfer rate and thus affect chamber cooling requirements and methods. The properties and flow rates of the propellants determine whether they are suitable for regenerative, transpiration, dump, or film cooling. Consequently, the propellants involved will be a primary consideration in the design of a chamber cooling system. [6]

### 1.7.2 Chamber pressure

The effect of chamber pressure on the heat flux in a nozzle is in general an increase in the heat flux with increasing pressure due to a progressive increase in higher heat-transfer rates with increasing combustion-gas density (i.e., higher combustion-gas mass flow rates per unit area of chamber cross section). Regenerative and film-cooling methods are usually combined to meet the stringent requirements of high-chamber-pressure applications. [1]

### 1.7.3 Propellant feed system

Type of propellant feed system used in an engine determines its pressure budget. In a turbo-pump-fed engine, a large pressure drop is usually available for chamber cooling. The availability of this pressure drop permits the use of regenerative cooling, which requires sufficient pressure to force the coolant through the cooling passages before entering the injector. A pressure-fed engine usually has more stringent pressure limitations and operates at relatively lower chamber pressures. This suggests the application of film, ablative, radiation cooling or combinations of these techniques. [6]

### 1.7.4 Thrust-chamber construction material

The properties of the thrust-chamber materials will profoundly affect the cooling system design. Strength at elevated temperature and thermal conductivity will determine the suitability of a given material for regenerative cooling. For film cooled chambers, higher allowable material working-temperatures are desired, for lower film-coolant flow rates. The application of radiation cooling to a chamber largely depends on the

availability of high-temperature (2000 K and up) materials. The success of ablative cooling entirely depends on the availability of suitable materials. In practice, the design of the thrust-chamber cooling system is a major link in the complete engine design. It cannot be treated independently, without consideration of other engine system aspects. For instance, optimization of the chamber pressure of a high-performance engine may be largely limited by the capacity and efficiency of the chamber-cooling system. In turn, chamber pressure affects other design parameters, such as the nozzle expansion ratio, propellant feed pressure, and weight. Because of the complex interrelations between these factors, the complete analysis of chamber-cooling systems is a specialized field, requiring thorough knowledge of heat transfer, fluid mechanics, thermodynamics, materials, and structure .Rocket engines are constructed of a combustion chamber exhausting through a supersonic nozzle. The nozzle consists of a converging section from the combustion chamber to the throat, or most narrow cross-section of the nozzle, and a diverging section from the throat to the exit. The combustion products provide the necessary high temperatures and pressures to induce the conversion into high-velocity exhaust gas. In supersonic flow, a preponderance of enthalpy is converted into kinetic energy resulting in thrust. Thrust force is due to Newton's third law of physics, the conservation of momentum. The pressure force on the wall are balanced by the equal and opposite reaction force by the walls; however, the pressure force at the exit is not compensated for. The high velocity gas exiting the nozzle propels the rocket in the opposite direction. [7]

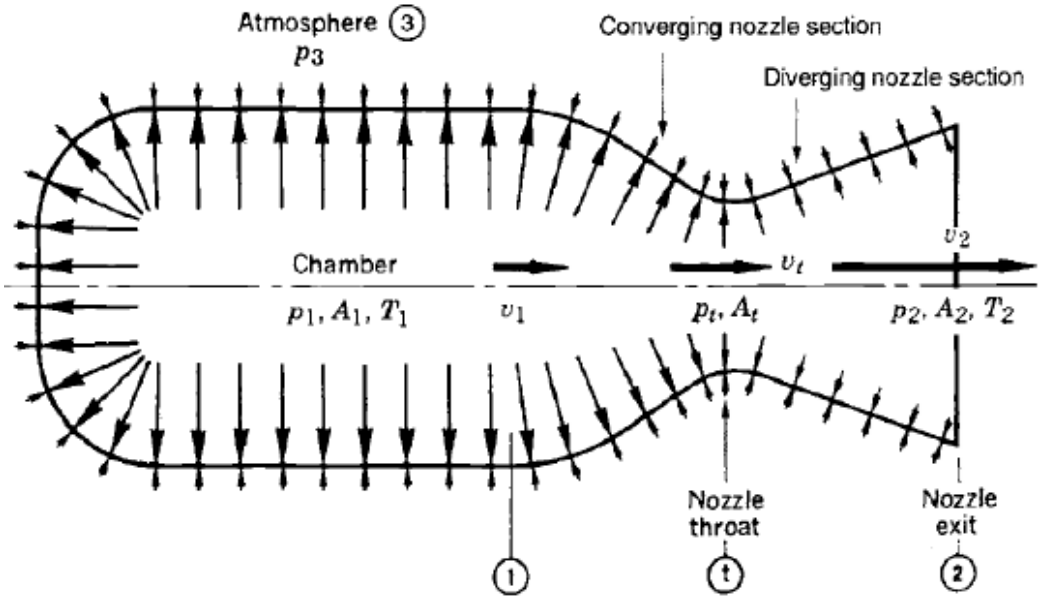


**Figure 1.10:** Rocket propulsion principles

The nozzle geometry produces high velocities by choking the high-pressure combustion gas through the throat. The geometrical convergence causes the pressure to decrease, and thus the velocity to increase from subsonic in the combustion chamber to Mach 1 at the throat. The subsequent rapid thermodynamic expansion of the gas into the diverging section causes the velocity to become supersonic. Mach number is the ratio of the velocity of the moving body to the velocity of the speed

of sound in the same medium. A Mach number of one indicates that the body is moving at the speed of sound in the given medium. Mach numbers less than one are called subsonic, while Mach numbers greater than one are supersonic. Local Mach numbers in rocket engines are referring to the velocity of the exhaust flow. The local Mach number is calculated at a particular location within the nozzle by:

$$M_x = v_x / \sqrt{\gamma R T_x}$$

Where the subscript $x$ implies at a given location in the nozzle, $M$ is the Mach number, $v$ is the velocity, $\gamma$ is the specific heat ratio, $R$ is the gas constant for the particular gas, and $T$ is the absolute temperature in Kelvin. The expansion area ratio of the exit to the throat combined with the chemical kinetics of the fuel determines what Mach numbers can be achieved, as well as the exit pressure. Rocket engines are considered perfectly expanded and have the most efficient performance when the outlet pressure is equal to the ambient pressure. Due to the precipitous altitude changes inherent to rockets, and the subsequent rapidly changing atmospheric pressure, a rocket engine would ideally have a dynamic expansion area ratio that adjusted with altitude. However, because thus far rockets have only been viable for one flight, this would involve impractical mechanical design complications. Since a dynamic area ratio is not yet feasible, the nozzle needs to be designed with an area ratio that is operative over a wide range of altitudes but most efficient at the target ambient pressure.

# 2 Basic concepts

## 2.1 introduction

Numerical simulation of flows within solid propellant engines (combustion chamber and nozzle) requires the use of a compressible formulation of fluid mechanics equations and dedicated treatments (mesh, boundary conditions, etc.). The main objective of this chapter 2 is to provide a comprehensive breakdown of all the formulations developed in this work.

## 2.2 Equations of fluid mechanics

The resolution of the equations of `Navier-Stokes` by the direct simulation approach remains for the moment and certainly for a long time still, limited to flows of `Reynolds` and for simple or even simplistic geometric configurations in relation to industrial concerns. When one is interested in realistic flows, one must therefore be interested in the mean quantities and obtain the system of equations verified by these quantities. To do this, we apply the decomposition of `Favre` on the unknowns of the problem. The new equations obtained are called averaging equations.

### 2.2.1 Reminder of instantaneous equations

The equations of fluid mechanics are written, respectively for the conservation of mass, momentum and energy:

$$\frac{\partial}{\partial t}\rho + \frac{\partial}{\partial x_j}\rho u_j = 0 \tag{2.1}$$

$$\frac{\partial}{\partial t}\rho u_i + \frac{\partial}{\partial x_j}\left(\rho u_i u_j + p\delta_{ij}\right) = \frac{\partial}{\partial x_j}\sigma_{ij} \tag{2.2}$$

$$\frac{\partial}{\partial t}\rho e_t + \frac{\partial}{\partial x_j}\left[u_j\left(\rho e_t + p\right)\right] = \frac{\partial}{\partial x_j}\sigma_{ij}u_i - \frac{\partial}{\partial x_j}q_j \tag{2.3}$$

Where $u_i$ are the velocity components, $p$ the pressure, $\rho$ the density, $\sigma_{ij}$ is the viscous stress tensor, $e_t$ is the total energy and $q_j$ is the heat flow. To close these equations, we add the thermodynamic relationships that link pressure, temperature and density.The heat flux intensity by conduction $q_j$ is, by designating by $\lambda_c$ the coefficient of thermal conduction of the fluid, proportional, according to the law de Fourier, with temperature gradient

$$q_j = -\lambda_c \frac{\partial T}{\partial x_j} \tag{2.4}$$

The choice of the $e_t$ total energy variable to write energy conservation is one form among others. Indeed the total energy conservation equation can be written as a function of the internal energy $e = c_v T$, for a perfect gas this relation is given by:

$$e_t = e + \frac{1}{2}u_k u_k \tag{2.5}$$

[1]:

$$\frac{\partial}{\partial t}\rho e_t + \frac{\partial}{\partial x_j}\rho h_t u_j = \frac{\partial}{\partial x_j}\sigma_{ij}u_i - \frac{\partial}{\partial x_j}q_j \tag{2.6}$$

where $h_t = h + \frac{1}{2}u_k u_k$ is the total enthalpy per unit mass. For compressible flows, the viscous stress tensor, $\sigma_{ij}$ depends on the second viscosity coefficient $\lambda$ (which represents the resistance that the viscous forces oppose to the compression of an elementary volume of fluid) in addition to the molecular viscosity $\mu$. The law of behaviour which links the tensor of viscous stresses to the tensor of average deformation rate is, for a Newtonian fluid

$$\sigma_{ij} = 2\mu S_{ij} + \lambda \frac{\partial u_k}{\partial x_k}\delta_{ij} \tag{2.7}$$

where $S_{ij} = \frac{1}{2}\left(\frac{\partial u_i}{\partial x_j} + \frac{\partial u_j}{\partial x_i}\right)$ is the symmetric portion of the velocity tensor and $\delta_{ij}$ is the symbol of Kronecker ($\delta_{ij}$ =1 if $i = j$, 0 otherwise).
With $2\mu + 3\lambda = 0$, because the changes in volume are made without viscosity (hypothesis of `Stokes`)
We consider the perfect gas state law, which links pressure, temperature and density:

$$p = \rho r T = \rho\left(\gamma - 1\right)e \tag{2.8}$$

Where $r$ is the perfect gas constant equal to the universal gas constant divided by the molecular mass of the fluid. We can also rewrite the heat flow by showing the number of `Prandtl` laminar, $Pr$ :

$$q_j = -\lambda_c \frac{\partial T}{\partial x_j} = -\frac{\gamma\mu}{Pr}\frac{\partial e}{\partial x_j} \tag{2.9}$$

[2]

The viscosity of a fluid varies according to its temperature, the law of `Sutherland` which connects viscosity and temperature, this law is given by:

$$\mu\left(T\right) = \mu_0\sqrt{\frac{T}{T_0}}\frac{1 + \frac{S}{T_0}}{1 + \frac{S}{T}}$$

1: With mass enthalpy $h = e + \frac{p}{\rho}$, the equation 2.3 can be written

2: with $Pr = \frac{\mu c_p}{\lambda_c} = \gamma\frac{\mu c_v}{\lambda_c}$

where $S = 110.4K$, $T_0 = 273.15K$ and $\mu_0 = 1.711.10^5 Pa.s$

## 2.3 The averaged Navier-Stokes equations

By a combination of the two averages, the resulting averaged equations can be simplified from a formulation that focuses solely on Reynolds decomposition. This method consists of decomposing pressure and density into an average centered on [3] and decomposing any other quantity (speed, temperature, energy) into an average weighted by density according to [4]. Introducing the hypothesis of negligible fluctuations in viscosity and thermal conductivity, the open form of the system of Navier-Stokes equations statistically averaged is:

3:

$$\phi = \bar{\phi} + \phi', \qquad \overline{\phi'} = 0 \tag{2.10}$$

4:

$$\begin{cases} \phi = \overline{\phi} + \phi' & moyenne \quad selon \quad \texttt{Reynolds} \\ \phi = \widetilde{\phi} + \phi'' & moyenne \quad selon \quad \texttt{Favre} \\ \rho = \overline{\rho} + \rho' \end{cases} \tag{2.11}$$

### 2.3.1 Average mass conservation equation

Using a weighted average for speed, the mass conservation equation becomes:

$$\frac{\partial \bar{\rho}}{\partial t} + \frac{\partial}{\partial x_j}\left(\bar{\rho}\tilde{u}_j\right) = 0 \tag{2.12}$$

The density fluctuation equation is obtained by subtracting the mean equation (2.12) from the instantaneous equation (2.3):

$$\frac{\partial \rho'}{\partial t} + \frac{\partial}{\partial x_j}\left(\rho'\tilde{u}_j\right) + \frac{\partial}{\partial x_j}\left(\rho u_j''\right) = 0 \tag{2.13}$$

### 2.3.2 Conservation equation of the mean momentum

Using a technique similar to that of the continuity equation, the equation of the momentum takes the form of :

$$\frac{\partial}{\partial t}\bar{\rho}\tilde{u}_i + \frac{\partial}{\partial x_j}\bar{\rho}\tilde{u}_i\tilde{u}_j = -\frac{\partial \bar{p}}{\partial x_i} + \frac{\partial}{\partial x_j}\left(\tilde{\sigma}_{ij} - \overline{\sigma_{ij}''}\right) - \frac{\partial}{\partial x_j}\bar{\rho}\widetilde{u_i''u_j''} \tag{2.14}$$

The equation of the momentum for the fluctuating component of the velocity is obtained by subtracting the mean equation (2.14) from the instantaneous equation of the momentum:

$$\frac{\partial}{\partial t}\left(\rho'\tilde{u}_i + \rho u_i''\right) + \frac{\partial}{\partial x_j}\left(\rho'\tilde{u}_j\tilde{u}_i + \rho\tilde{u}_i u_j'' + \rho u_i''\tilde{u}_j + \rho u_i''u_j'' - \overline{\rho u_i''u_j''}\right) = -\frac{\partial p'}{\partial x_i} + \frac{\partial}{\partial x_j}\left(\sigma_{ij}'' - \overline{\sigma_{ij}''}\right) \tag{2.15}$$

In addition to the conventional terms that already exist in the instantaneous equation, we have shown a new term; $\left(-\frac{\partial}{\partial x_j}\bar{\rho}\widetilde{u_i''u_j''}\right)$, Which has a dimension of a constraint and whose existence is the basis of the closure problem.

The decomposition of the viscous stress tensor $\sigma_{ij}$, shows not only an

average value of type $\tilde{\sigma}_{ij}$, but also a nonzero term l :

$$\overline{\sigma''_{ij}} = \bar{\mu}\left(\frac{\partial\overline{u''_i}}{\partial x_j} + \frac{\partial\overline{u''_j}}{\partial x_i}\right) - \frac{2}{3}\bar{\mu}\frac{\partial\overline{u''_k}}{\partial x_k} \tag{2.16}$$

this term can be overlooked by assuming that all terms involving fluctuations other than `Reynolds` tensions are negligible .The equation of the momentum averaged is written:

$$\frac{\partial}{\partial t}\bar{\rho}\tilde{u}_i + \frac{\partial}{\partial x_j}\bar{\rho}\tilde{u}_i\tilde{u}_j = -\frac{\partial\bar{p}}{\partial x_i} + \frac{\partial}{\partial x_j}\left(\bar{\mu}\left(\frac{\partial\tilde{u}_i}{\partial x_j} + \frac{\partial\tilde{u}_j}{\partial x_i} - \frac{2}{3}\delta_{ij}\frac{\partial\tilde{u}_k}{\partial x_k}\right) - \bar{\rho}\widetilde{u''_i u''_j}\right) \tag{2.17}$$

### 2.3.3 Average energy conservation equation

The transport equation of energy, when it applies formalism of Favre, becomes:

$$\begin{aligned}\frac{\partial}{\partial t}\left(\bar{\rho}\left(\tilde{e} + \frac{\tilde{u}_i\tilde{u}_i}{2}\right) + \frac{\overline{\rho u''_i u''_i}}{2}\right) + \frac{\partial}{\partial x_j}\left(\bar{\rho}\tilde{u}_j\left(\tilde{e} + \frac{\tilde{u}_i\tilde{u}_i}{2}\right) + \tilde{u}_j\bar{p} + \tilde{u}_j\overline{\rho u''_i u''_j}\right)\\ = -\frac{\partial}{\partial x_j}\left(\overline{\rho u''_j e''} + \bar{p}\overline{u''_j} + \overline{p' u''_j} + \tilde{u}_i\overline{\rho u''_j u''_i} + \frac{1}{2}\overline{\rho u''_j u''_i u''_i}\right)\\ + \frac{\partial}{\partial x_j}\left(\tilde{\sigma}_{ij}\tilde{u}_i + \tilde{\sigma}_{ij}\overline{u''_i} + \overline{\sigma''_{ij}}\tilde{u}_i + \overline{\sigma''_{ij}u''_i}\right) - \frac{\partial}{\partial x_j}\left(\tilde{q}_j + \overline{q''_j}\right)\end{aligned} \tag{2.18}$$

As for the equation of momentum, new terms appear: [5] Subtracting the mean equation (2.18) from the instantaneous equation (2.3). the energy fluctuation equation can be derived:

$$\begin{aligned}\frac{\partial}{\partial t}\rho\left(e'' + \tilde{u}_i u''_i + \frac{1}{2}u''_i u''_i\right) - \frac{\partial}{\partial t}\frac{1}{2}\overline{\rho u''_i u''_i} + \frac{\partial}{\partial t}\rho'\left(\tilde{e} + \frac{1}{2}\tilde{u}_i\tilde{u}_i\right) +\\ \frac{\partial}{\partial x_j}\rho\tilde{u}_j\left(e'' + \tilde{u}_i u''_i + \frac{1}{2}u''_i u''_i\right) + \frac{\partial}{\partial x_j}\rho'\tilde{u}_j\left(\tilde{e} + \frac{1}{2}\tilde{u}_i\tilde{u}_i\right) +\\ \frac{\partial}{\partial x_j}\rho u''_j\left(\tilde{e} + e'' + \frac{1}{2}\tilde{u}_i\tilde{u}_i + \tilde{u}_i u''_i + \frac{1}{2}u''_i u''_i\right) -\\ \frac{\partial}{\partial x_j}\left(\frac{1}{2}\tilde{u}_j\overline{\rho u''_i u''_i} + \overline{\rho u''_j e''} + \tilde{u}_i\overline{\rho u''_i u''_j} + \frac{1}{2}\overline{\rho u''_i u''_i u''_j}\right) +\\ \frac{\partial}{\partial x_j}\left(\tilde{u}_j p' + u''_j\bar{p} + u''_j p'\right) - \frac{\partial}{\partial x_j}\left(\overline{u''_j}\bar{p} + \overline{u''_j p'}\right) =\\ \frac{\partial}{\partial x_j}\left(\tilde{\sigma}_{ij}u''_i + \sigma''_{ij}\tilde{u}_i + \sigma''_{ij}u''_i\right) - \frac{\partial}{\partial x_j}\left(\tilde{\sigma}_{ij}\overline{u''_i} + \overline{\sigma''_{ij}}\tilde{u}_i + \overline{\sigma''_{ij}u''_i}\right) - \frac{\partial}{\partial x_j}\left(q''_j - \overline{q''_j}\right)\end{aligned} \tag{2.20}$$

The velocity-temperature correlation can be expressed by:

$$\overline{\rho u''_j e''} = c_v\overline{\rho u''_j T''} \tag{2.21}$$

5:

$\frac{1}{2}\overline{\rho u''_i u''_i}$ :kinetic energy of turbulent fluctuations per unit of volume, noted $\bar{\rho}k$ where:

$$k = \frac{1}{2}\widetilde{u''_i u''_i} \tag{2.19}$$

$\frac{1}{2}\bar{\rho}\tilde{u}_i\tilde{u}_i$ :kinetic energy of average motion per unit volume

$\overline{\rho u''_j e''}$ :turbulent transport of heat

$\frac{1}{2}\overline{\rho u''_j u''_i u''_i}$ :turbulent transport of turbulent energy

$\overline{\sigma_{ij}u''_i} = \left(\tilde{\sigma}_{ij}\overline{u''_i} + \overline{\sigma''_{ij}u''_i}\right)$ :molecular diffusion of turbulent energy

The pressure-velocity correlation :

$$\begin{aligned}\bar{p}\overline{u_j''} + \overline{p'u_j''} = \overline{pu_j''} &= (\gamma-1)\,\overline{\rho e u_j''} \\ &= (\gamma-1)\,\overline{\rho e'' u_j''} \\ &= c_v\,(\gamma-1)\,\overline{\rho T'' u_j''}\end{aligned} \tag{2.22}$$

with :

$$\overline{\rho u_j'' e''} + \overline{pu_j''} = \gamma c_v \overline{\rho u_j'' T''} \tag{2.23}$$

2.23 is the overall expression of 2.21 and 2.22 The correlation of viscous stress and velocity fluctuations is given by:

$$\overline{\sigma_{ij} u_i''} = \tilde{\sigma}_{ij}\overline{u_i''} + \overline{\sigma_{ij}'' u_i''} \tag{2.24}$$

For the analysis of terms $\left(\tilde{\sigma}_{ij}\overline{u_i''}\right)$ and $\left(\overline{\sigma_{ij}'' u_i''}\right)$,the speed fluctuation $u_i''$ needs to be expressed in other known terms, while keeping the conventional average for $\rho$ and $p$, , and that of Favre for the speed, the temperature, etc. . . . Vandromme[**8**] proposes two possible approaches:

1. Knowing that the total temperature $T_t$ is constant in vortices. In this case the temperature fluctuation $T''$ is expressed in a function of the mean value of the speed fluctuation.

$$\begin{aligned}T_t &= T + \tfrac{1}{2c_p} u_i u_i = C_0 \\ T_t &= \tilde{T} + \tfrac{1}{2c_p}\left(\tilde{u}_i\tilde{u}_i + \widetilde{u_i'' u_i''}\right) \\ T'' &= -\tfrac{\tilde{u}_i u_i''}{c_p} - \tfrac{1}{2c_p}\left(u_i'' u_i'' - \widetilde{u_i'' u_i''}\right)\end{aligned} \tag{2.25}$$

   Where $C_0$ is a constant. In the case of a unidirectional flow,we can write:

$$T'' = -\frac{\tilde{u}_i u_i''}{c_p} \tag{2.26}$$

   Introducing the hypothesis of Rubesin , for a behavior polytropic turbulence:

$$\frac{p'}{\bar{p}} = n\frac{\rho'}{\bar{\rho}} = \frac{n}{n-1}\frac{\rho T''}{\bar{\rho}\tilde{T}} \tag{2.27}$$

   Where n is the polytropic exponent, we obtain an expression giving fluctuation in density $\rho$:

$$\rho' = -\frac{\rho\tilde{u}_i u_i''}{(n-1)\,c_p\tilde{T}} \tag{2.28}$$

   Using the relations between conventional and weighted by mass taking into account the expression of fluctuation of $\rho$, , we obtain:

$$\overline{u_i''} = -\frac{\overline{\rho' u_i''}}{\bar{\rho}} = \frac{\tilde{u}_j\widetilde{u_i'' u_j''}}{(n-1)\,c_p\tilde{T}} \tag{2.29}$$

2. This approach uses the polytropic relationship (2.27), we obtain:

$$\overline{u_i''} = -\frac{\overline{\rho' u_i''}}{\bar{\rho}} = \frac{\widetilde{u_i'' T''}}{(n-1)\,\tilde{T}} \tag{2.30}$$

It appears in this expression the correlation speed-temperature,which takes into account the case of a heat flux or temperature imposed as conditions on limits, as opposed to the expression (2.29).

the term $\left(\tilde{\sigma}_{ij}\overline{u_i''}\right)$can be expressed either from (2.29) or (2.30), its role is negligible .for Mach values below 5 [**9**]-[**10**]. the term $\left(\overline{\sigma_{ij}'' u_i''}\right)$ is modeled :

$$\begin{aligned}\overline{\sigma_{ij}'' u_i''} &= \overline{\mu u_i'' \left(\frac{\partial u_i''}{\partial x_j} + \frac{\partial u_j''}{\partial x_i} - \frac{2}{3}\delta_{ij}\frac{\partial u_k''}{\partial x_k}\right)} \\ &= \bar{\mu}\left(\frac{\partial}{\partial x_j}\frac{\overline{u_i'' u_i''}}{2} + \overline{u_i''\frac{\partial u_j''}{\partial x_i}} - \frac{2}{3}\delta_{ij}\overline{u_i''\frac{\partial u_k''}{\partial x_k}}\right)\end{aligned} \tag{2.31}$$

the termes $\overline{\sigma_{ij}''}\tilde{u}_i$, $\overline{q_j''}$ et $-\frac{1}{2}\overline{\rho u_j'' u_i'' u_i''}$ being neglected, for we hold Only correlations involving Reynolds stress are accounted for.Equation (2.18) can be written as follows:

$$\begin{aligned}&\frac{\partial}{\partial t}\bar{\rho}\left(\tilde{e} + \frac{\tilde{u}_i\tilde{u}_i}{2} + k\right) + \frac{\partial}{\partial x_j}\left(\bar{\rho}\tilde{u}_j\left(\tilde{e} + \frac{\tilde{u}_i\tilde{u}_i}{2} + k\right) + \tilde{u}_j\bar{p}\right) = \\ &\frac{\partial}{\partial x_j}\tilde{u}_i\left(\bar{\mu}\left(\frac{\partial\tilde{u}_i}{\partial x_j} + \frac{\partial\tilde{u}_j}{\partial x_i} - \frac{2}{3}\delta_{ij}\frac{\partial\tilde{u}_k}{\partial x_k}\right) - \overline{\rho u_i'' u_j''}\right) - \\ &\frac{\partial}{\partial x_j}\left(-\lambda_c\frac{\partial\tilde{T}}{\partial x_j} + \gamma c_v\overline{\rho T'' u_j''}\right)\end{aligned} \tag{2.32}$$

In addition, the averaging equation is taken into account:

$$\bar{p} = \bar{\rho}\left(c_p - c_v\right)\tilde{T} = (\gamma - 1)\,\bar{\rho}\tilde{e} \tag{2.33}$$

We can also write an equation giving the pressure fluctuation:

$$p' = (\gamma - 1)\left(\rho'\tilde{e} + \rho e''\right) \tag{2.34}$$

The state equation can still be put in the form:

$$\frac{p'}{\bar{p}} = \frac{T''}{\tilde{T}} + \frac{\rho'}{\bar{\rho}} + \frac{\rho' T''}{\bar{\rho}\tilde{T}} \tag{2.35}$$

## 2.4 closing of equations

The establishment of the system of previously written equations testifies to the appearance of additional terms which are expressed in the form of correlations, which reflect the effect of turbulence on the movement of the middle field and which make the system of equations open. The problem of closure then arises in establishing the link between the correlations and the mean field.
The search for algebraic equations or relationships to close the equation system constitutes the modelling procedure that must be based on experimental validation.
The Reynolds tension is the main correlation as it largely determines the behavior of the mean velocity field. In the closure of the first order, the double correlations are expressed as a function of the gradient of

the mean field and a viscosity of the turbulence through a hypothesis of Boussinesq [**11**] . The closure of the second order is based on the balance equations for the components of the double velocity correlation, the third order approach of the triple correlations [**12**] semple at present very complex.
For turbulent heat flow, the closure can be carried to different levels up to the transport model by a partial differential balance equation [13]. The question arises: at what level should the closure of the thermal correlation be carried out in relation to the closure of the kinematic correlation? The answer depends on the nature of the flows that are being considered and is at the same time a compromise between the complexity of the model and its performance. Very schematically we can consider that obtaining a system close of equations can be done from the system opened by:

- Reduction of unknown numbers
- Addition of additional equations
- Combinations of the two previous procedures.

## 2.5 The Turbulent Kinetic Energy Transport Equation

A differential equation for turbulent kinetic energy $k$ can be obtained by:

1. Considering the instantaneous equation of the momentum written in primitive variables, a Navier-Stokes equation can be written as:

$$\mathscr{E}_{\mathcal{NS}}(u_i) = \rho\frac{\partial u_i}{\partial t} + \rho u_j\frac{\partial u_i}{\partial x_j} + \frac{\partial p}{\partial x_i} - \frac{\partial \sigma_{ij}}{\partial x_j} \tag{2.36}$$

In this case the equation of the momentum is obtained by:

$$\mathscr{E}_{\mathcal{NS}}(u_i) = 0 \tag{2.37}$$

2. We multiply the previous equation by $u_i''$ and we average in time:

$$\overline{u_i''\mathscr{E}_{\mathcal{NS}}(u_i) = 0} \tag{2.38}$$

$$\overline{u_i''\rho\frac{\partial u_i}{\partial t}} + \overline{u_i''\rho u_j\frac{\partial u_i}{\partial x_j}} + \overline{u_i''\frac{\partial p}{\partial x_i}} - \overline{u_i''\frac{\partial \sigma_{ij}}{\partial x_j}} = 0 \tag{2.39}$$

with

a)

$$\overline{u_i''\rho\frac{\partial u_i}{\partial t}} = \overline{u_i''\rho\frac{\partial u_i''}{\partial x_j}}$$

$$= \frac{\partial}{\partial t}\frac{1}{2}\overline{\rho u_i'' u_i''} - \frac{1}{2}\overline{u_i'' u_i''\frac{\partial \rho}{\partial t}}$$

b)

$$\begin{aligned}\overline{u_i'' \rho u_j \frac{\partial u_i}{\partial x_j}} &= \tilde{u}_j \overline{\rho \frac{\partial}{\partial x_j} \frac{1}{2} u_i'' u_i''} + \overline{\rho u_j'' \frac{\partial}{\partial x_j} \frac{1}{2} u_i'' u_i''} + \overline{\rho u_j'' u_i''} \frac{\partial \tilde{u}_i}{\partial x_j} \\ &= \overline{\rho u_j'' u_i''} \frac{\partial \tilde{u}_i}{\partial x_j} + \frac{\partial}{\partial x_j} \tilde{u}_j \frac{1}{2} \overline{\rho u_i'' u_i''} - \frac{1}{2} \overline{\rho u_i'' u_i'' \frac{\partial}{\partial x_j} \rho \tilde{u}_j} \\ &\quad + \frac{\partial}{\partial x_j} \frac{1}{2} \overline{\rho u_j'' u_i'' u_i''} - \frac{1}{2} \overline{u_i'' u_i'' \frac{\partial}{\partial x_j} \rho u_j''}\end{aligned}$$

c)

$$\overline{u_i'' \frac{\partial p}{\partial x_i}} = \overline{u_i''} \overline{\frac{\partial p}{\partial x_i}} + \frac{\partial}{\partial x_i} \overline{u_i'' p'} - \overline{p' \frac{\partial u_i''}{\partial x_i}}$$

d)

$$-\overline{u_i'' \frac{\partial \sigma_{ij}}{\partial x_j}} = \overline{\sigma_{ij} \frac{\partial u_i''}{\partial x_j}} - \frac{\partial}{\partial x_j} \overline{u_i'' \sigma_{ij}}$$

From the continuity equation, the following can be deduced:

$$\frac{1}{2} \overline{u_i'' u_i'' \frac{\partial \rho}{\partial t}} + \frac{1}{2} \overline{\rho u_i'' u_i'' \frac{\partial}{\partial x_j} \rho \tilde{u}_j} + \frac{1}{2} \overline{u_i'' u_i'' \frac{\partial}{\partial x_j} \rho u_j''} = 0 \tag{2.40}$$

We obtain the following scalar equation:

$$\begin{aligned}&\underbrace{\frac{\partial}{\partial t} \frac{1}{2} \overline{\rho u_i'' u_i''} + \frac{\partial}{\partial x_j} \tilde{u}_j \frac{1}{2} \overline{\rho u_i'' u_i''}}_{1} = \underbrace{- \overline{\rho u_j'' u_i''} \frac{\partial \tilde{u}_i}{\partial x_j}}_{2} \\ &\underbrace{- \frac{\partial}{\partial x_j} \left( \frac{1}{2} \overline{\rho u_j'' u_i'' u_i''} + \overline{u_j'' p'} - \overline{u_i'' \sigma_{ij}} \right)}_{3} \\ &\underbrace{- \overline{u_i''} \frac{\partial \bar{p}}{\partial x_i}}_{4} + \underbrace{p' \overline{\frac{\partial u_i''}{\partial x_i}}}_{5} \underbrace{- \overline{\sigma_{ij} \frac{\partial u_i''}{\partial x_j}}}_{6}\end{aligned} \tag{2.41}$$

The terms represent respectively:

1. Temporal variation of $k$ and its convection by the mean velocity field
2. Represents the production of turbulence kinetic energy by mean motion
3. represent respectively
   a) diffusion by turbulent movements: $\frac{1}{2} \overline{\rho u_j'' u_i'' u_i''}$
   b) diffusion by pressure fluctuations: $\overline{u_j'' p'}$
   c) molecular motion diffusion: $\overline{u_i'' \sigma_{ij}}$
4. the interaction of the medium pressurized field with velocity fluctuations
5. Correlation between fluctuation of pressure and divergence of fluctuating velocities
6. Corresponds to the destruction of turbulence kinetic energy by the effect of viscosity

## 2.6 Reynolds Stress Transport Equation

This equation plays an important role in the closure to the second order with transport equations or in its simple form in the closure to the first order which is presented as an equation of the kinetic energy of turbulence.
Consider the products $\mathcal{E}_{\mathcal{NS}}(u_i$ by the speed fluctuation $u_j''$) and $\mathcal{E}_{\mathcal{NS}}(u_j$ by $u_i''$).The statistical average of the sum of the two products gives:

$$\overline{u_j''\mathcal{E}_{\mathcal{NS}}(u_i) + u_i''\mathcal{E}_{\mathcal{NS}}(u_j)} = 0 \tag{2.42}$$

$$\begin{cases} \mathcal{E}_{\mathcal{NS}}(u_i) = \rho\dfrac{\partial u_i}{\partial t} + \rho u_k\dfrac{\partial u_i}{\partial x_k} + \dfrac{\partial p}{\partial x_i} - \dfrac{\partial \sigma_{ik}}{\partial x_k} \\ \mathcal{E}_{\mathcal{NS}}(u_j) = \rho\dfrac{\partial u_j}{\partial t} + \rho u_k\dfrac{\partial u_j}{\partial x_k} + \dfrac{\partial p}{\partial x_j} - \dfrac{\partial \sigma_{jk}}{\partial x_k} \end{cases} \tag{2.43}$$

We start with the development of unsteady terms:

$$\overline{u_j''\rho\frac{\partial u_i}{\partial t}} + \overline{u_i''\rho\frac{\partial u_j}{\partial t}} = \frac{\partial}{\partial t}\overline{\rho u_i'' u_j''} - \overline{u_i'' u_j''\frac{\partial \rho}{\partial t}} \tag{2.44}$$

The convective term is written :

$$\begin{aligned} &\overline{u_j''\rho u_k\frac{\partial u_i}{\partial x_k}} + \overline{u_i''\rho u_k\frac{\partial u_j}{\partial x_k}} = \frac{\partial}{\partial x_k}\tilde{u}_k\overline{\rho u_i'' u_j''} - \overline{u_i'' u_j''\frac{\partial \rho\tilde{u}_k}{\partial x_k}} + \\ &\frac{\partial}{\partial x_k}\overline{\rho u_k'' u_i'' u_j''} - \overline{u_i'' u_j''\frac{\partial \rho u_k''}{\partial x_k}} + \rho\overline{u_k'' u_i''}\frac{\partial \tilde{u}_j}{\partial x_k} + \rho\overline{u_k'' u_j''}\frac{\partial \tilde{u}_i}{\partial x_k} \end{aligned} \tag{2.45}$$

The term of the pressure gradient:

$$\begin{aligned} &\overline{u_i''\frac{\partial p}{\partial x_j}} + \overline{u_j''\frac{\partial p}{\partial x_i}} = \overline{u_i''}\frac{\partial \bar{p}}{\partial x_j} + \overline{u_j''}\frac{\partial \bar{p}}{\partial x_i} + \overline{u_i''\frac{\partial p'}{\partial x_j}} + \overline{u_j''\frac{\partial p'}{\partial x_i}} \\ &= \overline{u_i''}\frac{\partial \bar{p}}{\partial x_j} + \overline{u_j''}\frac{\partial \bar{p}}{\partial x_i} + \frac{\partial}{\partial x_j}\overline{u_i'' p'} + \frac{\partial}{\partial x_i}\overline{u_j'' p'} - \overline{p'\left(\frac{\partial u_i''}{\partial x_j} + \frac{\partial u_j''}{\partial x_i}\right)} \end{aligned} \tag{2.46}$$

The viscous term :

$$-\overline{u_j''\frac{\partial \sigma_{ik}}{\partial x_k}} - \overline{u_i''\frac{\partial \sigma_{jk}}{\partial x_k}} = -\frac{\partial}{\partial x_k}\overline{u_j''\sigma_{ik}} + \overline{\sigma_{ik}\frac{\partial u_j''}{\partial x_k}} - \frac{\partial}{\partial x_k}\overline{u_i''\sigma_{jk}} + \overline{\sigma_{jk}\frac{\partial u_i''}{\partial x_k}} \tag{2.47}$$

Using equation (2.40), we obtain the transport equation for the Reynolds stresses:

$$\begin{aligned} &\frac{\partial}{\partial t}\overline{\rho u_i'' u_j''} + \frac{\partial}{\partial x_k}\tilde{u}_k\overline{\rho u_i'' u_j''} = -\overline{\rho u_k'' u_i''}\frac{\partial \tilde{u}_j}{\partial x_k} - \overline{\rho u_k'' u_j''}\frac{\partial \tilde{u}_i}{\partial x_k} \\ &-\frac{\partial}{\partial x_k}\left(\overline{\rho u_k'' u_i'' u_j''} + \overline{u_i'' p'}\delta_{jk} + \overline{u_j'' p'}\delta_{ik} - \overline{u_j''\sigma_{ik}} - u_i''\sigma_{jk}\right) \\ &-\overline{u_i''}\frac{\partial \bar{p}}{\partial x_j} - \overline{u_j''}\frac{\partial \bar{p}}{\partial x_i} + \overline{p'\left(\frac{\partial u_i''}{\partial x_j} + \frac{\partial u_j''}{\partial x_i}\right)} - \overline{\sigma_{ik}\frac{\partial u_j''}{\partial x_k}} - \overline{\sigma_{jk}\frac{\partial u_i''}{\partial x_k}} \end{aligned} \tag{2.48}$$

This transport equation is used as an alternative to Reynolds $-\rho\overline{u_i'' u_j''}$, tensor modeling, it contains triple correlation terms, which will need to be modeled

## 2.7 The transport equation of turbulent dissipation

Dissipation equation requires much more effort, dissipation is given from the following expression:

$$\bar{\rho}\varepsilon = \overline{\sigma_{ik}\frac{\partial u_j''}{\partial x_k}} = \bar{\mu}\overline{\left(\frac{\partial u_i}{\partial x_k} + \frac{\partial u_k}{\partial x_i} - \frac{2}{3}\delta_{ik}\frac{\partial u_n}{\partial x_n}\right)\frac{\partial u_i''}{\partial x_k}} \tag{2.49}$$

we can express an equation for viscous stress $\sigma_{ik}$ using expressions (2.36) and (2.37). By adding kinematic viscosity to have a dimension of a constraint.

$$\nu\left(\frac{\partial}{\partial x_k}\mathscr{E}_{\mathcal{NS}}(u_i) + \frac{\partial}{\partial x_i}\mathscr{E}_{\mathcal{NS}}(u_k) - \frac{2}{3}\delta_{ik}\frac{\partial}{\partial x_n}\mathscr{E}_{\mathcal{NS}}(u_n)\right) \tag{2.50}$$

The terms of equation (248) are given respectively by:

$$\begin{aligned}\frac{\partial}{\partial x_k}\mathscr{E}_{\mathcal{NS}}(u_i) = \rho\frac{\partial}{\partial t}\left(\frac{\partial u_i}{\partial x_k}\right) + \rho u_l\frac{\partial}{\partial x_l}\left(\frac{\partial u_i}{\partial x_k}\right) + \frac{\partial\rho}{\partial x_k}\frac{\partial u_i}{\partial t} + \frac{\partial\rho u_l}{\partial x_k}\frac{\partial u_i}{\partial x_l}\\ -\frac{\partial^2}{\partial x_k\partial x_l}\mu\left(\frac{\partial u_i}{\partial x_l} + \frac{\partial u_l}{\partial x_i} - \frac{2}{3}\delta_{il}\frac{\partial u_j}{\partial x_j}\right) + \frac{\partial^2 p}{\partial x_k\partial x_i} = 0\end{aligned} \tag{2.51}$$

$$\begin{aligned}\frac{\partial}{\partial x_i}\mathscr{E}_{\mathcal{NS}}(u_k) = \rho\frac{\partial}{\partial t}\left(\frac{\partial u_k}{\partial x_i}\right) + \rho u_l\frac{\partial}{\partial x_l}\left(\frac{\partial u_k}{\partial x_i}\right) + \frac{\partial\rho}{\partial x_i}\frac{\partial u_k}{\partial t} + \frac{\partial\rho u_l}{\partial x_i}\frac{\partial u_k}{\partial x_l}\\ -\frac{\partial^2}{\partial x_i\partial x_l}\mu\left(\frac{\partial u_k}{\partial x_l} + \frac{\partial u_l}{\partial x_k} - \frac{2}{3}\delta_{kl}\frac{\partial u_j}{\partial x_j}\right) + \frac{\partial^2 p}{\partial x_k\partial x_i} = 0\end{aligned} \tag{2.52}$$

$$\begin{aligned}-\frac{2}{3}\delta_{ik}\frac{\partial}{\partial x_n}\mathscr{E}_{\mathcal{NS}}(u_n) = -\frac{2}{3}\delta_{ik}\left\{\rho u_l\frac{\partial}{\partial x_l}\left(\frac{\partial u_n}{\partial x_n}\right) + \rho\frac{\partial}{\partial t}\left(\frac{\partial u_n}{\partial x_n}\right) + \frac{\partial\rho u_l}{\partial x_n}\frac{\partial u_n}{\partial x_l}\right.\\ \left.-\frac{\partial^2}{\partial x_n\partial x_l}\mu\left(\frac{\partial u_n}{\partial x_l} + \frac{\partial u_l}{\partial x_n} - \frac{2}{3}\delta_{nl}\frac{\partial u_j}{\partial x_j}\right) + \frac{\partial^2 p}{\partial x_n\partial x_n} + \frac{\partial\rho}{\partial x_n}\frac{\partial u_n}{\partial t}\right\}\end{aligned} \tag{2.53}$$

Equation (2.50) can take the form:

$$\nu\rho\left(\frac{\partial}{\partial t}\left(\frac{\partial u_i}{\partial x_k}+\frac{\partial u_k}{\partial x_i}-\frac{2}{3}\delta_{ik}\frac{\partial u_n}{\partial x_n}\right)+u_l\frac{\partial}{\partial x_l}\left(\frac{\partial u_i}{\partial x_k}+\frac{\partial u_k}{\partial x_i}-\frac{2}{3}\delta_{ik}\frac{\partial u_n}{\partial x_n}\right)\right)=$$
$$+\nu\frac{\partial^2}{\partial x_k\partial x_l}\mu\left(\frac{\partial u_i}{\partial x_l}+\frac{\partial u_l}{\partial x_i}-\frac{2}{3}\delta_{il}\frac{\partial u_j}{\partial x_j}\right)+\frac{2}{3}\delta_{ik}\nu\frac{\partial^2 p}{\partial x_n\partial x_n}-2\nu\frac{\partial^2 p}{\partial x_k\partial x_i}-$$
$$\frac{2}{3}\delta_{ik}\nu\frac{\partial^2}{\partial x_n\partial x_l}\mu\left(\frac{\partial u_n}{\partial x_l}+\frac{\partial u_l}{\partial x_n}-\frac{2}{3}\delta_{nl}\frac{\partial u_j}{\partial x_j}\right)+\nu\frac{\partial^2}{\partial x_i\partial x_l}\mu\left(\frac{\partial u_k}{\partial x_l}+\frac{\partial u_l}{\partial x_k}-\frac{2}{3}\delta_{kl}\frac{\partial u_j}{\partial x_j}\right)-$$
$$\nu\frac{\partial\rho}{\partial x_i}\frac{\partial u_k}{\partial t}-\nu\frac{\partial\rho u_l}{\partial x_i}\frac{\partial u_k}{\partial x_l}-\nu\frac{\partial\rho}{\partial x_k}\frac{\partial u_i}{\partial t}-\nu\frac{\partial\rho u_l}{\partial x_k}\frac{\partial u_i}{\partial x_k}+\frac{2}{3}\delta_{ik}\nu\frac{\partial\rho}{\partial x_n}\frac{\partial u_n}{\partial t}+\frac{2}{3}\delta_{ik}\nu\frac{\partial\rho u_l}{\partial x_n}\frac{\partial u_n}{\partial x_l} \tag{2.54}$$

Deriving from $x_k$ the equation for the speed fluctuation $u_i''$, we get:

$$\rho\frac{\partial}{\partial t}\left(\frac{\partial u_i''}{\partial x_k}\right)+\rho u_l\frac{\partial}{\partial x_l}\left(\frac{\partial u_i''}{\partial x_k}\right)=-\frac{\partial\rho'}{\partial x_k}\frac{\partial\tilde{u}_i}{\partial t}-\rho'\frac{\partial^2\tilde{u}_i}{\partial t\partial x_k}-\frac{\partial\rho}{\partial x_k}\frac{\partial u_i''}{\partial t}-\frac{\partial\rho'\tilde{u}_l}{\partial x_k}\frac{\partial\tilde{u}_i}{\partial x_l}$$
$$-\rho'\tilde{u}_l\frac{\partial^2\tilde{u}_i}{\partial x_l\partial x_k}-\frac{\partial\rho u_l}{\partial x_k}\frac{\partial u_i''}{\partial x_l}-\frac{\partial\rho u_l''}{\partial x_k}\frac{\partial\tilde{u}_i}{\partial x_l}-\rho u_l''\frac{\partial^2\tilde{u}_i}{\partial x_l\partial x_k}-\frac{\partial^2 p'}{\partial x_i\partial x_k}+\frac{\partial^2}{\partial x_l\partial x_k}\overline{\rho u_i''u_l''}+$$
$$\frac{\partial^2}{\partial x_l\partial x_k}\mu\left(\frac{\partial u_i''}{\partial x_l}+\frac{\partial u_l''}{\partial x_i}-\frac{2}{3}\delta_{il}\frac{\partial u_j''}{\partial x_j}\right)-\frac{\partial^2}{\partial x_l\partial x_k}\overline{\mu\left(\frac{\partial u_i''}{\partial x_l}+\frac{\partial u_l''}{\partial x_i}-\frac{2}{3}\delta_{il}\frac{\partial u_j''}{\partial x_j}\right)} \tag{2.55}$$

By multiplying the equations (2.54) and (2.55) respectively by $\left(\frac{\partial u_i''}{\partial x_k}\right)$ and $\left(\nu\sigma_{ik}^*\right)$, where:

$$\sigma_{ik}^*=\frac{\partial u_i}{\partial x_k}+\frac{\partial u_k}{\partial x_i}-\frac{2}{3}\delta_{ik}\frac{\partial u_n}{\partial x_n} \tag{2.56}$$

The sum of two resulting equations gives a transport equation $\left(\frac{\partial u_i''}{\partial x_k}\mu\sigma_{ik}^*\right)$:

$$\nu\rho\left(\frac{\partial u_i''}{\partial x_k}\frac{\partial\sigma_{ik}^*}{\partial t}+\frac{\partial u_i''}{\partial x_k}u_l\frac{\partial\sigma_{ik}^*}{\partial x_l}+\sigma_{ik}^*\frac{\partial}{\partial t}\left(\frac{\partial u_i''}{\partial x_k}\right)+\sigma_{ik}^*u_l\frac{\partial}{\partial x_l}\left(\frac{\partial u_i''}{\partial x_k}\right)\right)=$$
$$+\frac{2}{3}\delta_{ik}\nu\frac{\partial u_i''}{\partial x_k}\frac{\partial^2 p}{\partial x_n\partial x_n}-2\nu\frac{\partial u_i''}{\partial x_k}\frac{\partial^2 p}{\partial x_k\partial x_i}+\nu\frac{\partial u_i''}{\partial x_k}\frac{\partial^2}{\partial x_k\partial x_l}\mu\left(\frac{\partial u_i}{\partial x_l}+\frac{\partial u_l}{\partial x_i}-\frac{2}{3}\delta_{il}\frac{\partial u_j}{\partial x_j}\right)-$$
$$\nu\frac{\partial u_i''}{\partial x_k}\frac{\partial\rho}{\partial x_i}\frac{\partial u_k}{\partial t}-\nu\frac{\partial u_i''}{\partial x_k}\frac{\partial\rho u_l}{\partial x_i}\frac{\partial u_k}{\partial x_l}-\nu\frac{\partial u_i''}{\partial x_k}\frac{\partial\rho}{\partial x_k}\frac{\partial u_i}{\partial t}-\nu\frac{\partial u_i''}{\partial x_k}\frac{\partial\rho u_l}{\partial x_k}\frac{\partial u_i}{\partial x_l}$$
$$+\frac{2}{3}\delta_{ik}\nu\frac{\partial u_i''}{\partial x_k}\frac{\partial\rho}{\partial x_n}\frac{\partial u_n}{\partial t}+\frac{2}{3}\delta_{ik}\nu\frac{\partial u_i''}{\partial x_k}\frac{\partial\rho u_l}{\partial x_n}\frac{\partial u_n}{\partial x_l}$$
$$-\nu\sigma_{ik}^*\rho'\tilde{u}_l\frac{\partial^2\tilde{u}_i}{\partial x_l\partial x_k}-\nu\sigma_{ik}^*\frac{\partial\rho'\tilde{u}_l}{\partial x_k}\frac{\partial\tilde{u}_i}{\partial x_l}-\nu\sigma_{ik}^*\frac{\partial\rho}{\partial x_k}\frac{\partial u_i''}{\partial t}-\nu\sigma_{ik}^*\rho'\frac{\partial^2\tilde{u}_i}{\partial t\partial x_k}$$
$$-\nu\sigma_{ik}^*\frac{\partial\rho'}{\partial x_k}\frac{\partial\tilde{u}_i}{\partial t}-\nu\sigma_{ik}^*\frac{\partial\rho u_l''}{\partial x_k}\frac{\partial\tilde{u}_i}{\partial x_l}-\nu\sigma_{ik}^*\frac{\partial^2 p'}{\partial x_i\partial x_k}-\nu\sigma_{ik}^*\frac{\partial\rho u_l}{\partial x_k}\frac{\partial u_i''}{\partial x_l}-\nu\sigma_{ik}^*\rho u_l''\frac{\partial^2\tilde{u}_i}{\partial x_l\partial x_k}+$$
$$\nu\sigma_{ik}^*\frac{\partial^2}{\partial x_l\partial x_k}\overline{\rho u_i''u_l''}+\nu\sigma_{ik}^*\frac{\partial^2}{\partial x_l\partial x_k}\mu\left(\frac{\partial u_i''}{\partial x_l}+\frac{\partial u_l''}{\partial x_i}-\frac{2}{3}\delta_{il}\frac{\partial u_j''}{\partial x_j}\right)$$
$$-\nu\sigma_{ik}^*\frac{\partial^2}{\partial x_l\partial x_k}\overline{\mu\left(\frac{\partial u_i''}{\partial x_l}+\frac{\partial u_l''}{\partial x_i}-\frac{2}{3}\delta_{il}\frac{\partial u_j''}{\partial x_j}\right)} \tag{2.57}$$

The first line of equation (2.57), taking into account the equation of

continuity, after the passage to the temporal mean, we obtain:

$$\frac{\partial}{\partial t}\overline{\left(\nu\rho\sigma^*_{ik}\frac{\partial u''_i}{\partial x_k}\right)}+\frac{\partial}{\partial x_l}\overline{\left(\nu\rho u_l\sigma^*_{ik}\frac{\partial u''_i}{\partial x_k}\right)}=\frac{\partial}{\partial t}\bar{\rho}\varepsilon+\frac{\partial}{\partial x_l}\tilde{u}_l\bar{\rho}\varepsilon+\frac{\partial}{\partial x_l}\overline{\left(u''_l\nu\rho\sigma^*_{ik}\frac{\partial u''_i}{\partial x_k}\right)}$$

## 2.8 closing models of the Navier Stokes equations

### 2.8.1 Models with turbulent viscosity

To avoid solving transport equations of components tensor of turbulent stresses, a hypothesis can be established to model the term $-\rho\widetilde{u''_i u''_j}$. The hypothesis of closure is that of the Boussinesq [**14**], and similarly for the closure of the energy equation:

$$-\rho\widetilde{u''_i u''_j}=2\mu_t\left(\tilde{S}_{ij}-\frac{1}{3}\tilde{u}_{k,k}\delta_{ij}\right)-\frac{2}{3}\rho k\delta_{ij} \tag{2.58}$$

the term $-\frac{2}{3}\mu_t\tilde{u}_{k,k}\delta_{ij}$ presents the volume expansion used in the case of compressible flows.

#### 2.8.1.1 Zero equation models

The zero equation models used to model the `Reynolds` constraints in motion quantity equations use an algebraic turbulent viscosity or mixing length. It was `Ludwig Prandtl` who proposed a relationship linking turbulent viscosity to the gradient of average velocity by introducing a length lm called mixing length $l_m$, for flows of the boundary layer type:

$$\mu_t=\rho l_m^2\left|\frac{\partial u}{\partial y}\right| \tag{2.59}$$

This relationship reflects the state of equilibrium between the medium field and the fluctuating field. To determine $l_m$, `Von Karman` [**15**], `Klebanoff` [**16**] and `Michel` and al [**17**] al proposed different models depending on wall distance, boundary layer thickness and mean velocity gradient. To take into account the effect of the wall,`Van Driest` [**18**] proposed a damping function F in relation $\mu_t$.

$$\begin{aligned}&\mu_t=\rho F^2 l_m^2\left|\tfrac{\partial u}{\partial y}\right|\\&F=1-\exp(-\tfrac{y^+}{26})\\&y^+=\tfrac{u_\tau y}{\nu_p}\ ,\ u_\tau=\sqrt{\tau_p/\rho}\ ,\ \tau_p=\left(\mu\tfrac{\partial u}{\partial y}\right)_p\end{aligned} \tag{2.60}$$

Other models have been developed by `Cebeci-Smith` [**19**], `Alber`[**20**] and the known `Baldwin-Lomax`[**21**] model . The advantage of this type of model is its simplicity of implementation, but the disadvantages are diverse, a lot of empiricism, absence of the history of turbulence .

#### 2.8.1.2 Single Equation Models

Among the different models in this group, we consider only the Spalart and Allmaras (SA) model, which, unlike the Cebeci-Smith model which uses algebraic expressions for turbulent viscosity ($\nu_t$), the model (SA) uses a transport equation.
The `Spalart-Allmaras` [**21**] [**22**] [**23**]model is a viscosity model relatively recent turbulent based on a transport equation for turbulent viscosity. This model was inspired by an old model developed by Baldwin and Barth[**24**]. Its formulation and coefficients have been defined using dimensional analysis, and empirical results selected. The empirical results used in its development were for two-dimensional (2-D) type, mixing layers, wake, and boundary layer flow on a flat plate.
The aim of this model is to improve the predictions obtained with the algebraic models of mixing length to develop a model local for complex flows, and provide an alternative more simple to two-equation turbulence models.
The model uses the distance closest to the wall in its formulation, and provides a smooth transition from laminar to turbulent, provided that the transition start position is given. It does not require a very fine mesh in the case of flows with walls as in two-equation turbulence models, and it shows good convergence in simple flows.
The model does not give good predictions in jet flow, but gives enough good predictions in the 2-D flow of mixing layers, wake, and flat plate boundary layers and shows improved flow forecasting with adverse pressure gradients relative to models $k-\varepsilon$ and $k-\omega$ , but not as much as the SST model.

**`model equation`** :

The function of turbulent viscosity is defined as a function of a variable viscosity, $\tilde{\nu}$, and a wall function, , $f_{\nu_1}$, as follows:

$$\nu_t = \tilde{\nu} f_{\nu_1} \tag{2.61}$$

In remote wall areas, function , $f_{\nu_1}$, is equal to one and et $\nu_t = \tilde{\nu}$. The convective transport equation of turbulent viscosity is given by:

$$\begin{aligned}\frac{\partial \rho\tilde{\nu}}{\partial t} + \frac{\partial}{\partial x_j}\left(\rho\tilde{\nu}u_j\right) = c_{b_1}\left(1-f_{t_2}\right)\rho\tilde{S}\tilde{\nu} + \frac{1}{\sigma}\left(\frac{\partial}{\partial x_j}\left(\rho\left(\nu+\tilde{\nu}\right)\frac{\partial\tilde{\nu}}{\partial x_j}\right) + c_{b_2}\rho\frac{\partial\tilde{\nu}}{\partial x_j}\frac{\partial\tilde{\nu}}{\partial x_j}\right) \\ -\left(c_{w_1}f_w - \frac{c_{b_1}}{\kappa^2}f_{t_2}\right)\rho\left(\frac{\tilde{\nu}}{d}\right)^2 + f_{t_1}\rho\Delta U^2\end{aligned} \tag{2.62}$$

Where the right-hand terms represent, turbulent viscosity production, preservation of diffusion, non-conservative diffusion, dissipation turbulence near the wall, transition damping, and source of turbulence transition. The index b means "basic", w for "wall", $\nu$ means "viscous", and t means "trip".
Model constants and auxiliary functions are defined in terms of basic model for free sheared flows, the wall for boundary layers, the viscous model of integration with the wall, and transition model for laminar-turbulent transition.

Basic model constants for free sheared flows to control the production and diffusion of turbulent viscosity are:

$$c_{b_1} = 0.1355 \qquad c_{b_2} = 0.622 \qquad \sigma = 2/3$$

Additional model constants and auxiliary functions for the destruction of turbulent viscosity in the zone of the layer limits are:

$$\begin{aligned} c_{w_1} &= \frac{c_{b_1}}{\kappa^2} + \frac{(1+c_{b_2})}{\sigma} & r &= \frac{\tilde{\nu}}{\tilde{S}\kappa^2 d^2} \\ c_{w_2} &= 0.3 & g &= r + c_{w_2}\left(r^6 - r\right) \\ c_{w_3} &= 2 & f_w &= g\left(\frac{1+c_{w_3}^6}{g^6+c_{w_3}^6}\right)^{1/6} \end{aligned}$$

These auxiliary functions allow the model to predict the layer logarithmic, although the particular balance of the shear stress Reynolds is not in quantitative agreement with the experimental data. Modeling functions and constants for regions close to the wall are given by :

$$\begin{aligned} \tilde{S} &= S + \frac{\tilde{\nu}}{(\kappa d)^2} f_{v2} & S &= \sqrt{2S_{ij}S_{ij}} & \chi &= \frac{\tilde{\nu}}{\nu} \\ f_{v_1} &= \frac{\chi^3}{\chi^3 + c_{v_1}^3} & f_{v_2} &= 1 - \frac{\chi}{1+\chi f_{v_1}} & c_{v_1} &= 7.1 \end{aligned}$$

Auxiliary functions and constants of the model to control the laminar region of the shear layers and the transition to the turbulence are defined with a source term controlled with the $f_{t_1}$ and a reduction in production controlled by the function $f_{t_2}$

$$\begin{aligned} f_{t_1} &= c_{t_1} g_t e^{\left(-c_{t_2}\frac{w_t^2}{\Delta U^2}\left(d^2 + (g_t d_t)^2\right)\right)} \\ f_{t_2} &= c_{t_3} e^{\left(-c_{t_4}\chi^2\right)} \\ g_t &= \min\left(0.1,\ \frac{\Delta U}{w_t \Delta x_t}\right) \\ c_{t_1} &= 1 \quad c_{t_2} = 2 \quad c_{t_3} = 1.2 \quad c_{t_4} = 0.5 \end{aligned}$$

where $w_t$is the vorticity at the point of disjunction of the boundary layer, $\Delta U$ is the standard of the difference between the velocity at the flow point and speed at trigger point,$\Delta x_t$ is the spacing of the mesh along the wall at the trip point, and $d_t$is the distance from the wall.
Despite the existence of too many empiricism, many constants and damping functions, the `Spalart-Allmaras` model is considered as a compromise between algebraic approaches and two-equation models.

**`Boundary conditions`**:

The ideal value for turbulent viscosity in free flow regions is zero. Some solvers have problems with zero $\tilde{\nu}$ values in free flow, and lower $\frac{\tilde{\nu}}{2}$ values have been recommended. Small values are recommended for free sheared flows, otherwise solutions show dependence on regions outside the boundary layer in velocity profiles and decay rates. On the walls the turbulent viscosity is zero.

### 2.8.2 Models with two equations

AAlthough the models of an equation have found little success, except for the SA model, and where the transport of turbulence characteristics is important as in the case of flows of strong adverse gradients or separate flows, Two-equation models have found wide use. Different two-equation models were proposed and more details were given, for example in **[22]**,**[25]**. Three famous models based on this approach are the $k-\varepsilon$ model, the Wilcox $k-w$ model, and the Menter SST model **[22]**,**[25]**, which groups the two models, $k-\varepsilon$ in the outer region and $k-w$ in the wall region.

**2.8.2.0.1** $k-\omega$ **model (Wilcox)** :

$k-\omega$ (**[22]** and **[26]**) is a well-known and widely-tested turbulence viscosity model of two equations. The main reference for this model is given by Wilcox , and its formulation is used here. The roots of this model can be attributed to Kolmogorov, Prandtl,Saffman, and Wilcox, in collaboration with other scientists.
This model was developed at the same time and in parallel with the $k-\varepsilon$ model as an alternative to define a turbulent viscosity function. Convective transport equations are solved for turbulent kinetic energy and its specific rate of dissipation, $k$ and $\omega = \varepsilon/\beta^* k$ respectively.
Obtaining a transport equation for the frequency $w$ is just as delicate as for pseudo-dissipation and therefore an analogous strategy is implemented by considering a prototype equation form inspired by the equation $k$. The $k-\omega$ model by Wilcox's proved to be superior numerical stability model $k-\varepsilon$ mainly in the viscous underlayment near the wall.This model does not require any damping functions as in the two-equation model $k-\varepsilon$ and others due to the large values of $w$ in the wall region. Wall boundary conditions require specification of the distance between the wall and the first point of the mesh. In the logarithmic region, the model gives good agreement with the experimental results for flows with a moderate gradient of adverse pressure.
In the free shear layer and the adverse pressure gradient boundary layer flows, the results of the $k-\omega$ model are sensitive to low values of $w$ outside the boundary layer (references **[26]** and **[27]**). In calculating complex flows, it is difficult to exercise enough control over the turbulence of the external region to avoid small values of w in the free flow and still avoid ambiguities in the results.

**`Models equation`**:

Reynolds stress are modeled in terms of turbulent viscosity as follows:

$$\tau_{t_{ij}} = 2\mu_t \left(S_{ij} - S_{nn}\delta_{ij}/3\right) - 2\rho k \delta_{ij}/3 \tag{2.63}$$

where $\mu_t$ is turbulent viscosity,$S_{ij}$ is the deformation tensor of the average velocity. $\rho$ is fluid density ,$k$ is turbulent kinetic energy ,$\delta_{ij}$is kronecker symbol.Turbulent viscosity is defined as a function of turbulent kinetic

energy, and specific dissipation rate, $\varepsilon$ :

$$\mu_t = c_\mu f_\mu \rho \frac{k^2}{\varepsilon} \tag{2.64}$$

The two transport equations for $k$ and $\omega$ are defined below by:

$$\frac{\partial \rho k}{\partial t} + \frac{\partial}{\partial x_j}\left(\rho u_j k - (\mu + \sigma^* \mu_t)\frac{\partial k}{\partial x_j}\right) = \tau_{t_{ij}} S_{ij} - \beta^* \rho \omega k \tag{2.65}$$

and

$$\frac{\partial \rho \omega}{\partial t} + \frac{\partial}{\partial x_j}\left(\rho u_j \omega - (\mu + \sigma \mu_t)\frac{\partial \omega}{\partial x_j}\right) = \alpha \frac{\omega}{k} \tau_{t_{ij}} S_{ij} - \beta \rho \omega^2 \tag{2.66}$$

with

$$\begin{array}{lll} \alpha = \frac{5}{9} & \beta = \frac{3}{40} & \beta^* = \frac{9}{100} \\ \sigma = 0.5 & \sigma^* = 0.5 & \end{array}$$

**Boundary conditions**

The selection of recommended external values for boundary layer flows is:

$$\omega_\infty > \lambda \frac{U_\infty}{L} \qquad \mu_{t\infty} < 10^{-2} \mu_{tmax} \quad k_\infty = \frac{\mu_{t\infty}}{\rho_\infty} \omega_\infty$$

Where $L$ is the approximate length of the computation range, and $U_\infty$ is the characteristic speed. A proportionality factor $\lambda = 10$ was recommended. Free shear layers are more sensitive to low $\omega_\infty$ free flow values and higher de $\omega$ values are needed. Following a self-similarity analysis, a value of $\lambda$ can be determined from which a value of at least $\lambda = 10$ for mixing layers, increased to $\lambda = 80$ for round jets. Wall boundary conditions are given by the following relationships.

$$k = 0 \qquad et \qquad \omega = 10 \frac{6\mu}{\beta \rho \left(y_1\right)^2}$$

Where $y_1$ is the distance from the first point to the wall and $y^+ < 1$, zero gradient conditions are applied to the symmetry limits.

#### 2.8.2.0.2 The $k - \omega$ BSL (Menter model) :

The $k - \omega$ models generally do not require additional damping functions and therefore appear to exhibit a more universal behaviour in the near-wall region than the k e "low-Reynolds" models.Taking into account this remark and the fact that the k w models are, contrary to the $k - \varepsilon$ models, sensitive to the definition of the conditions of the distant flow, Menter proposes to define a mixed model with two equations, Having the characteristics of a closure The $k - \omega$ near the walls and those of a model $k - \varepsilon$ in remote areas.
To develop this combination, Menter first considers the Wilcox $k - \omega$

formulation, the transport equations of $k$ and $w$ are given respectively by:

$$\frac{\partial \rho k}{\partial t} + \frac{\partial}{\partial x_j}\left(\rho u_j k - (\mu + \sigma_{k_1}\mu_t)\frac{\partial k}{\partial x_j}\right) = \tau_{t_{ij}} S_{ij} - \beta^* \rho \omega k \tag{2.67}$$

$$\frac{\partial \rho \omega}{\partial t} + \frac{\partial}{\partial x_j}\left(\rho u_j \omega - (\mu + \sigma_{\omega_1}\mu_t)\frac{\partial \omega}{\partial x_j}\right) = \rho\frac{\gamma_1}{\mu_t}\tau_{t_{ij}} S_{ij} - \beta \rho \omega^2 \tag{2.68}$$

Considering that $f_2 = 1$ to exclude aspects of base Reynolds, the equation of pseudo-dissipation :

$$\frac{\partial \rho \varepsilon}{\partial t} + \frac{\partial}{\partial x_j}\left(\rho u_j \varepsilon - \left(\mu + \frac{\mu_t}{\sigma_\varepsilon}\right)\frac{\partial \varepsilon}{\partial x_j}\right) = c_{\varepsilon 1}\frac{\varepsilon}{k}\tau_{t_{ij}} S_{ij} - c_{\varepsilon 2} f_2 \rho \varepsilon \frac{\varepsilon}{k} + \phi_\varepsilon \tag{2.69}$$

is modified to take into account the relation between $\varepsilon$ and $\omega$ given by:

$$\omega = \frac{\varepsilon}{c_\mu k} \tag{2.70}$$

We obtain the following transport equations:

$$\frac{\partial \rho k}{\partial t} + \frac{\partial}{\partial x_j}\left(\rho u_j k - (\mu + \sigma_{k2}\mu_t)\frac{\partial k}{\partial x_j}\right) = \tau_{t_{ij}} S_{ij} - \beta^* \rho \omega k \tag{2.71}$$

$$\begin{aligned}\frac{\partial \rho \omega}{\partial t} + \frac{\partial}{\partial x_j}\left(\rho u_j \omega - (\mu + \sigma_{\omega_2}\mu_t)\frac{\partial \omega}{\partial x_j}\right) &= \rho\frac{\gamma_2}{\mu_t}\tau_{t_{ij}} S_{ij} - \beta \rho \omega^2 \\ &+2\rho\sigma_{\omega_2}\frac{1}{\omega}\frac{\partial k}{\partial x_j}\frac{\partial \omega}{\partial x_j}\end{aligned} \tag{2.72}$$

The transport equation for turbulent kinetic energy $k$ remains unchanged with changes in the coefficients. For the equation of $\omega$, a new term appeared following the passage of the equation of $\varepsilon$ to the equation of $\omega$, called the term of cross diffusion.
To take advantage of the two models $k-\varepsilon$ far from the boundary layer and $k-\omega$ near the wall, Menter has introduced an $F_1$ function that allows switching between the two models. Now equation, equation (2.67) and equation (2.68) are multiplied by $F_1$ and equation (2.71) and equation (2.72) are multiplied by $(1-F_1)$ and the corresponding equations of each set are summed to give the new model:

$$\frac{\partial \rho k}{\partial t} + \frac{\partial}{\partial x_j}\left(\rho u_j k - (\mu + \sigma_k \mu_t)\frac{\partial k}{\partial x_j}\right) = \tau_{t_{ij}} S_{ij} - \beta^* \rho \omega k \tag{2.73}$$

$$\begin{aligned}\frac{\partial \rho \omega}{\partial t} + \frac{\partial}{\partial x_j}\left(\rho u_j \omega - (\mu + \sigma_\omega \mu_t)\frac{\partial \omega}{\partial x_j}\right) &= \rho\frac{\gamma}{\mu_t}\tau_{t_{ij}} S_{ij} - \beta \rho \omega^2 \\ &+2\rho(1-F_1)\sigma_{\omega_2}\frac{1}{\omega}\frac{\partial k}{\partial x_j}\frac{\partial \omega}{\partial x_j}\end{aligned} \tag{2.74}$$

Turbulence viscosity is given by:

$$\mu_t = \frac{\rho k}{\omega} \tag{2.75}$$

The $F_1$ function allows you to select the `Wilcox` $k-\omega$ model in the viscous underlayer and logarithmic region and gradually switch to the $k-\varepsilon$ model as you move away from the wall. This allows us to benefit from the robustness of w in the near wall area and the insensitivity of e in the free flow. The function of Menter $F_1$ is written:

$$F_1 = tanh\left(arg_1^4\right) \tag{2.76}$$

With

$$arg_1 = min\left(max\left(\frac{\sqrt{k}}{0.09\omega y}, \frac{500\nu}{\omega y^2}\right), \frac{4\rho k\sigma_{\omega_2}}{CD_{k\omega}y^2}\right)$$

where $y$ is the normal distance to the wall and

$$CD_{k\omega} = max\left(2\rho\sigma_{\omega_2}\frac{1}{\omega}\frac{\partial k}{\partial x_j}\frac{\partial \omega}{\partial x_j}, 10^{-20}\right)$$

With
The term $\sqrt{k}\Big/0.09\omega y$ is a scale of turbulent length, enlarged by the distance to the wall, occurs mainly in the logarithmic zone, then decreases further away from the boundary layer.
The term $500\nu\Big/\omega y^2$ ensures the activation of the $k-\omega$ model in the viscous sub-layer, and tends to zero the further away from the wall.
The term $4\rho k\sigma_{\omega_2}\Big/CD_{k\omega}y^2$ is to prevent the degeneration of the solution for small values of w in the external flow.
Let $\phi_1$ represent the constants in the original model ($\sigma_{k1}$...), $\phi_2$ the constants in the transformed model $k-\varepsilon$ ($\sigma_{k2}$...) and $\phi_1$ the corresponding constants of the new model ($\sigma_k$...), then the relationship between them is:

$$\begin{aligned} &\phi = F_1\phi_1 + (1-F_1)\phi_2 \\ &\phi = \{\sigma_k, \sigma_\omega, \beta, \gamma\} \end{aligned} \tag{2.77}$$

The following two groups of constants will be used: Group 1 (Wilcox):

$$\begin{aligned} &\sigma_{k_1} = 0.5, \quad \sigma_{\omega_1} = 0.5, \quad \beta_1 = 0.075 \\ &\beta^* = 0.09, \quad \kappa = 0.41, \quad \gamma_1 = \beta_1/\beta^* - \sigma_{\omega_1}\kappa^2\Big/\sqrt{\beta^*} \end{aligned}$$

Group 2 (Jones-Launder):

$$\begin{aligned} &\sigma_{k_2} = 1.0, \quad \sigma_{\omega_2} = 0.856, \quad \beta_2 = 0.0828 \\ &\beta^* = 0.09, \quad \kappa = 0.41, \quad \gamma_2 = \beta_2/\beta^* - \sigma_{\omega_2}\kappa^2\Big/\sqrt{\beta^*} \end{aligned}$$

#### 2.8.2.1 Second order closure model (SSG/LRR-RSM-w2012)

This model was developed within the framework of the European project FLOMANIA for application to aeronautical flow problems. It uses a

mixture of two different pressure-strain models (the LRR part is based on an earlier version of the WilcoxRSM-W2006 [**28**]. The main references of this model are those of Cecora and al [**29**], Eisfeld [**30**], Eisfeld and al [**31**], Eisfeld [**32**] .
Unlike turbulent viscosity models, the Reynolds Stress Model (RSM) considers Reynolds tensor terms as unknowns. The purpose of this model is to remove the hypothesis introduced by the gradient transport approximation. Experiments show that correlations still do not follow a change of sign with the gradients that connect them with a turbulence viscosity.
According to the motion quantity equation, a transport equation for the Reynolds stress can be derived:

$$\frac{\partial}{\partial t}\left(\bar{\rho}\tilde{R}_{ij}\right)+\frac{\partial}{\partial x_k}\left(\bar{\rho}\tilde{u}_k\tilde{R}_{ij}\right)=\bar{\rho}P_{ij}+\bar{\rho}\Pi_{ij}-\bar{\rho}\varepsilon_{ij}+\bar{\rho}D_{ij}+\bar{\rho}M_{ij} \quad (2.78)$$

with

$$\bar{\rho}\tilde{R}_{ij}=-\tau_{ij}=\overline{\rho u_i'' u_j''}$$

In this equation the term production $P_{ij}$ is correct, while the other terms on the right side need modeling.

$$\bar{\rho}P_{ij}=\bar{\rho}\tilde{R}_{ik}\frac{\partial\tilde{u}_j}{\partial x_k}-\bar{\rho}\tilde{R}_{jk}\frac{\partial\tilde{u}_i}{\partial x_k} \quad (2.79)$$

In the European project FLOMANIA [**33**] the SSG/LRR-w model [**30**],[**31**] was developed, transferring Menter's SST model ideas [**34**] into the framework of differential Reynolds stress models. In particular, the term redistribution has been harmonized between the Launder-Reece-Rodi model (LRR) [**35**] near the walls, omitting the terms of so-called wall reflection as suggested by Wilcox [**36**] and the Speziale-Sarkar-Gatski model (SSG) [**37**] to the far field.
The resulting redistribution term can be written in the following unified notation:

$$\begin{aligned}\bar{\rho}\Pi_{ij}=&-\left(C_1\bar{\rho}\varepsilon+\frac{1}{2}C_1^*\bar{\rho}P_{kk}\right)\tilde{b}_{ij}+C_2\bar{\rho}\varepsilon\left(\tilde{b}_{ik}\tilde{b}_{kj}-\frac{1}{3}\tilde{b}_{mn}\tilde{b}_{mn}\delta_{ij}\right)\\&+\left(C_3-C_3^*\sqrt{II}\right)\bar{\rho}\tilde{k}\tilde{S}_{ij}^*+C_4\bar{\rho}\tilde{k}\left(\tilde{b}_{ik}\tilde{S}_{jk}^*+\tilde{b}_{jk}\tilde{S}_{ik}^*-\frac{2}{3}\tilde{b}_{mn}\tilde{S}_{mn}^*\delta_{ij}\right)\\&+C_5\bar{\rho}\tilde{k}\left(\tilde{b}_{ik}\widetilde{W}_{jk}+\tilde{b}_{jk}\widetilde{W}_{ik}\right)\end{aligned} \quad (2.80)$$

Which is formally identical to the SSG model and where $\tilde{b}_{ij}=\tilde{R}_{ij}/(2\tilde{k})-\delta_{ij}/3$ is the anisotropy tensor with its second invariant $II=\tilde{b}_{ij}\tilde{b}_{ij}$.
Note that the specific turbulence kinetic energy is equivalent to half of the specific Reynolds stress trace, that is $\tilde{k}=\tilde{R}_{ii}/2$ in addition, $\widetilde{W}_{ij}=1/2\left(\partial\tilde{u}_i/\partial x_j-\partial\tilde{u}_j/\partial x_i\right)$is the mean rotation tensor.
with:

$$\tilde{S}_{ij}^*=\frac{1}{2}\left(\frac{\partial\tilde{u}_i}{\partial x_j}+\frac{\partial\tilde{u}_j}{\partial x_i}\right)-\frac{1}{3}\frac{\partial\tilde{u}_k}{\partial x_k}\delta_{ij}$$

finally,$\varepsilon=C_\mu\tilde{k}\omega$, where $C_\mu=0.09$,and $\omega$ is provided by the BSL Menter [**34**] equation given below. The dissipation term is modelled by an

isotropic tensor according to Rotta [38].

$$\bar{\rho}\varepsilon_{ij} = \frac{2}{3}C_{\mu}\bar{\rho}\tilde{k}\omega\delta_{ij} \tag{2.81}$$

A single gradient or generalized gradient diffusion models can be used alternatively.According to [39] , we can write:

$$\bar{\rho}D_{ij} = \frac{\partial}{\partial x_k}\left[\left(\bar{\mu}\delta_{kl} + \hat{D}\frac{\bar{\rho}}{\omega}\tilde{R}_{kl}\right)\frac{\partial\tilde{R}_{ij}}{\partial x_l}\right] \tag{2.82}$$

The contribution due to mass fluctuations , $\bar{\rho}M_{ij}$, is neglected, as it is a common practice for transsonic flows.The turbulence model is closed by the equation of $w$ of the model BSL de Menter [34] .

$$\frac{\partial(\bar{\rho}\omega)}{\partial t} + \frac{\partial}{\partial x_k}(\bar{\rho}\tilde{u}_k\omega) = \alpha\frac{\omega}{\tilde{k}}\frac{\bar{\rho}P_{kk}}{2} - \beta\bar{\rho}\omega^2 + \frac{\partial}{\partial x_k}\left(\left(\bar{\mu} + \sigma\frac{\bar{\rho}\tilde{k}}{\omega}\right)\frac{\partial\omega}{\partial x_k}\right) + \sigma_d\frac{\bar{\rho}}{\omega}max\left(\frac{\partial k}{\partial x_j}\frac{\partial\omega}{\partial x_j};0\right) \tag{2.83}$$

The relation giving the assembly between the SSG and LRR regions is obtained by:

$$\phi = F_1\phi^{(LRR)} + (1 - F_1)\,\phi^{(SSG)} \tag{2.84}$$

where the Menter function is given by

$$F_1 = tanh\left(\zeta^4\right) \tag{2.85}$$

with

$$\zeta = min\left[max\left(\frac{\sqrt{\tilde{k}}}{C_{\mu}\omega d};\frac{500\bar{\mu}}{\bar{\rho}\omega d^2}\right);\frac{4\sigma^{(SSG)}\bar{\rho}\tilde{k}}{max\left\{2\sigma^{(SSG)}\frac{\bar{\rho}}{\omega}\frac{\partial\tilde{k}}{\partial x_k}\frac{\partial\omega}{\partial x_k};10^{-20}\right\}}\right] \tag{2.86}$$

The values for the overall limit of the closure coefficients for SSG and LRR are given in Table :

Table 2.1: SSG/LRR-$\omega$ model constants

| | $C_1$ | $C_1$* | $C_2$ | $C_3$ | $C_3$* | $C_4$ |
|---|---|---|---|---|---|---|
| SSG | 3.4 | 1.8 | 4.2 | 0.8 | 1.3 | 1.25 |
| LRR | 3.6 | 0.0 | 0.0 | 0.8 | 0.0 | 2.0 |
| | $C_5$ | $\hat{D}$ | $\alpha$ | $\beta$ | $\sigma$ | $\sigma_d$ |
| SSG | 0.4 | 2.44 | 0.44 | 0.0828 | 0.856 | 1.712 |
| LRR | 0.11 | 0.5 | 0.5556 | 0.075 | 0.5 | 0.0 |

**boundary conditions**:

$$\tilde{R}_{ij,farfield} = \frac{2}{3}\tilde{k}_{farfield}\delta_{ij} \qquad \omega_{farfield} = \frac{\bar{\rho}\tilde{k}_{farfield}}{\mu_{t,farfield}}$$

The initial value is a function of the intensity of the far field turbulence $Tu$, with:

$$\tilde{k}_{farfield} = (3/2)(Tu)^2 U^2_{farfield}$$

Typical values are:

$$Tu = 0.001(= 0.1\%) \qquad \mu_{t,farfield} \big/ \bar{\mu}_{farfield} = 0.1$$

for solid surfaces (walls):

$$\tilde{R}_{ij,paroi} = 0 \qquad \omega_{paroi} = 10\frac{6\bar{\nu}}{\beta^{(LRR)}\left(\Delta d_1\right)^2}$$

where $(\Delta d_1)^2$ is the distance between the wall and the nearest point.

#### 2.8.2.2 RSM omega

The system of equations governed the turbulent compressible gas may be written as:

$$\frac{\partial \bar{\rho}}{\partial \mathrm{t}} + \frac{\partial}{\partial x_j}\left(\bar{\rho}\widetilde{U_j}\right) = 0 \tag{2.87}$$

$$\frac{\partial \bar{\rho}\widetilde{U_j}}{\partial t} + \frac{\partial}{\partial x_j}\left(\bar{\rho}\widetilde{U_i}\widetilde{U_j} + \bar{\rho}\widetilde{u_i'' u_j''}\right) = \frac{\partial \overline{\sigma_{ij}}}{\partial x_j} - \frac{\partial \bar{p}}{\partial x_i} \tag{2.88}$$

$$\begin{aligned}\frac{\partial \bar{\rho}\widetilde{E_t}}{\partial \mathrm{t}} + \frac{\partial \widetilde{U_j}\left(\bar{\rho}\widetilde{E_t}+\bar{P}\right)}{\partial x_j} = \frac{\partial}{\partial x_j}\Big(\overline{\sigma_{lj}U_l} - \bar{\rho}\overline{u_l'' u_l''}\widetilde{U_l} - \\ \frac{1}{2}\bar{\rho}\widetilde{u_l'' u_j''}\Big) - \frac{\partial}{\partial x_j}\left(\bar{\rho}\gamma c_v \overline{T'' u_j''} - \overline{k_c \frac{\partial T}{\partial x_j}}\right)\end{aligned} \tag{2.89}$$

Where $\bar{\rho}, \tilde{U}_j, \bar{P}$ and $\tilde{E}_t$ are the density, velocity and the pressure and the total energy respectively.

$$\bar{\rho}R_{ij} = -\overline{\rho u_t'' u_j''} \tag{2.90}$$

$$\frac{\partial \bar{\rho}R_{ij}}{\partial t} + \frac{\partial\left(\bar{\rho}U_k R_{ij}\right)}{\partial x_k} = P_{ij} + \Pi_{ij} - \frac{2}{3}\beta^* f_\beta \cdot \bar{\rho}\omega k\delta_{ij} + \frac{\partial}{\partial x_k}\left[\left(\mu + \frac{\mu_t}{\sigma_k}\right)\frac{\partial R_{ij}}{\partial x_k}\right] \tag{2.91}$$

$$\frac{\partial \bar{\rho}\omega}{\partial t} + \frac{\partial(\bar{\rho}U_k\omega)}{\partial x_k} = \frac{\alpha\bar{\rho}\omega}{k}R_{ij}\frac{\partial U_i}{\partial x_j} - \bar{\rho}\beta f_\beta \omega^2 + \frac{\partial}{\partial x_k}\left[\left(\mu + \frac{\mu_t}{\sigma}\right)\frac{\partial \omega}{\partial x_k}\right] + \sigma_d \frac{\bar{\rho}}{\omega}\frac{\partial k}{\partial x_j}\frac{\partial \omega}{\partial x_j} \tag{2.92}$$

The pressure stain correlation is given by:

$$\Pi_{ij} = \beta^* f_\beta \cdot C_1 \bar{\rho}\omega\left(R_{ij} + \tfrac{2}{3}k\delta_{ij}\right) - \hat{\alpha}\left(P_{ij} - \tfrac{2}{3}P\delta_{ij}\right) - \hat{\beta}\left(D_{ij} - \tfrac{2}{3}P\delta_{ij}\right) - \hat{\gamma}\bar{\rho}k\left(S_{ij} - \tfrac{1}{3}S_{kk}\delta_{ij}\right) \tag{2.93}$$

The production tensor of Reynolds stresses is given by:

$$P_{ij} = -\overline{\rho u_i'' u_k''}\frac{\partial U_j}{\partial x_k} - \overline{\rho u_j'' u_k''}\frac{\partial U_i}{\partial x_k} \tag{2.94}$$

With $k = -R_{it}/2$, $\mu_t = \bar{\rho}k/\omega$ and $P = P_{kk}/2$ The tensor $D_{ij}$ differs in the dot-product indices from the production tensor

$$D_{ij} = -\overline{\rho u_i'' u_k''}\frac{\partial U_k}{\partial x_j} - \overline{\rho u_1'' u_k''}\frac{\partial U_k}{\partial x_i} \tag{2.95}$$

The closure coefficients of the modelare:

$\hat{\alpha} = (8 + C_2)/11, \hat{\beta} = (8C_2 - 2)/11, \hat{\gamma} = (60C_2 - 4)/55, C_1 = 9/5$
$, C_2 = 10/19, \alpha = 13/25, \beta = \beta_0 f_\beta, \beta^* = 9/100, \sigma_k = 2, \sigma = 5/3, \beta_0 = 0.0708$
$, \sigma_d = 0,$ for $\left(\frac{\partial k}{\partial x_j}\frac{\partial \omega}{\partial x_j} \le 0\right)$ and $\sigma_d = \frac{1}{8},$ for $\left(\frac{\partial k}{\partial x_j}\frac{\partial \omega}{\partial x_j} > 0\right),$
$f_\beta = (1 + 70X_\omega)/(1 + 80X_\omega), X_\omega = \left|W_{ij}W_{jk}S_{ki}/(\beta^*\omega)^3\right|, \hat{S}_{ki} = S_{ki} - \frac{1}{2}\frac{\partial \hat{u}_m}{\partial x_m}\delta_{ki}$
$, S_{ij} = \frac{1}{2}\left(\frac{\partial U_i}{\partial x_j} + \frac{\partial U_j}{\partial x_i}\right), W_{ij} = \frac{1}{2}\left(\frac{\partial u_i}{\partial x_j} - \frac{\partial u_j}{\partial x_i}\right), f_{\beta^*} = 1$ if $x_k \le 0$
$\& f_{\beta^*} = \left(1 + 640x_k{}^2\right)/\left(1 + 400x_k{}^2\right)$ if $x_k > 0$

In the standard $k$ - $\boldsymbol{\omega}$ model, you also have the option of including corrections to improve the accuracy in predicting free shear flows. The Shear Flow Corrections option under the k-omega Options is enabled by default in the Viscous Model dialog box, as these corrections are included in the standard $k - \omega$ model. When this option is enabled, ANSYS FLUENT will calculate $f_{\beta^*}$ using this equation (in the separate Theory Guide) and $f_\beta$ using this equation (in the separate Theory Guide). If this option is disabled, $f_{\beta^*}$ and $f_\beta$ will be set equal to 1 .

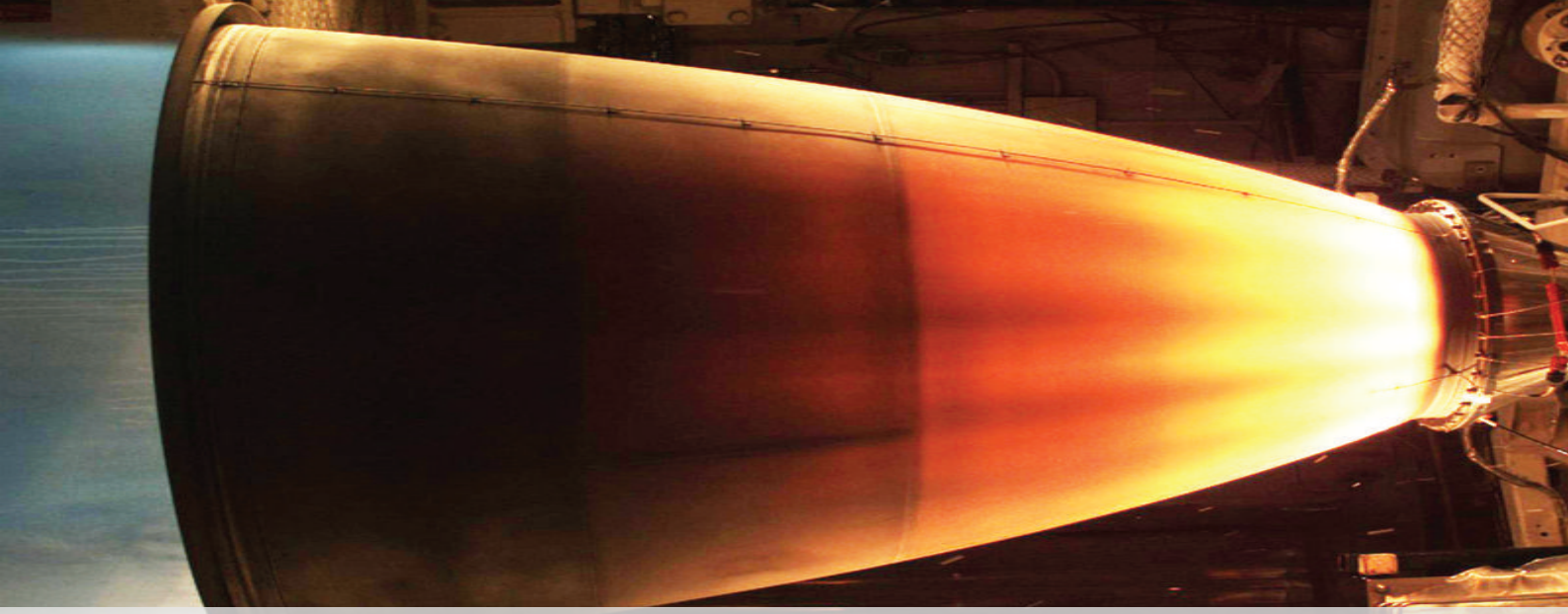

# 3 Results and discussion



## 3.1 Introduction

For model implemented in this research, a combination of NASA JPL (Jet Propulsion Laboratory) and ANSYS CFD (computational fluid dynamics) were employed to calculate thermophysical properties, heat transfer rates, wall, and fluid temperatures. CFD software was implemented to simulate the fluid dynamics and heat transfer within the rocket engine and cooling process.

We study the effect of cooling channel's length in regenerative cooled-nozzle, where we simulate a rocket nozzle in 2D with Ansys fluent. We took the dimensions According to JPL nozzle (Figure 3.1) [84].

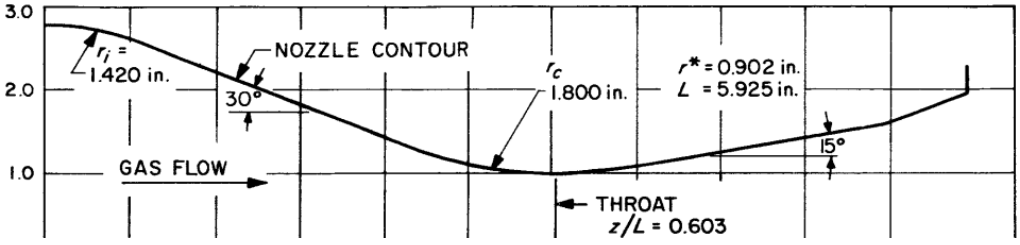


**Figure 3.1:** Nozzle dimensions diagram

Numerical models of the fluid dynamics and heat transfer within the rocket nozzle were created using ANSYS Fluent software. ANSYS Fluent was chosen because it is a powerful simulation tool for a wide range of physics problems including finite volume analysis (FVA) and computational fluid dynamics (CFD), providing accurate predictive models in a relatively short timeframe. It was determined that Fluent was a high-quality computer-aided engineering (CAE) tool for modeling the flow and heat transfer from the exhaust gas through the walls of the rocket nozzle within the required computational constraints. ANSYS Fluent has four integral software components, the Workbench, Design Modeler CFD software, ANSYS Meshing, and the solver.
To draw the geometry in CFD software, text files with the data points for the curves need to be imported. For this project, the text files were developed through derived functions written in MATLAB for the nozzle and the channels.
The wall and channel geometry was created with functions to compute the actual nozzle offsets. The MATLAB code created text files of the points for the curves that were then converted to the format required to upload to the particular CFD software. The data points created for these lines by MATLAB were then uploaded to either Design Modeler.

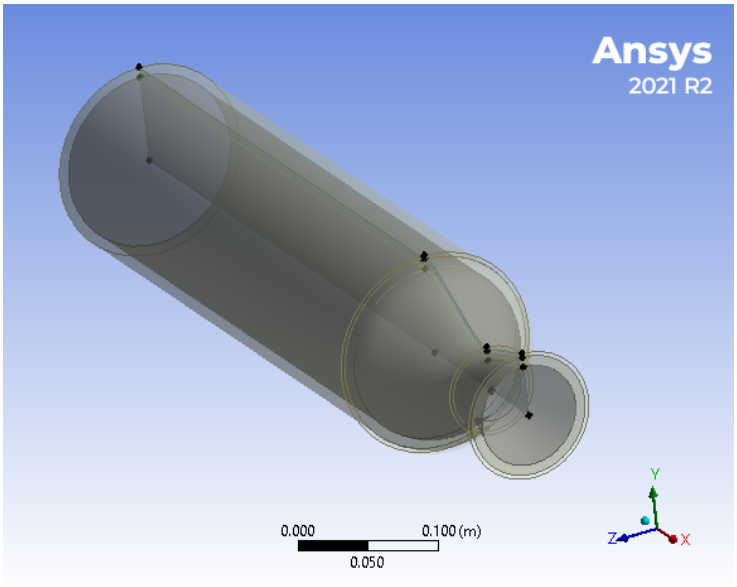


**Figure 3.2:** Nozzle geometry in 3D

ANSYS Design Modeler was effective for drawing the 2D geometry, we utilized to create four parts. The parts consisted of the nozzle wall (solid), the channel (fluid), nozzle-gas (fluid) and external air (fluid), we did use water in the channel, methyl-vapor in nozzle-gas and steel 502 as solid.
In ANSYS Meshing, parameters for sizing and boundary conditions need to be established.
The named-selections tool is used to stipulate inlets, outlets, zones, and walls such that the solver was able to identify each boundary type correctly. Fluent auto-generates arbitrary boundary conditions if sectors are not named appropriately, as well as for contact regions and walls with

convection on both sides. The quality of a mesh is often attributed to low skewness, which is defined as the difference between the shape of the element and the shape of an equilateral element with an equivalent volume. According to the ANSYS Fluent user manual, a skewness value of less than 0.9 is indicative of a high-quality mesh that will provide a converged solution, given the boundaries are also specified properly [**83**]. We took four length in cooling channel (0, 6, 12, 18) inches as we can see in the figures below:

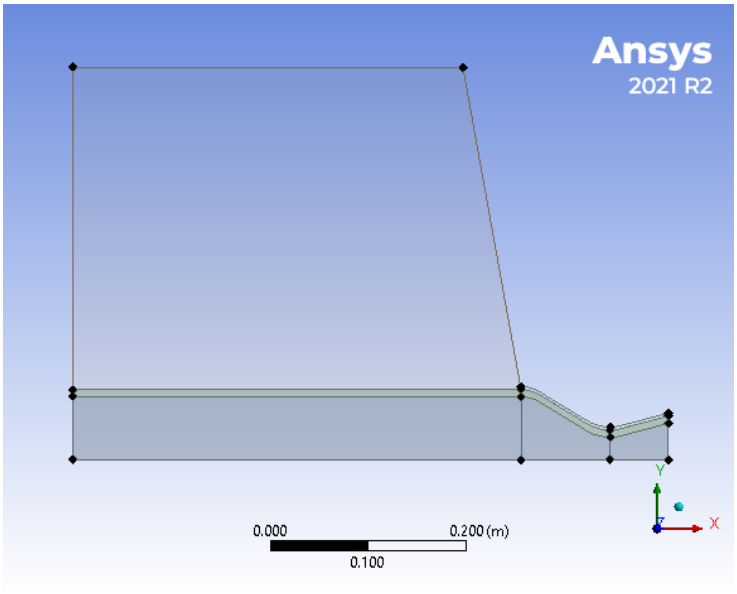


**Figure 3.3:** Nozzle geometry (0 inch)

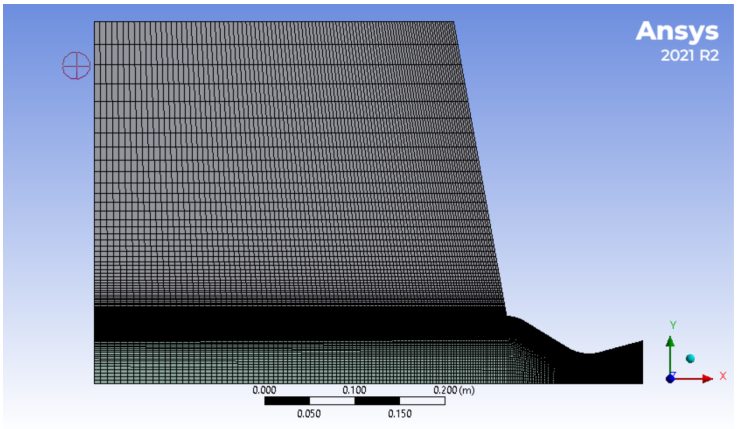


**Figure 3.4:** Nozzle mesh (0 inch)

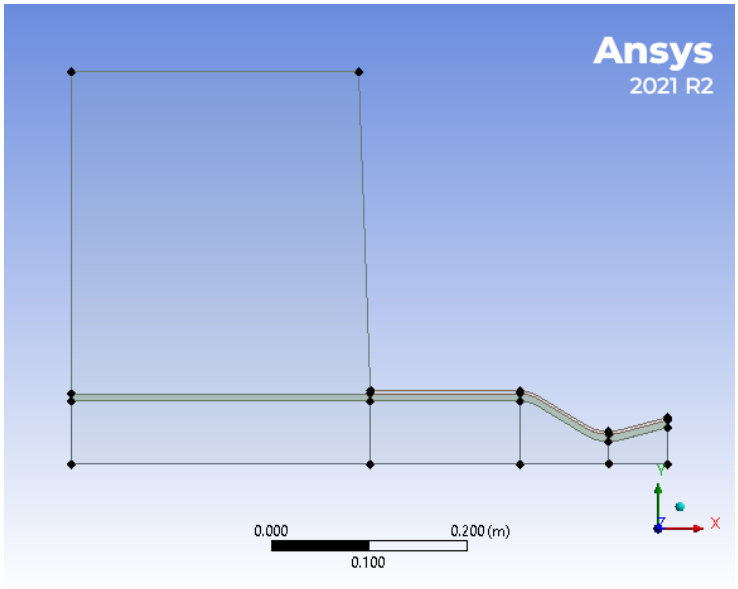


**Figure 3.5:** Nozzle geometry (6 inch)

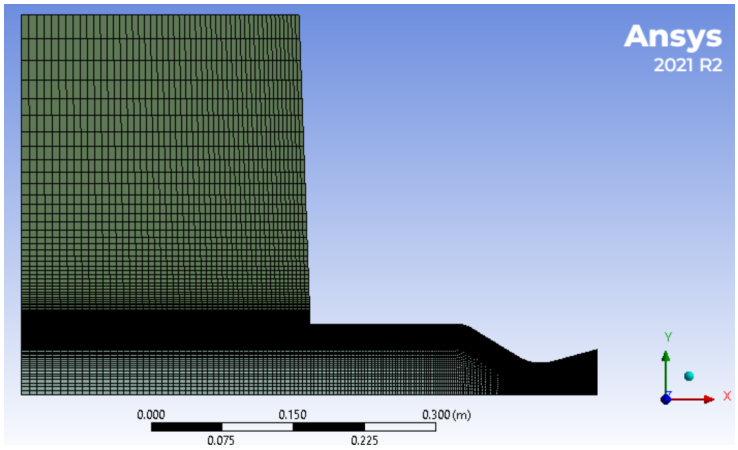


**Figure 3.6:** Nozzle mesh (6 inch)

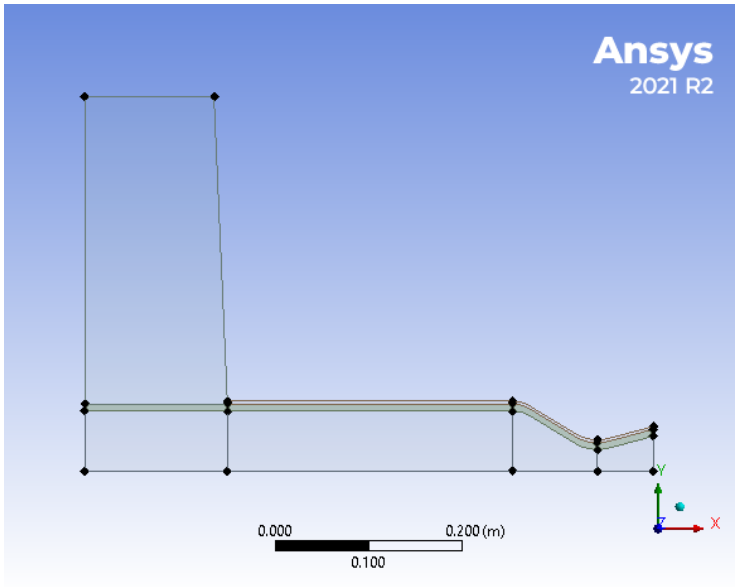


**Figure 3.7:** Nozzle geometry (12 inch)

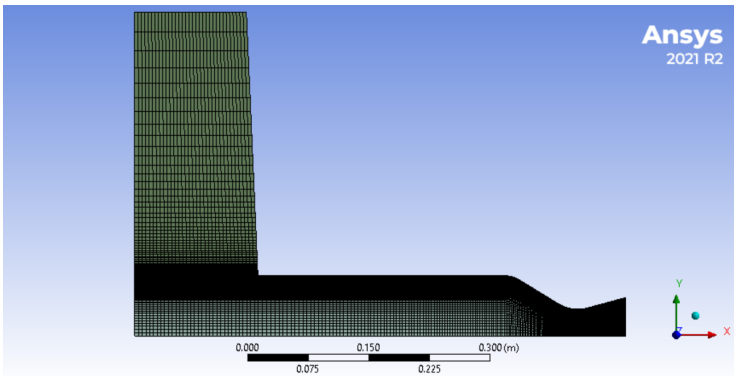


**Figure 3.8:** Nozzle mesh (12 inch)

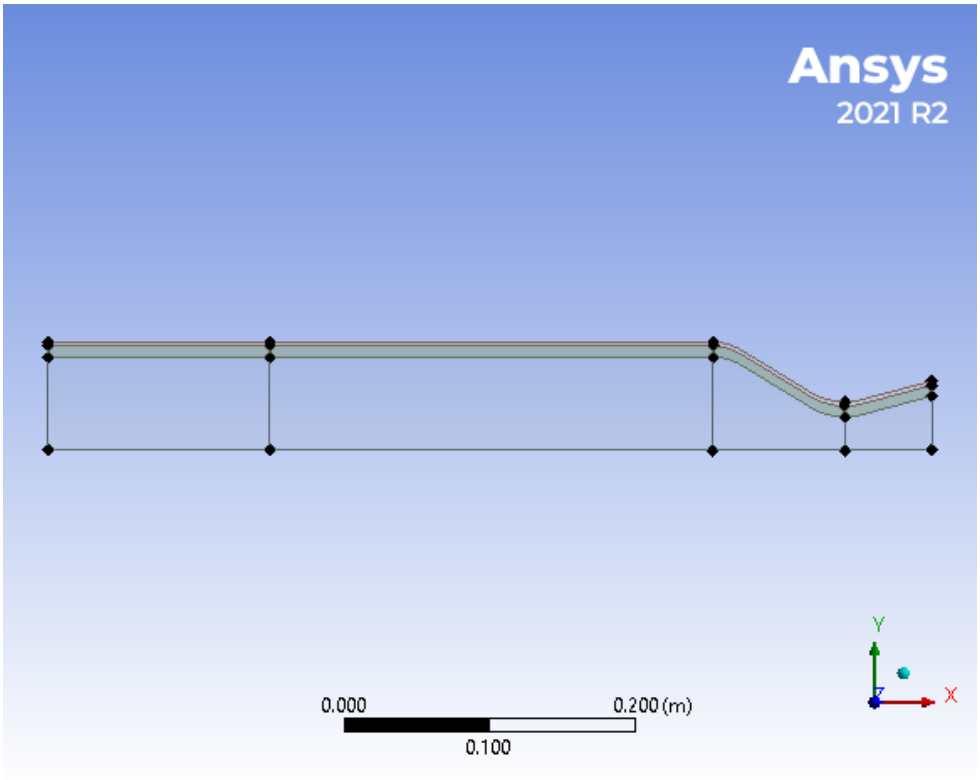


**Figure 3.9:** Nozzle geometry (18 inch)

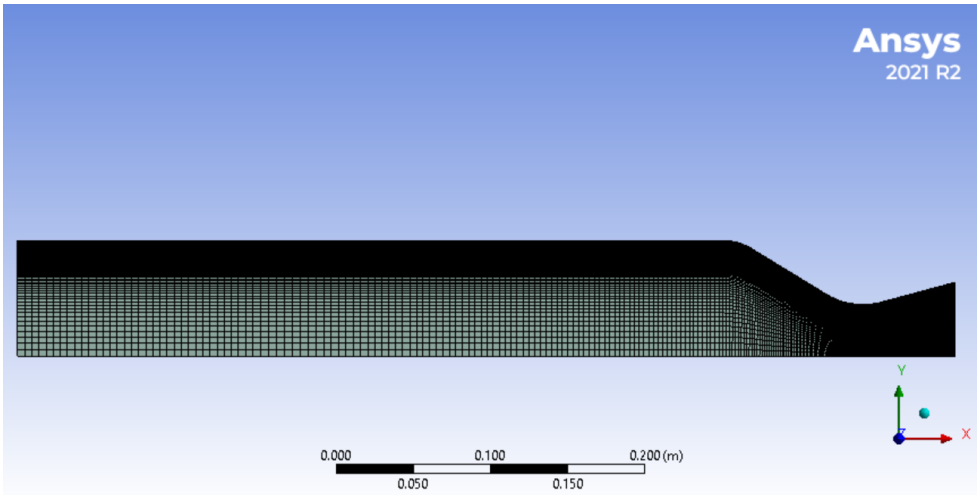


**Figure 3.10:** Nozzle mesh (18 inch)

## 3.2 Properties

Several in-depth studies have found that the use of constant values of physical properties in some cases can give erroneous results or far from the exact solution. Because as we know between 0 and 1 there is an infinity of numbers. Then preferably we use a function that generally varies according to temperature or another variable to obtain a convergence of the exact solution.
We took all properties from NASA NIST (National Institute of Standards and Technology) data-base web site :`https://webbook.nist.gov/chemistry/fluid/`

### 3.2.1 Water properties

The properties of water are given for pressure $P = 10$ bar
vaporization temperature $T_V$=453 K

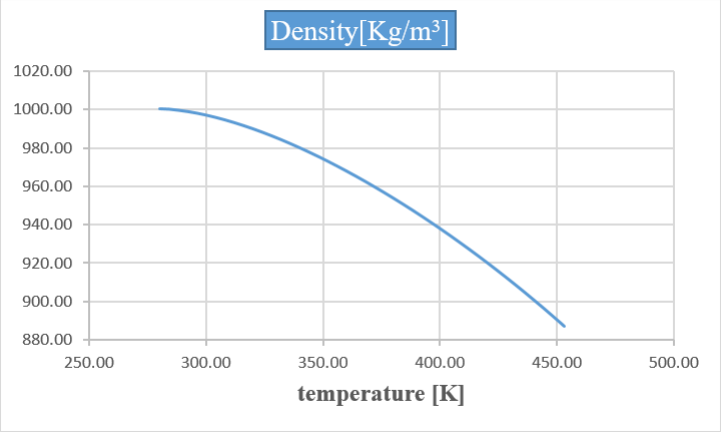


**Figure 3.11:** water density

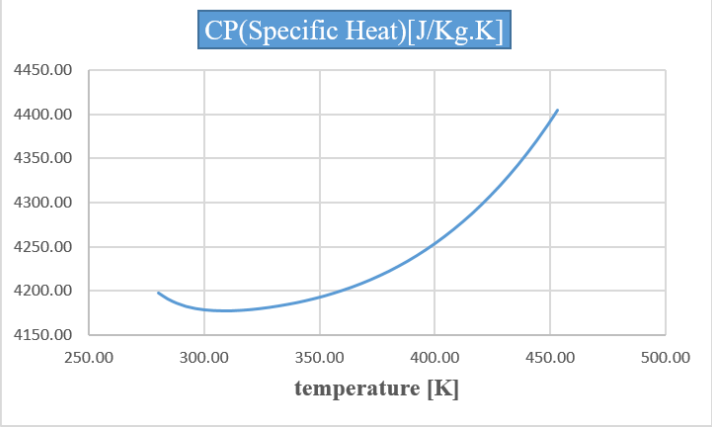


**Figure 3.12:** water specific heat

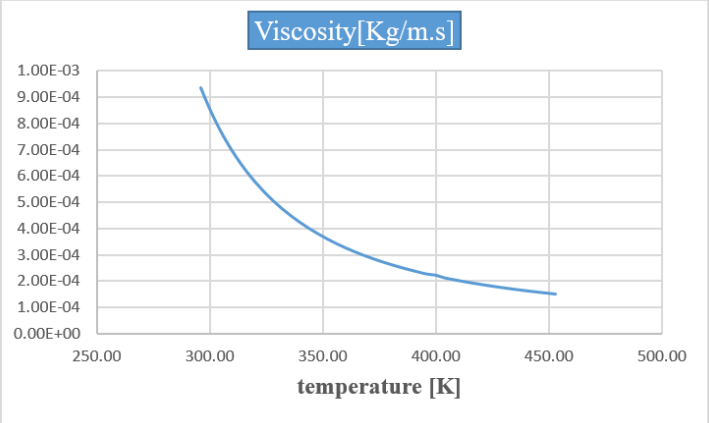


**Figure 3.13:** water viscosity

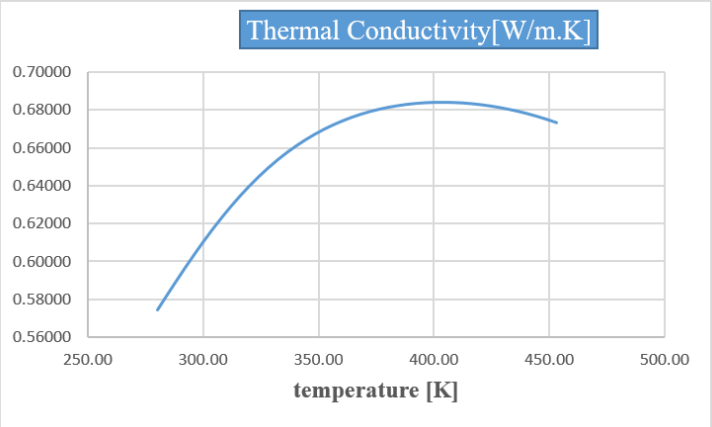


**Figure 3.14:** water thermal conductivity

### 3.2.2 Methyl-Alcohol-Vapor properties

The gas used in these simulation is Methyl-Alcohol-Vapor which enter from the chamber in different total pressure and temperature, the properties are given by:
Chemical formula: ch3oh
Density [Kg/m3]: ideal gas
Molecular weight M=32.04 [g/mol]

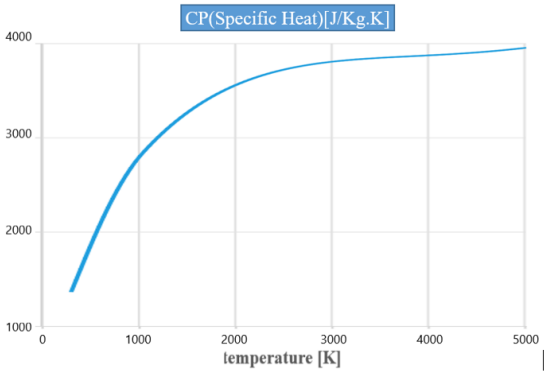


**Figure 3.15:** specific heat of ch3oh

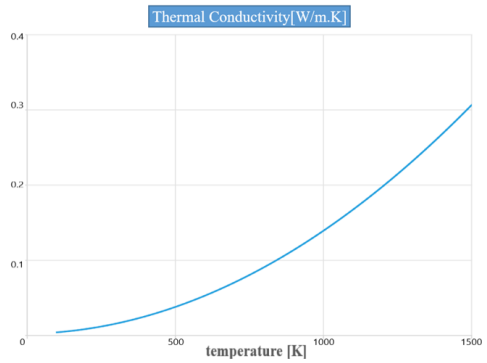


**Figure 3.16:** thermal conductivity of ch3oh

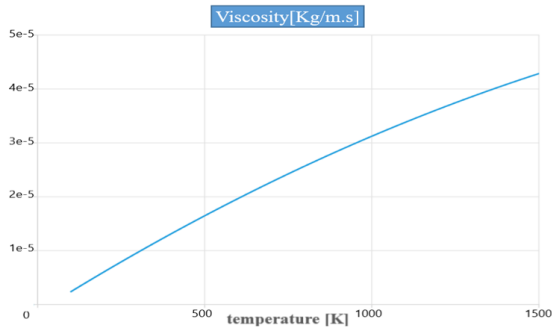


**Figure 3.17:** viscosity of ch3oh

### 3.2.3 Stainless-Steel 502 properties

The nozzle and plugs were made from the same billet of 502-type stainless steel. The available data on this material's thermal conductivity indicated a small temperature variation in the attainable wall temperature range. [1]

1: Density $\rho$=7753 [Kg/m3], Specific Heat Cp =486 [J/Kg.k], melting point temperature T=1755K.

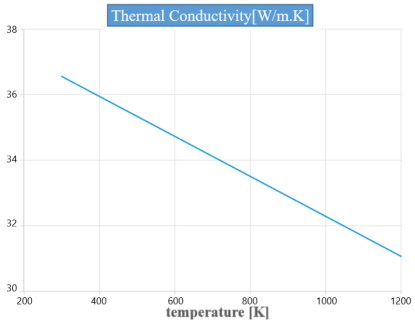


**Figure 3.18:** thermal conductivity of Stainless-Steel 502

### 3.2.4 Turbulence wall Y+

An extended grid refinement is obtained to ensure that the results are mesh-independent (Figure 3.19 and Figure 3.20), and when the change of resolution between the subsequent mesh refinement steps has been considered negligible, the fine mesh has been maintained. The laminar viscous sublayer had to be resolved; this has been achieved by keeping the maximum nondimensional wall distance (y+) of the first point near the wall equal to about 0.25 which is sufficiently smaller than 1 (see Fig.2). Results presented thereafter contain approximately 600.000 nodes.

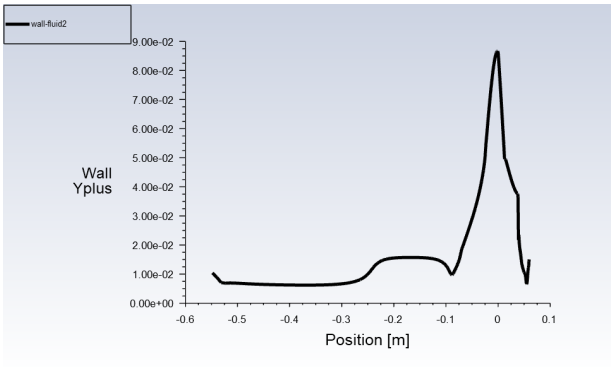


**Figure 3.19:** gas side $y^+$ for 6 inch cooled length

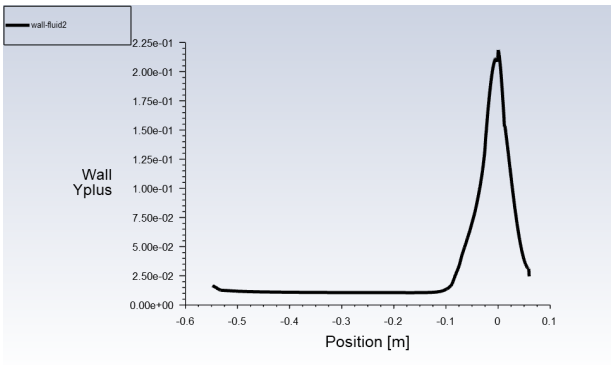


**Figure 3.20:** gas side $y^+$ for 0 inch cooled length

## 3.3 Validation

With advances in computing power, engineers increasingly rely on modeling and simulation for the design, analysis, and certification of engineering systems. Validation provides the primary means by which the overall accuracy of computational simulations can be assessed. Validation can be separated into two parts, code and solution validation. Code validation is used to find coding errors in the discrete solution to a given set of governing equations and boundary conditions. Code validation can be assessed by comparison to exact analytical solutions or experimental data, comparison to highly accurate numerical benchmark solutions, and code-to-code comparisons. Solution validation (or numerical error assessment) is concerned with quantifying the numerical error of a given simulation. Solution validation should be performed for each application of the code that is significantly different from previous applications. For steady-state problems, the two main aspects of solution validation are iterative convergence and grid convergence.
The former deals with the marching of a solution in pseudo-time toward a steady-state, whereas the latter addresses the adequacy of the mesh on which the discrete equations are being solved. The spatial order of accuracy is also an important metric for assessing the errors due to spatial resolution.
In this section, solution validation have been performed on two-dimensional test cases for gas temperature. Solution verification has been achieved by an analysis of iterative convergence and grid convergence. These solutions have been compared with experimental data, thus providing the validation of the code.
after a multiple change in the boundary conditions we get the result below:

### 3.3.1 First case 0 inch (test 315)

The temperature, pressure and mass flow of the inlet of the coolant channel (water) were specified to be 300 K, 10 bar and 2 kg/s respectively. For the gas (methyl vapor) 842.222 k, 514348.89 Pa and 1.15 kg/s respectively.
For the external air we chose velocity inlet V=0.3 m/s, T=300 K, P=101325 Pa

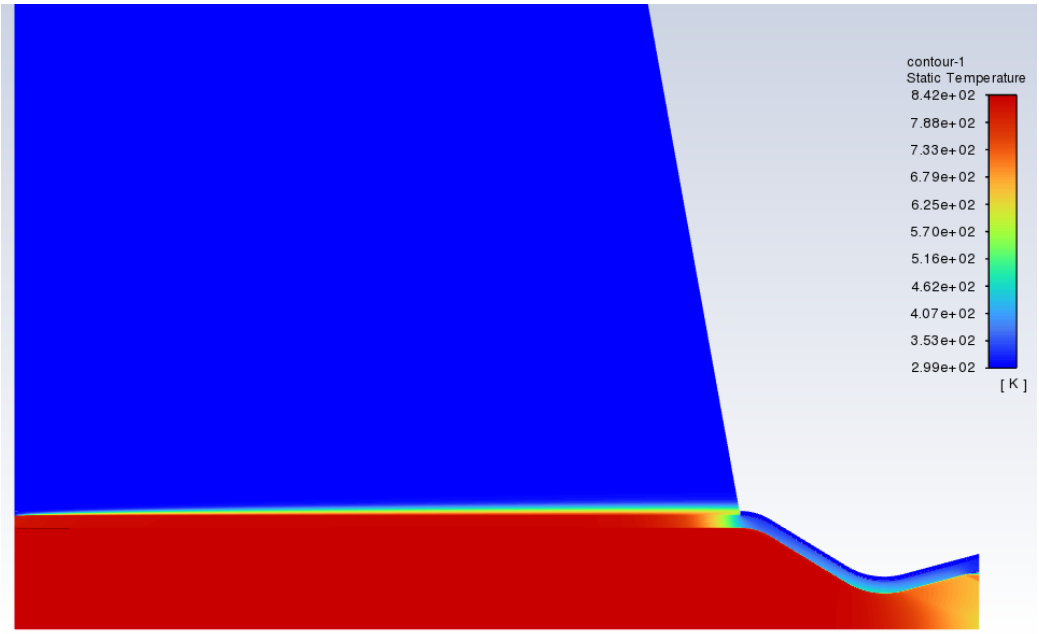


**Figure 3.21:** Static temperature contour of methyl, water and external air

this Figure 3.21 represents the contour of static temperature of the Rocket (engine, nozzle) we note graduation of color from the cold blue 300K to the hot red 842 K where the max temperature of the methyl reaches 842K, water 364K, and gas side wall (wall fluid2) 482K as we can see in the Figure 3.22.

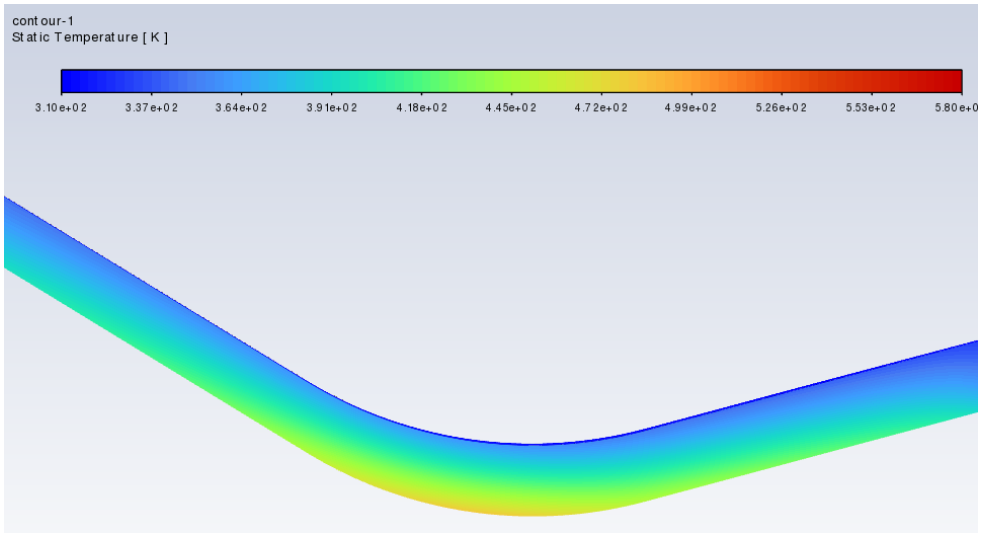


**Figure 3.22:** Static temperature contour in the of wall of nozzle and water

Figure 3.23 represents the axial evolution of static temperature, where the red curve represent gas side wall (wall fluid2), the temperature decrease from $T_{inlet}$=842K to T=372K (position x=-0.07m from the throat, this position correspond to the inlet nozzle) due the increase of the speed in the nozzle then increase to reach Tmax= 482K then decrease again, the most important observation, The maximum value of the temperature and heat-transfer occurs just upstream of the throat in the vicinity where the mass flux $\rho u$, as indicated in Figure 3.23, is a maximum [2].
For the black curve, the temperature of water side decrease from T=378K to T=337K (position -0.07m) then increase to Tmax=362K shows that the temperature exchange is quite important in that region (less than the vaporization temperature $T_c$=453 K) then decrease again.

2: The difference between chamber temperature and the maximum temperature obtained upstream of the throat is about $\Delta T$=842-482=360K

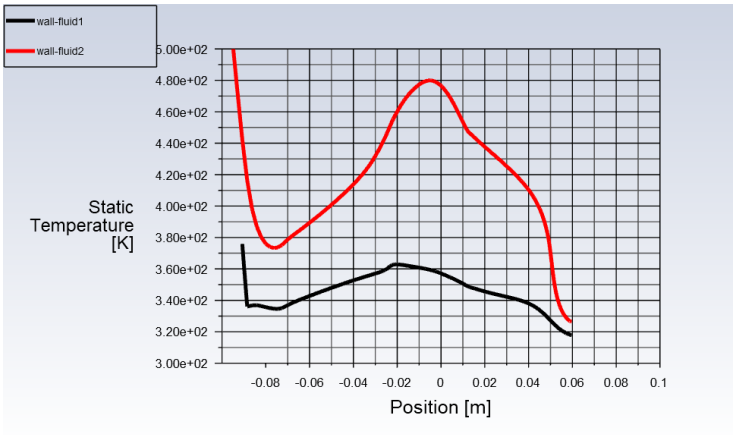


**Figure 3.23:** Axial distribution of static temperature of coolant side (wall-fluid1) and gas side wall (wall-fluid2), case of 0 inch cooled length

The Figure 3.24 shows that the gas side temperature distribution obtained is in very good agreement with the experimental data of Back and al.[**84**],

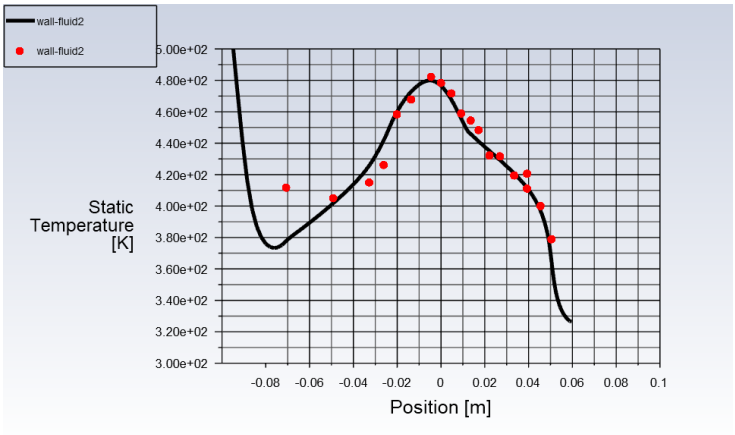


**Figure 3.24:** Comparison of gas side static temperature with experimental data of [**84**], case of 0 inch cooled length

### 3.3.2 Second case 6 inch (test 246)

In this case the coolant is 6 inches upstream of the nozzle entrance. The temperature, pressure and mass flow of the inlet of the coolant channel (water) were specified to be 300 K, 10 bar and 2 kg/s respectively.
For the gas (methyl vapor) 833.33 k and 518485.7 Pa respectively.
For the external air we chose velocity inlet V=0.3m/s, T=300 K, P=101325 pa

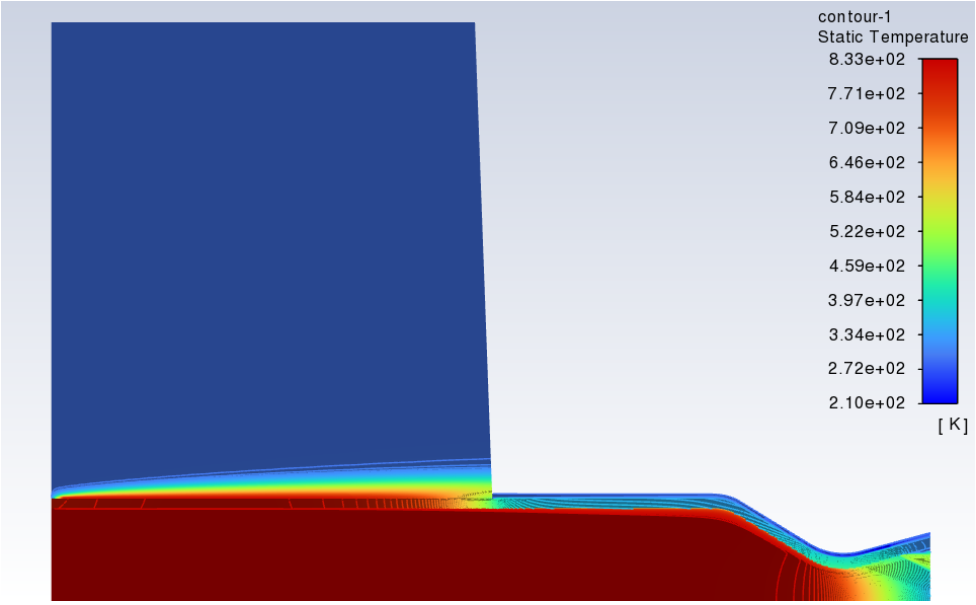


**Figure 3.25:** Static temperature contour of methyl, water and external air

this Figure 3.25 represents the contour of static temperature of the Rocket (engine nozzle), we note graduation of color from the blue 210K to the red 833 K where the max temperature of the methyl reaches 833K, water 344K, and gas side (wall fluid2) 457K as we can see in the Figure 3.26.[3]. The same trend of decreasing and increasing of the physical and thermodynamic properties is obtained due to the change of cooled length.

3: The difference between chamber temperature and the maximum temperature obtained upstream of the throat is about $\Delta T$=833-457=376K

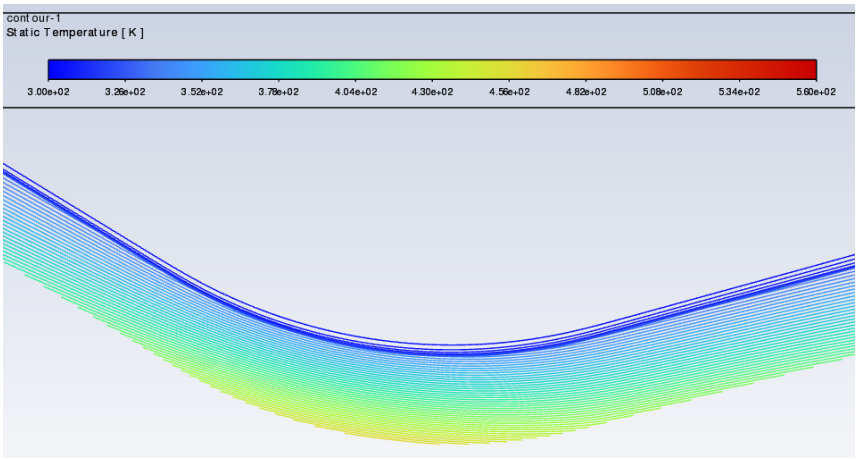


**Figure 3.26:** Static temperature contour of wall and water

Figure 3.27 represents the wall axial distribution of static temperature of the gas and coolant (water) side where the red curve represent gas side (wall fluid2), the temperature decrease from Tinlet=833K to T=347K (position -0.08m ) due to the decrease in total temperature or in other words to increase of the speed of the gas just in the entrance of the nozzle were the section area start to decrease in the convergent section of nozzle, then increase to reach a maximum just upstream of the throat traduced by the maximum location of the mass flux (Tmax= 457K), and

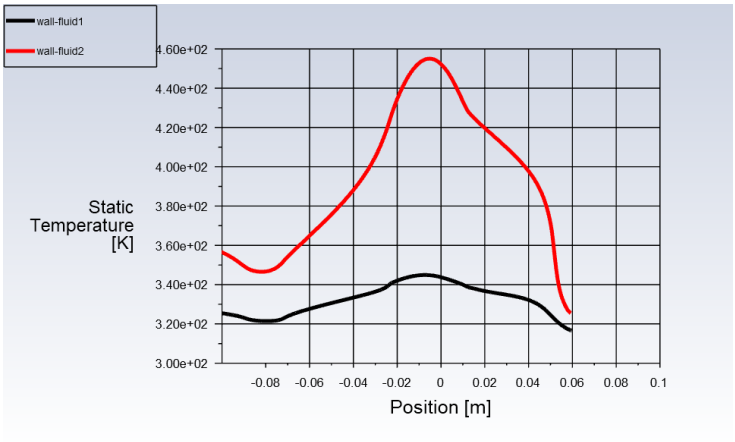


**Figure 3.27:** Axial distribution of static temperature of coolant side (wall-fluid1) and gas side wall (wall-fluid2), case of 6 inches cooled length

also this can be traduced by the maximum friction coefficient due also to the maximum of friction velocity, then decrease again in the divergent section due to the decrease in the friction velocity, although in this area the gas velocity continues to increase.
For the black curve, the temperature of water side decrease from T=325K (position -0.08m) to T=320K then increase to Tmax=344K (less than the vaporization temperature) then decrease again

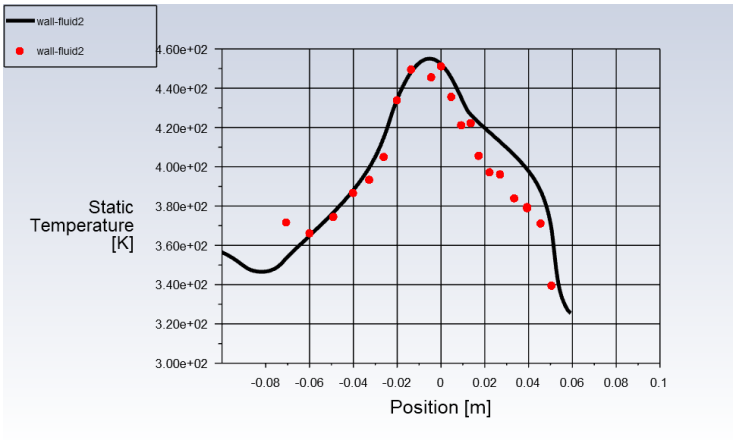


**Figure 3.28:** Comparison of gas side static temperature with experimental data of [**84**], case of 6 inches cooled length

a comparison of the simulation result against the experimental one has been made and shown on the Figure 3.28. The result is in agreement with experimental data of Back et al. [**84**]

### 3.3.3 Third case 12 inch (test 234)

In this case, the coolant starts at a distance equal to 12 inches upstream of the nozzle inlet. To study the survival of the nozzle, the effect of the cooling amount on the heat transfer and on the temperature distribution to finally maintain the wall of the nozzle and also to maintain the coolant (water) temperature from reaching the vaporization temperature.
The temperature, pressure and mass flow of the inlet of the coolant channel (water) were specified to be 300 K, 10 bar and 3 kg/s respectively.
For the gas (methyl vapor) 833.33 k and 518485.7 Pa respectively.
For the external air we chose velocity inlet V=0.3 m/s, T=300 K, P=101325 Pa.

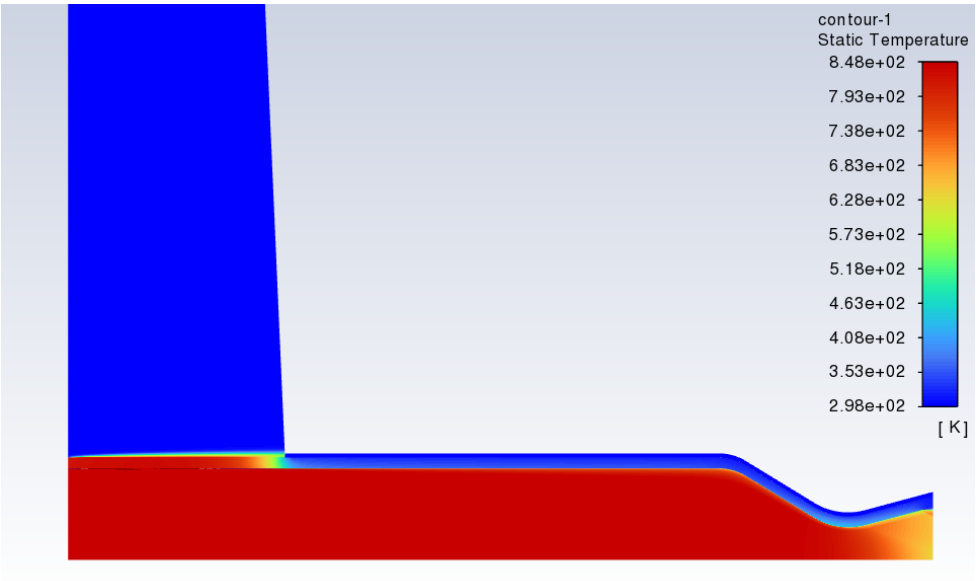


**Figure 3.29:** Static temperature contour of methyl, water and external air

4: The difference between chamber temperature and the maximum temperature obtained upstream of the throat is about $\Delta T$=848-445=403K

This Figure 3.29 [4] represents the contour of static temperature of the Rocket (engine nozzle), we can see the graduation of the colors from the blue one of about 298K to the red 848 K where the max temperature of the methyl reaches 848K, water 338K, and gas side (wall fluid2) 445K as we can see in the Figure 3.30.

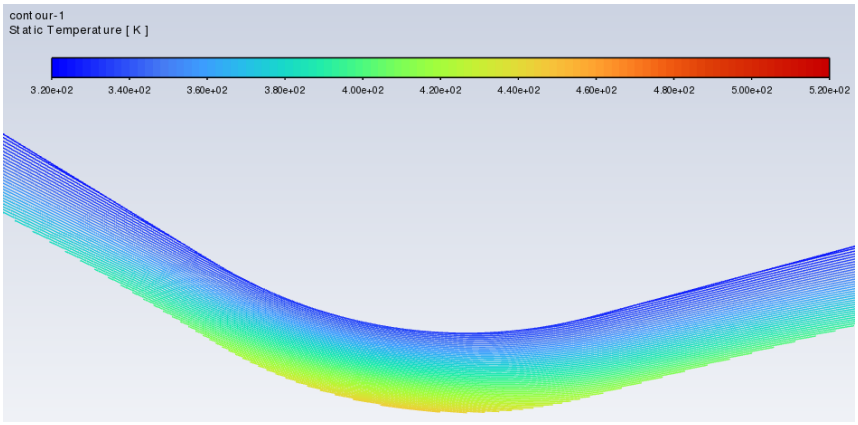


**Figure 3.30:** Static temperature contour of wall and water

The Figure 3.31 shows a graphical representation of the temperature distribution for the two sides, on the gas side where the temperature decreases because of the entry of the gas in the nozzle, where it is subjected to an increase in speed because of the decrease of temperature and consequently the increase of the Mach number with the decrease of the nozzle section (convergent section), the reason for the increase in temperature has the same explanation as mentioned for the previous cases. For the black curve, slight temperature of water side decrease from T=320K to T=317K (position -0.08m) then increase to Tmax=338K (less than the vaporization temperature) then decrease again.

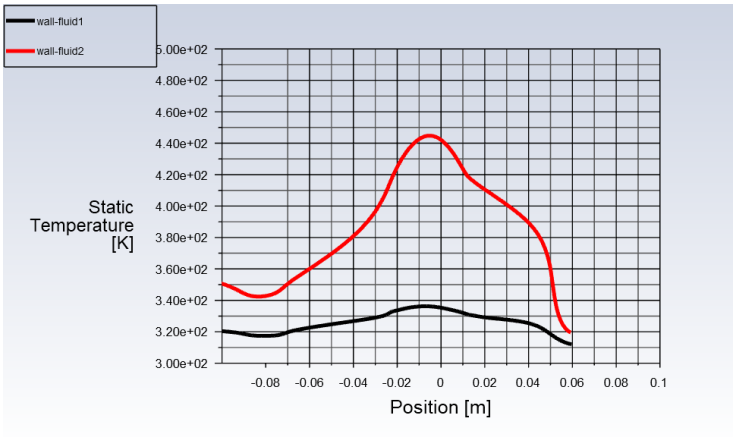


**Figure 3.31:** Axial distribution of static temperature of coolant side (wall-fluid1) and gas side wall (wall-fluid2), case of 12 inches cooled length

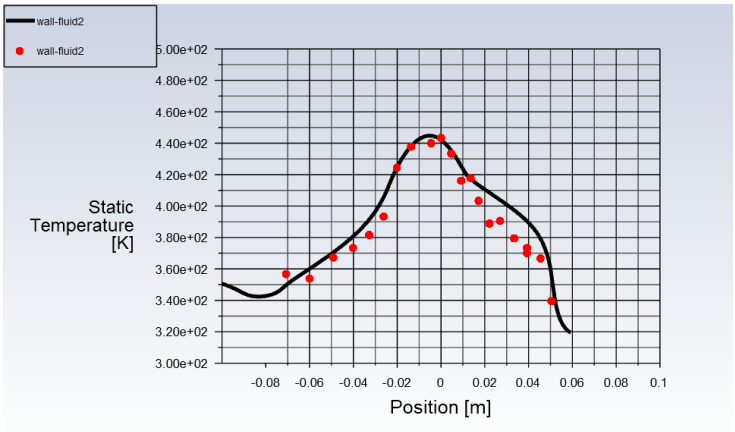


**Figure 3.32:** Comparison of gas side static temperature with experimental data of [**84**], case of 12 inches cooled length

The Figure 3.32 shows that the gas side temperature distribution obtained is in very good agreement with the experimental data of Back and al. [84],

### 3.3.4 Fourth case 18 inch (test 262)

in the case with 18 inches, the cooling covers both the combustion chamber and the nozzle wall, i.e. the cooling starts at a distance of 18 inches upstream of the nozzle.

The temperature, pressure and mass flow of the inlet of the coolant channel (water) were specified to be 300 K, 10 bar and 1.4 kg/s respectively. For the gas (methyl vapor) 843.333 k and 518485.7 Pa respectively.

The Figure 3.33 represents the contour of static temperature of the nozzle, the degradation in the colors clearly shows the effect of cooling, from the blue one of about 299K to the hot red temperature of about 843 K where the max temperature of the methyl is 843K (stagnation temperature or the temperature of the chamber), water temperature is 364K, and the gas side (wall fluid2) is 460K, located just upstream of the nozzle. [5].

See the note

5: The difference between chamber temperature and the maximum temperature obtained upstream of the throat is about $\Delta T$=843-460=383K

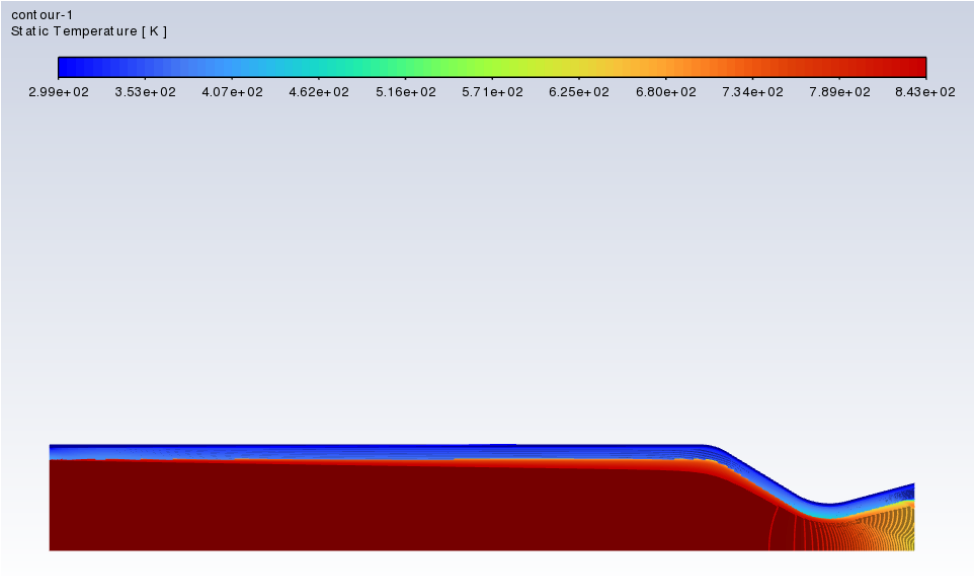


**Figure 3.33:** Static temperature contour of methyl, water and external air

**Note**

We note here that the temperature differences between the stagnation temperature and the max temperature shown on the sides notes $\Delta T$, are no longer directly comparable given the difference between the chamber pressure ($p_0$) and the chamber temperature ($T_0$).

The Figure 3.34 shows a zoom on the area of the nozzle wall just upstream of the throat, clearly showing the position of the maximum temperature.

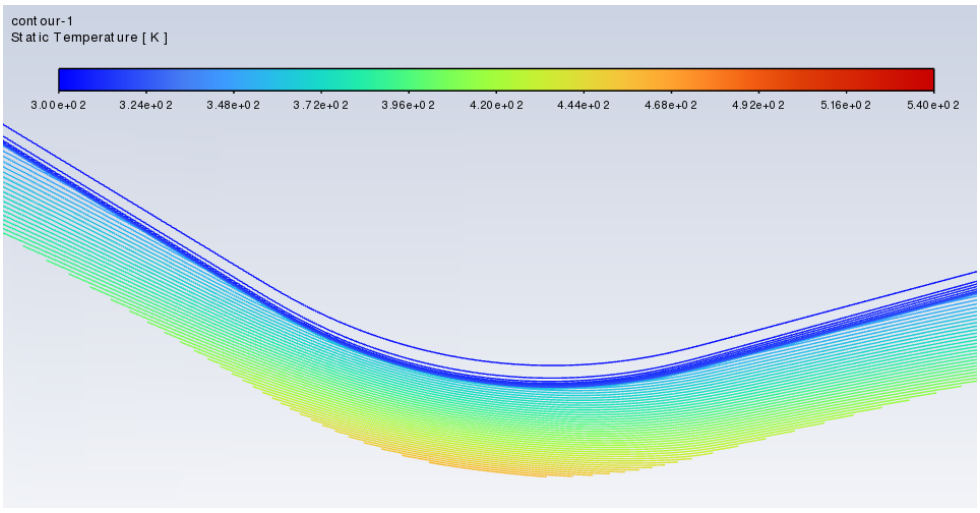


**Figure 3.34:** Static temperature contour of wall and water

Figure 3.35 represents the axial variation of wall static temperature, where the red curve represent gas side (wall fluid2), the temperature decrease from $T_{inlet}$=843K to T=355K (position -0.08m ) then increase to reach Tmax= 460K (upstream of throat) then decrease again in the divergent section due to the decrease in friction velocity.

For the black curve, the temperature of water side decrease from T=336K to T=330K (throat position) due to the increase of the speed of coolant and in the same time this correspond to the decrease in pressure then increase to Tmax=364K (less than the vaporization temperature of water at pressure equal to 10 bar $T_c$=453 K) then decrease again, we note here the bahavior of the density of the water is the opposite of the temperature behavior.

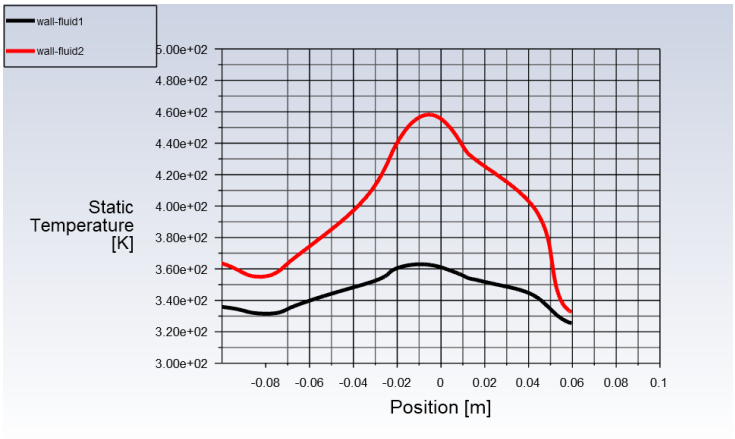


**Figure 3.35:** Axial distribution of static temperature of coolant side (wall-fluid1) and gas side wall (wall-fluid2), case of 18 inches cooled length

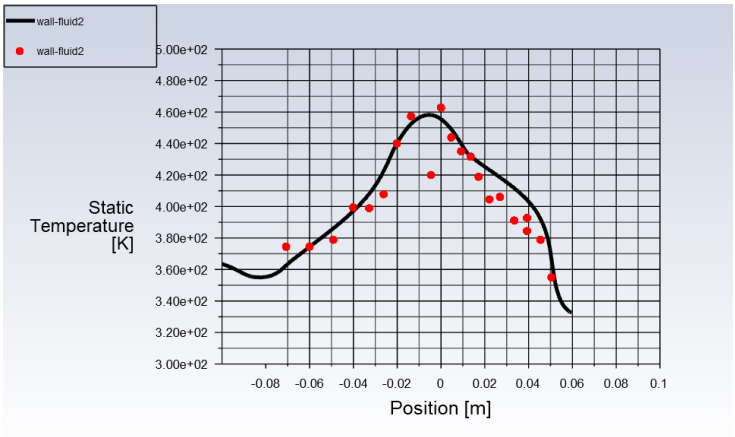


**Figure 3.36:** Comparison of gas side static temperature with experimental data of [**84**], case of 18 inches cooled length

A comparison is made against the experimental data of case TEST N° 262 in Back et al. [**84**] reference, the result of simulation agrees very well with the experimental data, and this in spite of the dispersion of the experimental results (see Figure 3.36 ).

## 3.4 Effect of cooled inlet length

For the comparison to be relevant between the different cases already mentioned, and to show the effect of the coolant length, it is necessary to keep constant all the conditions, either for the gas or the coolant. For that we fixed methyl inlet temperature and pressure to ($P_0$=9 bar, T=1000K) and we chose two values of water mass flow (2kg/s, 6kg/s) for more comparison of results, with ($P_0$=10 bar, T=300K) for water

### 3.4.1 0 inch

In this case, the coolant starts exactly at the nozzle entrance as shown in Figure 3.37

#### 3.4.1.1 water mass flow =6kg/s

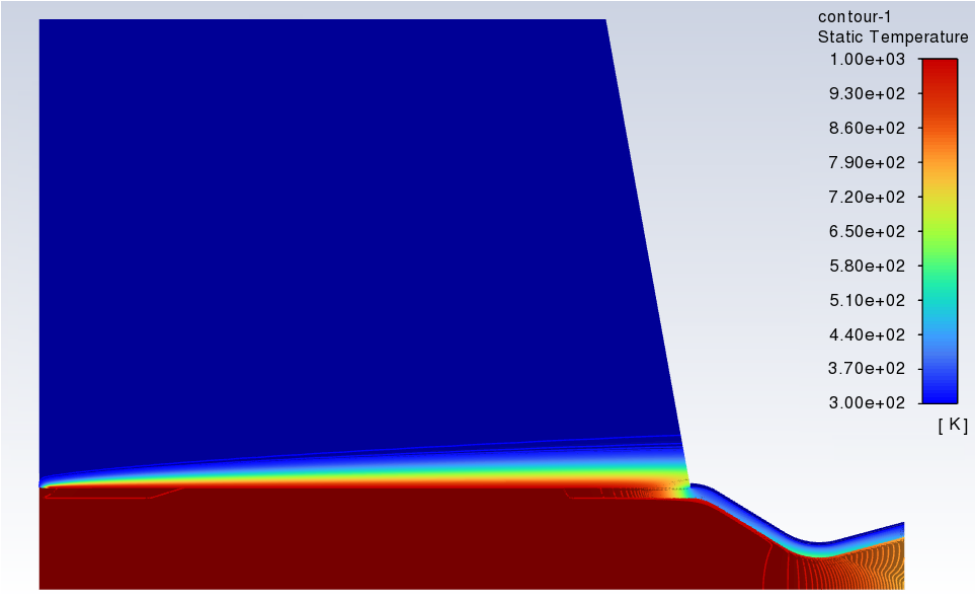


**Figure 3.37:** Static temperature contour of methyl, water and external air

The contour of the static temperature is displayed in the Figure 3.37. The temperature of the hot gas is cooled from 1000 K to 584 K, and the coolant extract the heat and its temperature increase from 300 K to 341 K.[6].

6: The difference between chamber temperature and the maximum temperature obtained upstream of the throat is about $\Delta T$=1000-584=416K

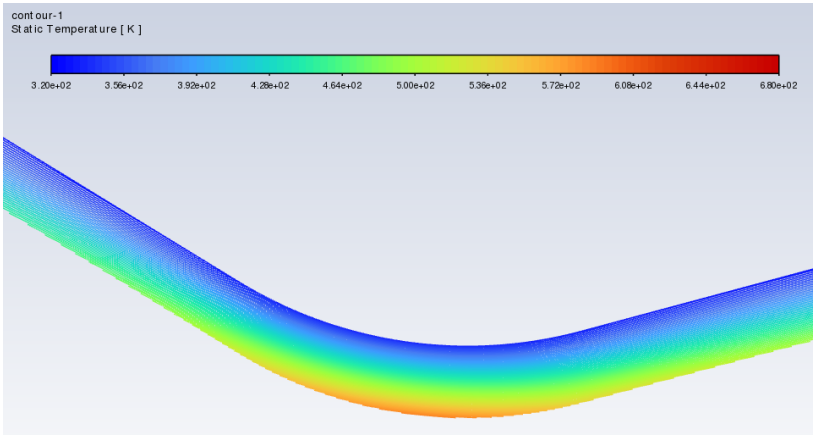


**Figure 3.38:** Static temperature contour of wall and water

Figure 3.39 represent axial evolution of static temperature in term of position where the red curve represent gas side (wall fluid2), the temperature decrease from $T_{inlet}$=1000K to T=410K (x=-0.076m throat position, this position is the intake nozzle) then increase to reach Tmax= 584K(before the throat 0m ) then decrease again.

Most essential observation is where the mass flux is maximal the value of temperature and heat transfer is maximum (just before the throat) This applies to all cases below.
For the black curve, the temperature of water side decrease from T=400K (position -0.09m) to T= 331K (position -0.06m) then a slight increase to Tmax=341K (less than the vaporization temperature) then decrease again.

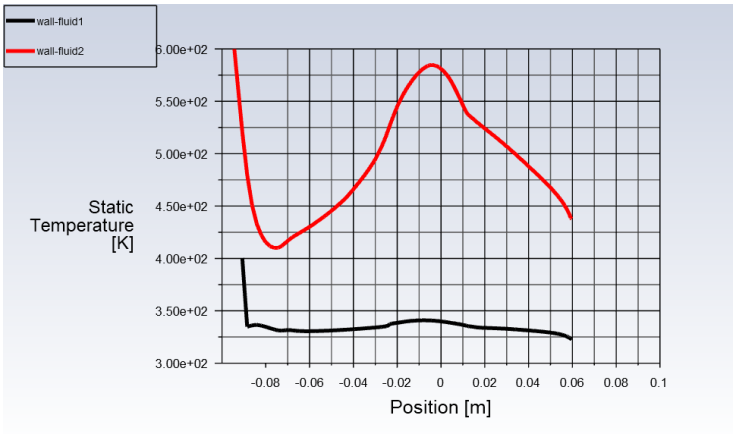


**Figure 3.39:** Axial distribution of static temperature of coolant side (wall-fluid1) and gas side wall (wall-fluid2), 6kg/s case of 0 inch cooled length

### 3.4.1.2 water mass flow =2kg/s

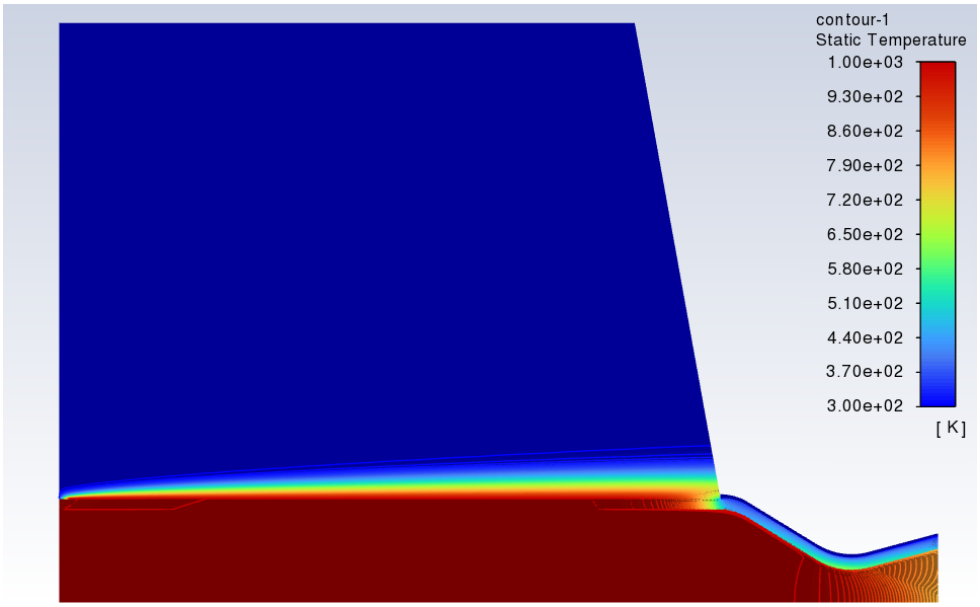


**Figure 3.40:** Static temperature contour of wall and water

This Figure 3.40 represents the Contour of static temperature of the Rocket (engine, nozzle) we note gradation of color from the blue 300K to the red 1000 K where the max temperature of the methyl reaches 1000K, water 399K, and gas side (wall fluid2) 619K as we can see in the Figure 3.41. [7]
We have an 8% drop in temperature from 6kg/s to 2kg/s in water mass flow.

7: The difference between chamber temperature and the maximum temperature obtained upstream of the throat is about $\Delta T$=1000-619=381K.

When we increase the mass flow rate, we notice that the temperature drops. Since viscosity is the resistance to flow expressed by fluids, this means that temperature has an effect to flow rate,This applies to all the following cases.

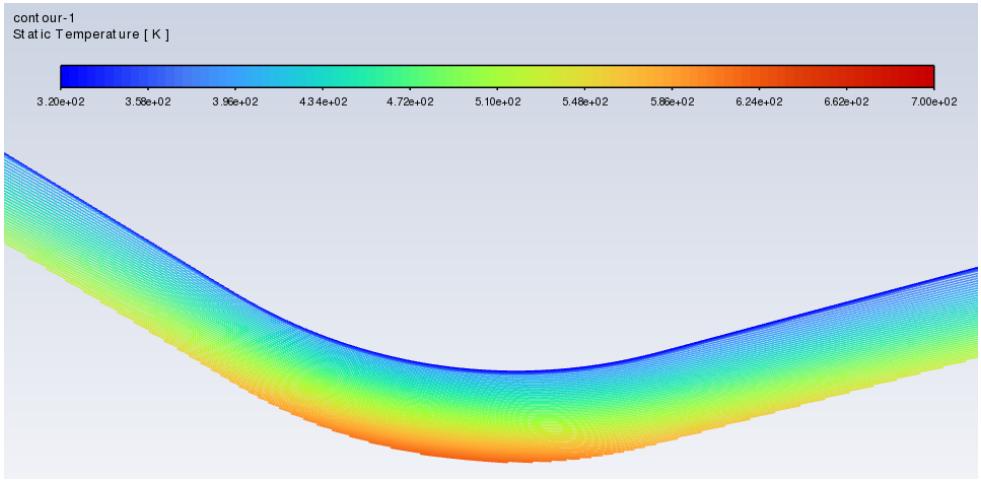


**Figure 3.41:** Static temperature contour of wall and water

Figure 3.42 represent the axial evolution of static temperature in term of position where the red curve represent gas side (wall fluid2) , the temperature decrease from $T_{inlet}$=1000K to T=438K (position -0.076m ) then increase to reach Tmax= 619K(before the throat 0m, we did mention the reason in the Previous cases), then decrease again.
For the black curve, the temperature of water decrease from T=422K (position -0.09m) to T= 360K (position -0.076m) then increase to Tmax=399K (less than the vaporization temperature) then decrease again.

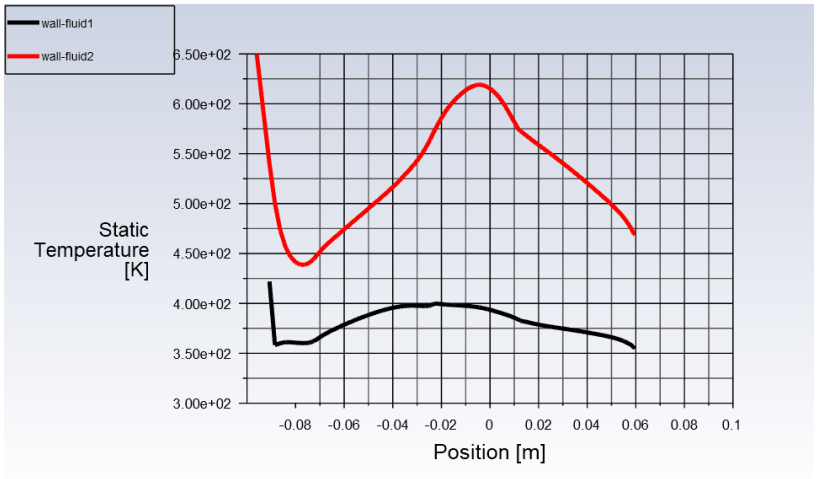


**Figure 3.42:** Axial distribution of static temperature of coolant side (wall-fluid1) and gas side wall (wall-fluid2), 2kg/s case of 0 inch cooled length

### 3.4.2 6 inch

The coolant is 6 inches upstream of the nozzle entrance.(that's means its above a part of the combustion chamber and the nozzle)

#### 3.4.2.1 water mass flow =6kg/s

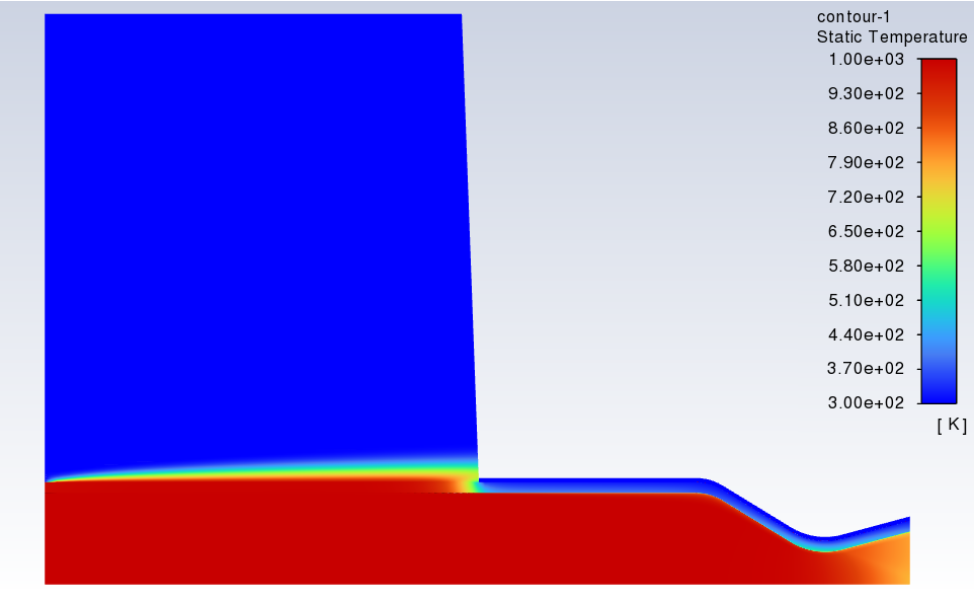


**Figure 3.43:** Static temperature contour of methyl, water and external air

This Figure 3.43 represents the axial evolution of static temperature of the Rocket (engine, nozzle) we note gradation of color from the blue 300K to the red 1000 K where the max temperature of the methyl reaches 1000K, water 336K, and gas side (wall fluid2) 561K as we can see in the Figure 3.44.[8].
as result of the change in cooled length we obtained a decreasing and increasing of the physical and thermodynamic properties.
Our increase is 5.2% in $\Delta T$ from 0 inch case to 6 inches 6kg/s water mass flow case.

8: The difference between chamber temperature and the maximum temperature obtained upstream of the throat is about $\Delta T$=1000-561=439K

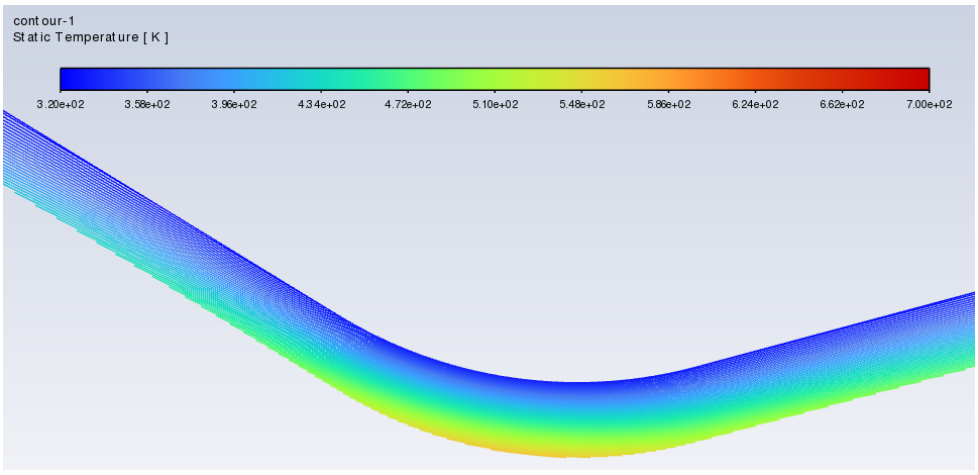


**Figure 3.44:** Static temperature contour of wall and water

Figure 3.45 represent axial evolution of static temperature in term of position where the red curve represent gas side (wall fluid2), the temperature decrease from $T_{inlet}$=1000K to T=375K (position -0.08m ) then increase to reach Tmax= 561K(before the throat 0m ) then decrease again.
For the black curve, Slight decrease in temperature of water side from T=322K (position -0.1m) to T=318K (position -0.08m) then increase to Tmax=336K (less than the vaporization temperature) then decrease again.

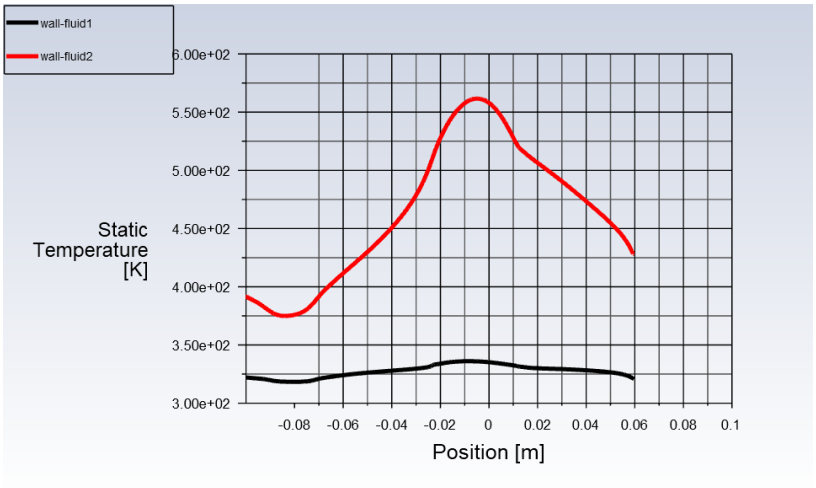


**Figure 3.45:** Axial distribution of static temperature of coolant side (wall-fluid1) and gas side wall (wall-fluid2), 6kg/s case of 6 inch cooled length

### 3.4.2.2 water mass flow =2kg/s

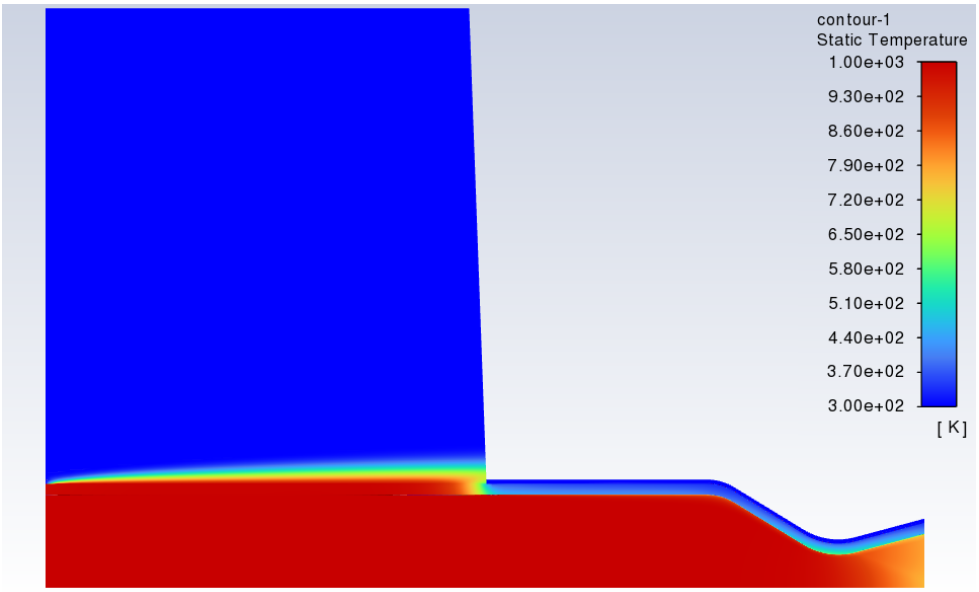


**Figure 3.46:** Static temperature contour of methyl, water and external air

This Figure 3.46 represents the Contour of static temperature of the Rocket (engine, nozzle) we note gradation of color from the blue 300K to the red 1000 K where the max temperature of the methyl reaches 1000K, water 376K, and gas side (wall fluid2) 586K as we can see in the Figure 3.47.[9]

9: The difference between chamber temperature and the maximum temperature obtained upstream of the throat is about $\Delta T$=1000-586=414K

Following the change in cooled length and mass flow, we obtained a decrease and an increase in physical and thermodynamic properties.
We have an 7.9% drop in $\Delta T$ from 6 inches case to 0 inch case (2kg/s water mass flow), and 5.7% drop in $\Delta T$ from 2kg/s to 6kg/s water mass flow.

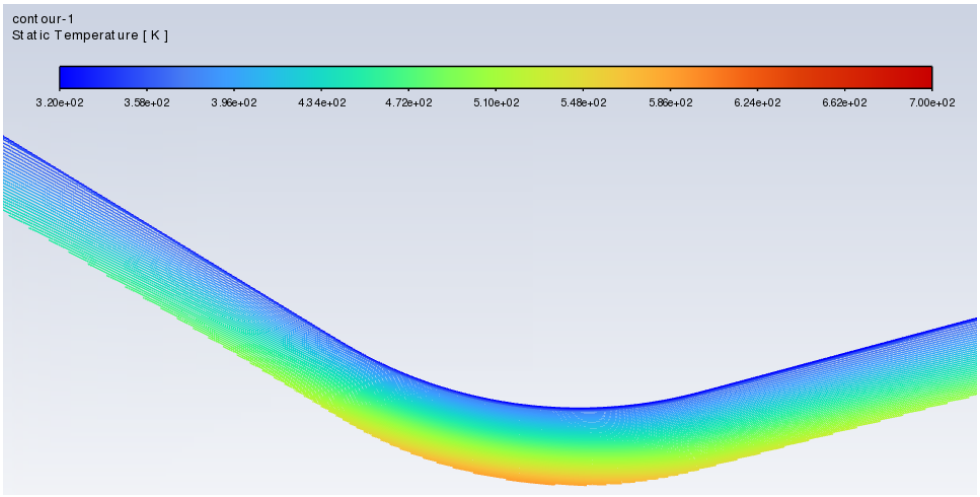


**Figure 3.47:** Static temperature contour of wall and water

Figure 3.48 represent axial evolution of static temperature in term of position where the red curve represent gas side (wall fluid2), the temperature decrease from $T_{inlet}$=1000K to T=397K (position -0.08m ) then increase to reach Tmax= 586K(before the throat 0m ) then decrease again.
For the black curve, Slight decrease in temperature of water side from T=348K (position -0.1m) to T=341K (position -0.08m) then increase to Tmax=376K (less than the vaporization temperature) then decrease again.

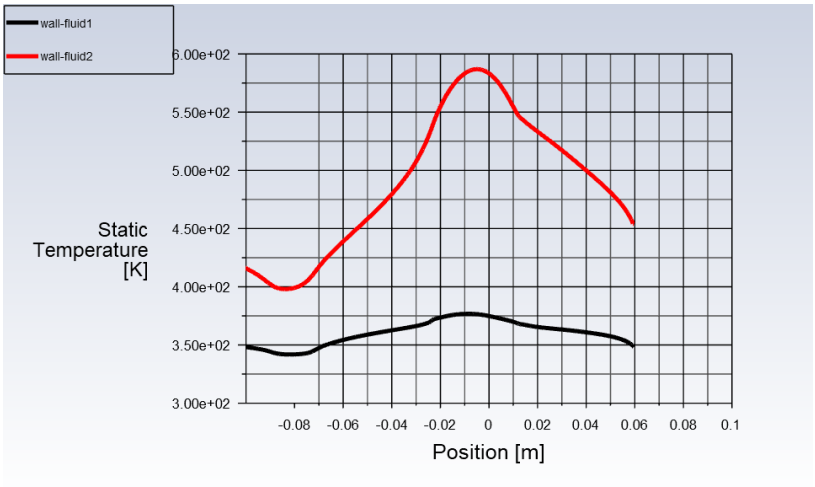


**Figure 3.48:** Axial distribution of static temperature of coolant side (wall-fluid1) and gas side wall (wall-fluid2), 2kg/s case of 6 inch cooled length

### 3.4.3 12 inch

#### 3.4.3.1 water mass flow =6kg/s

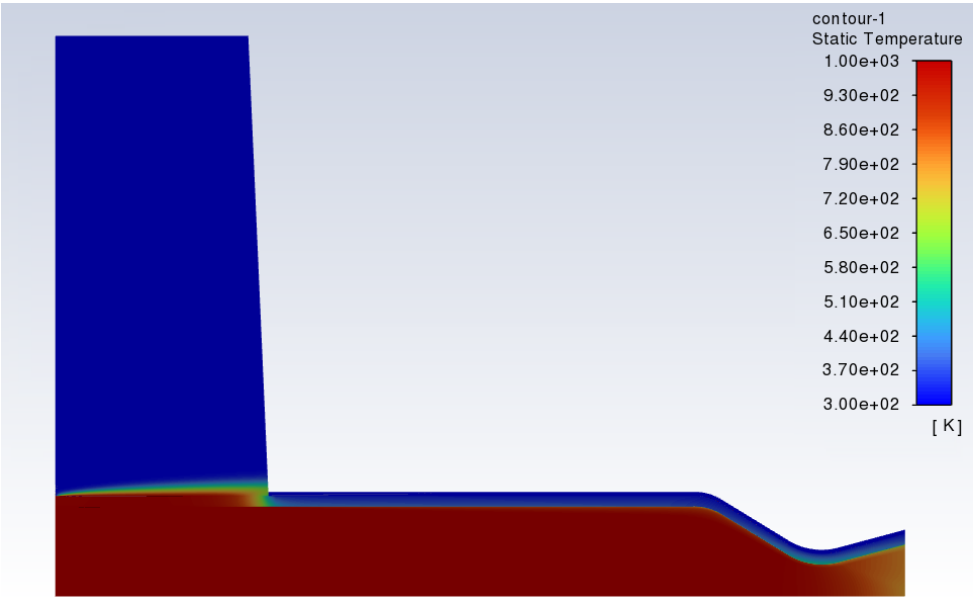


**Figure 3.49:** Static temperature contour of methyl, water and external air

This Figure 3.49 represents the Contour of static temperature of the Rocket(engine, nozzle) we note gradation of color from the blue 300K to the red 1000 K where the max temperature of the methyl reaches 1000K, water 337K, and gas side (wall fluid2) 546K as we can see in the Figure 3.50.[10]. A drop in temperature is observed due to the increase in the length of the cooling channel.
We have an increase of 8.4% $\Delta T$ from 0 inch case to 12 inches case ,from 6 to 12 inches 3.3% (6kg/s water mass flow).

10: The difference between chamber temperature and the maximum temperature obtained upstream of the throat is about $\Delta T$=1000-546=454K

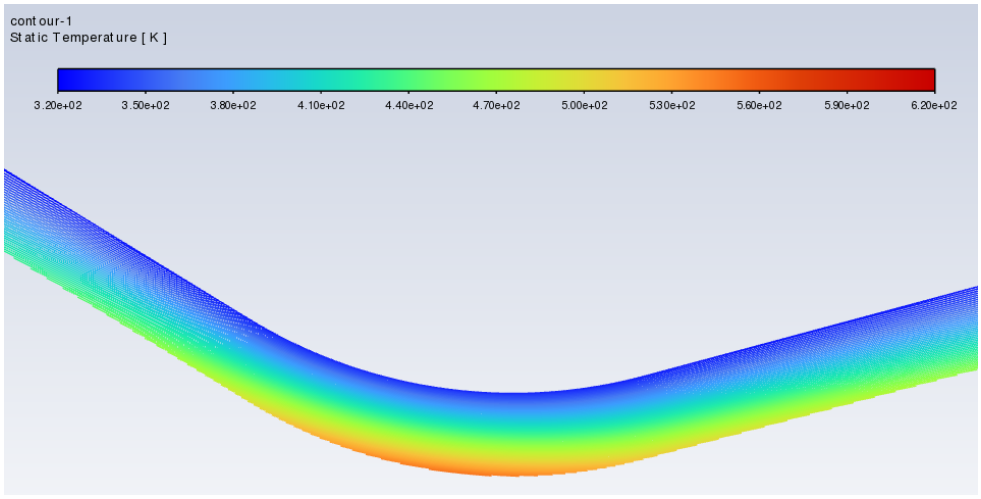


**Figure 3.50:** Static temperature contour of wall and water

Figure 3.51 represent axial evolution of static temperature in term of position where the red curve represent gas side (wall fluid2), the temperature decrease from $T_{inlet}$=1000K to T=370K (position -0.08m ) then increase to reach Tmax= 546K(before the throat 0m ) then decrease again.

For the black curve, Slight decrease in temperature of water side from T=323K (position -0.1m) to T=319K (position -0.08m) then increase to Tmax=337K (less than the vaporization temperature) then decrease again.

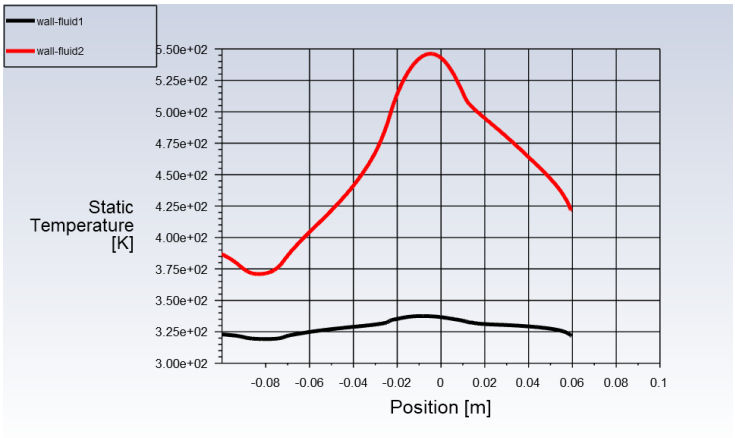


**Figure 3.51:** Axial distribution of static temperature of coolant side (wall-fluid1) and gas side wall (wall-fluid2), 6kg/s case of 12 inch cooled length

### 3.4.3.2 water mass flow =2kg/s

.

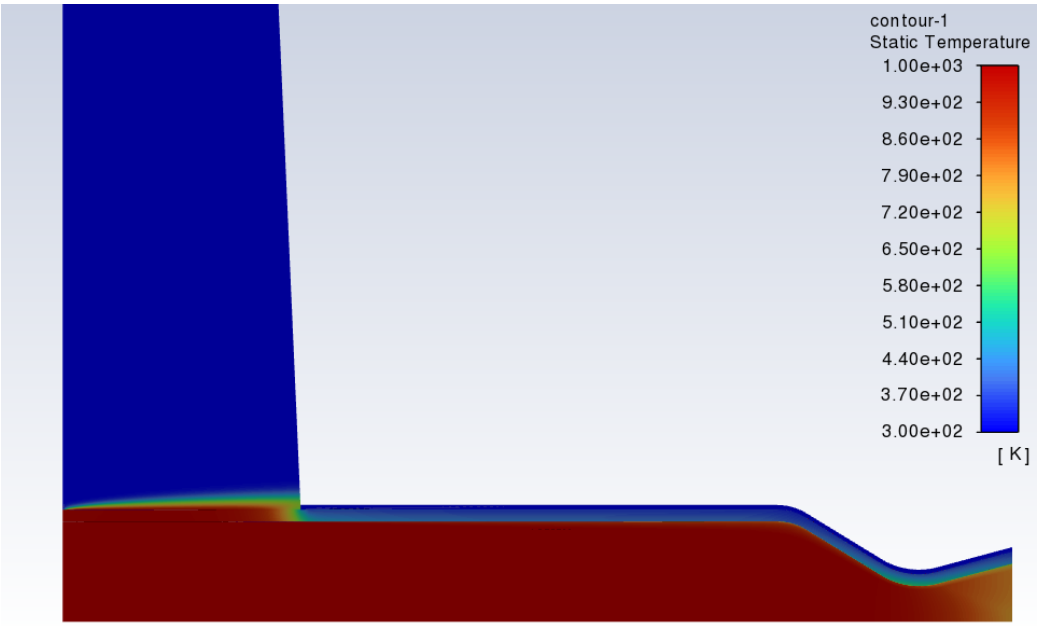


**Figure 3.52:** Static temperature contour of methyl, water and external air

This Figure 3.52 represents the Contour of static temperature of the Rocket(engine, nozzle) we note gradation of color from the blue 300K to the red 1000 K where the max temperature of the methyl reaches 1000K, water 383K, and gas side (wall fluid2) 575K as we can see in the Figure 3.53.[11]

11: The difference between chamber temperature and the maximum temperature obtained upstream of the throat is about $\Delta T$=1000-575=425K.

We have an increase of 10.4% in $\Delta T$ from 0 inch case to 12 inches case ,from 6 to 12 inches 2.6% (2kg/s water mass flow), and 6.3% drop in $\Delta T$ from 2kg/s to 6kg/s water mass flow.

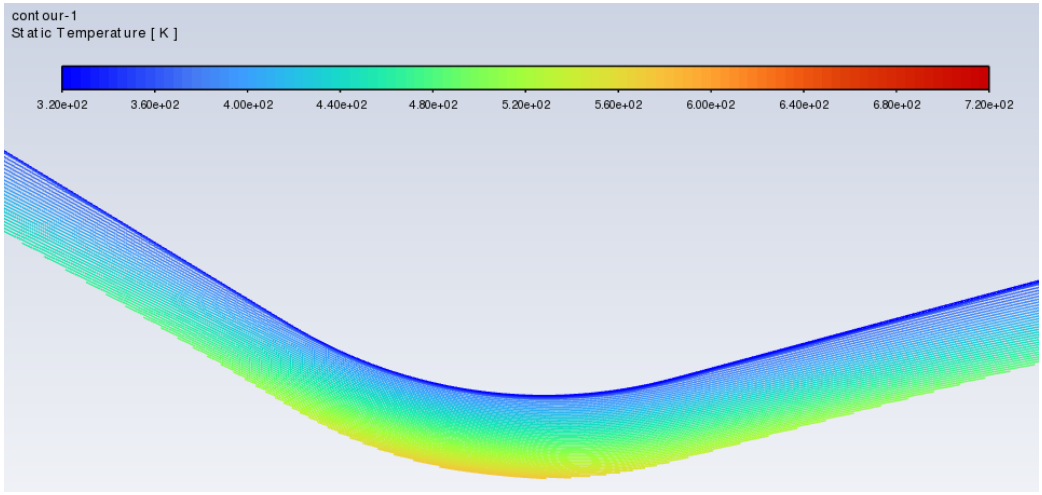


**Figure 3.53:** Static temperature contour of wall and water

Figure 3.54 represent diagram variation of static temperature in term of position where the red curve represent gas side (wall fluid2), the temperature decrease from $T_{inlet}$=1000K to T=397K (position -0.08m ) then increase to reach Tmax= 575K(before the throat 0m ) then decrease again.
For the black curve, Slight decrease in temperature of water side from T=352K (position -0.1m) to T=345K (position -0.08m) then increase to Tmax=383K (less than the vaporization temperature) then decrease again.

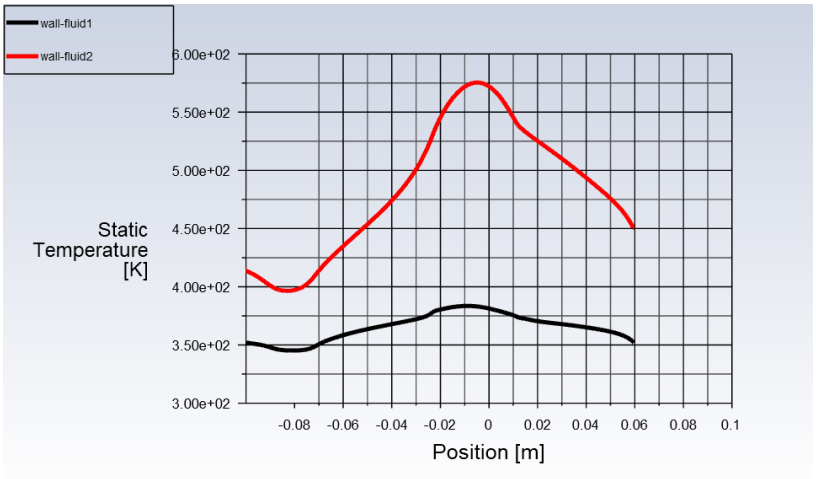


**Figure 3.54:** Axial distribution of static temperature of coolant side (wall-fluid1) and gas side wall (wall-fluid2), 2kg/s case of 12 inch cooled length

### 3.4.4 18 inch

#### 3.4.4.1 water mass flow =6kg/s

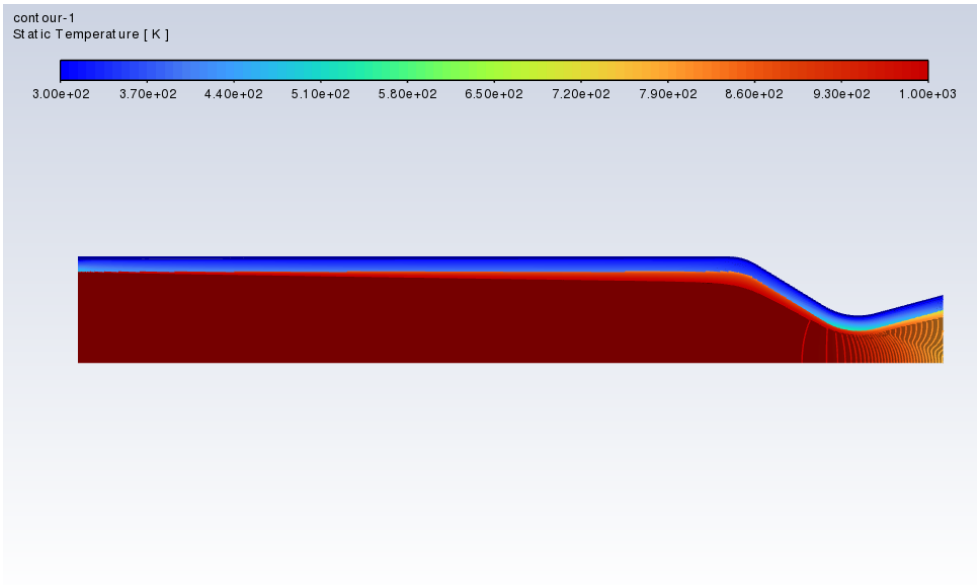


**Figure 3.55:** Static temperature contour of methyl, water and external air

This Figure 3.55 represents the Contour of static temperature of the Rocket(engine, nozzle) we note gradation of color from the blue 300K to the red 1000 K where the max temperature of the methyl reaches 1000K, water 337K, and gas side (wall fluid2) 535K as we can see in the Figure 3.56.[12].
10.5% drop in $\Delta T$ from 18 inches case to 0 inch case ,from 18 to 6 inches 6.6%,from 18 to 12 inches 2.4% (6kg/s water mass flow).

12: The difference between chamber temperature and the maximum temperature obtained upstream of the throat is about $\Delta T$=1000-535=465K

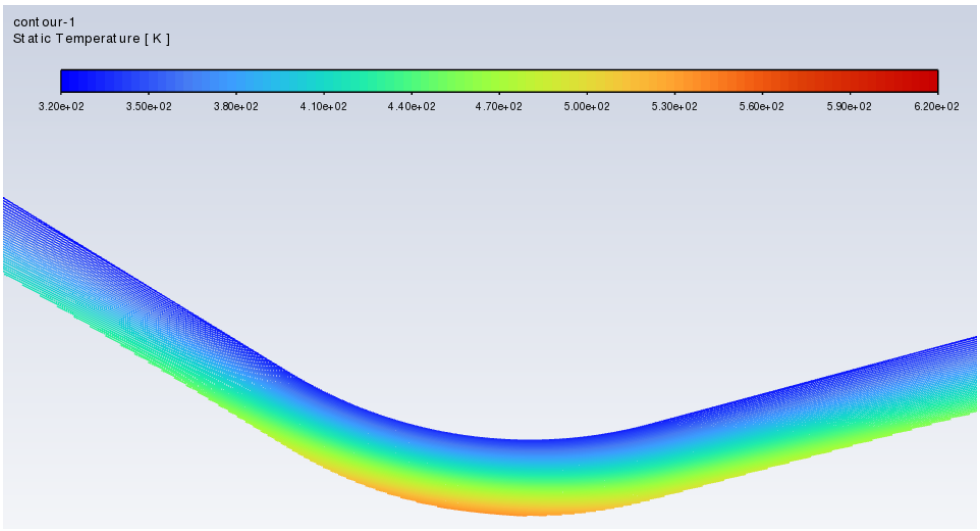


**Figure 3.56:** Static temperature contour of wall and water

Figure 3.57 represent axial evolution of static temperature in term of position where the red curve represent gas side (wall fluid2), the temperature decrease from $T_{inlet}$=1000K to T=368K (position -0.08m ) then increase to

reach Tmax= 535K(before the throat 0m ) then decrease again.
For the black curve, Slight decrease in temperature of water side from T=322K (position -0.1m) to T=319K (position -0.08m) then a slight increase to Tmax=337K (less than the vaporization temperature) then decrease again.

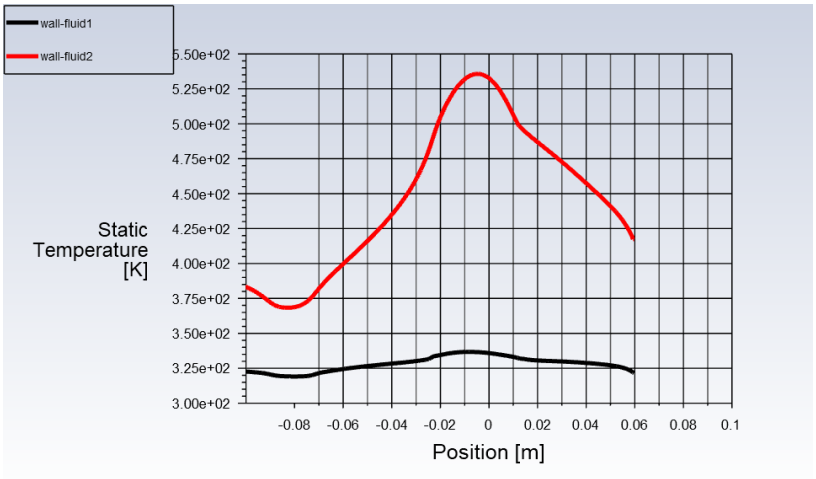


**Figure 3.57:** Axial distribution of static temperature of coolant side (wall-fluid1) and gas side wall (wall-fluid2), 6kg/s case of 18 inch cooled length

### 3.4.4.2 water mass flow =2kg/s

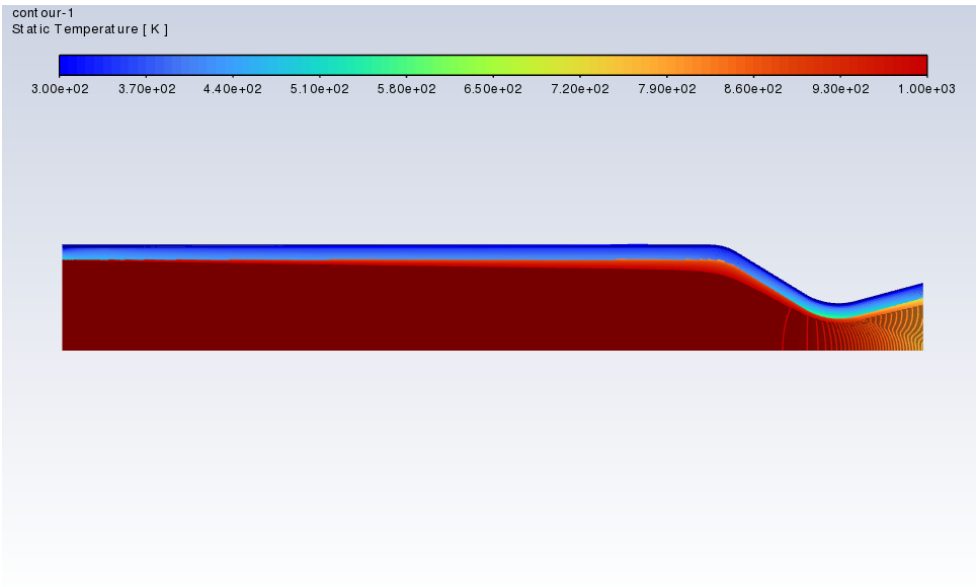


**Figure 3.58:** Static temperature contour of methyl, water and external air

This Figure 3.58 represents the Contour of static temperature of the Rocket(engine, nozzle) we note gradation of color from the blue 300K to the red 1000 K where the max temperature of the methyl reaches 1000K, water 382K, and gas side (wall fluid2) 565K as we can see in the Figure 3.59.[13]

12.4% down in $\Delta T$ from 18 inches case to 0 inch case ,from 18 to 6 inches 4.8%,from 18 to 12 inches 2.3% (2kg/s water mass flow), and 6.45% drop in temperature from 2kg/s to 6kg/s water mass flow.

13: The difference between chamber temperature and the maximum temperature obtained upstream of the throat is about $\Delta T$=1000-565=435K.

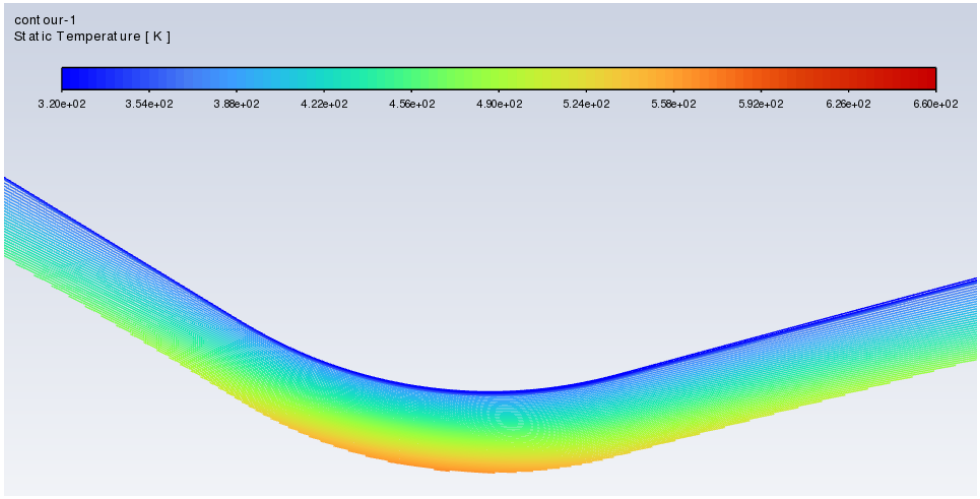


**Figure 3.59:** Static temperature contour of wall and water

Figure 3.60 represent axial evolution of static temperature in term of position where the red curve represent gas side (wall fluid2), the temperature decrease from $T_{inlet}$=1000K to T=394K (position -0.08m ) then increase to reach Tmax= 565K(before the throat 0m ) then decrease again. For the black curve, Slight decrease in temperature of water side from T=352K (position -0.1m) to T=345K (position -0.08m) then increase to Tmax=382K (less than the vaporization temperature) then decrease again.

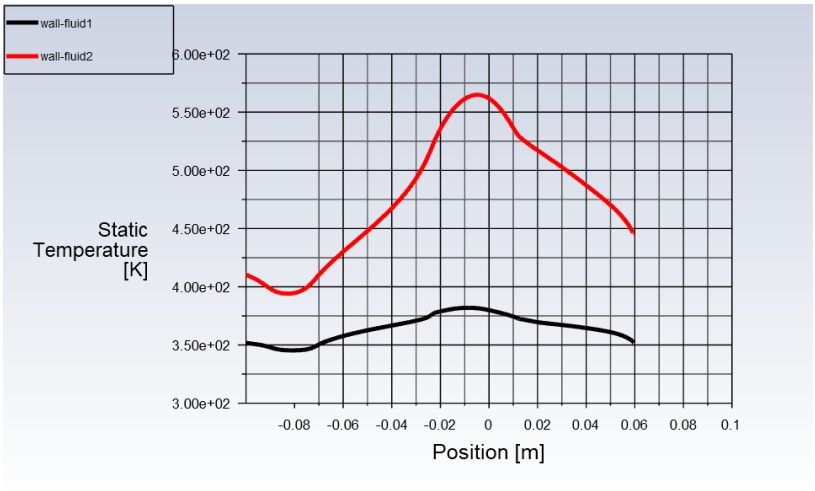


**Figure 3.60:** Axial distribution of static temperature of coolant side (wall-fluid1) and gas side wall (wall-fluid2), 2kg/s case of 18 inch cooled length

### 3.4.5 Comparison with the same nominal conditions

We have tabulated the result obtained for comparison as shown below:

| Case | $\Delta T$(2kg/s water mass flow) | $\Delta T$(6kg/s water mass flow) |
|---|---|---|
| **0 inch** | 381K | 416K |
| **6 inches** | 414K | 439K |
| **12 inches** | 425K | 454K |
| **18 inches** | 435K | 465K |

**Figure 3.61:** Table of The difference between chamber temperature and the maximum temperature obtained in all cases

The table in Figure 3.61 represent The difference between chamber and the maximum temperature obtained in all cases with two different mass flow (2 kg/s, 6kg/s).

| Case | Tmax(2 kg/s) | Tmax(6 kg/s) |
|---|---|---|
| **0 inch** | 619.143 | 584.628 |
| **6 inch** | 586.874 | 561.604 |
| **12 inch** | 575.396 | 546.143 |
| **18 inch** | 564.880 | 535.704 |

**Figure 3.62:** Table of wall fluid 2 max temperature in all cases

The table in Figure 3.62 represent the max temperature in K of the wall (gas side) in all cases with two different mass flow (2 kg/s, 6kg/s).

We converted the values of temperature in Figure 3.61 and Figure 3.62 into a percentage terms for understand more the thermal behavior

| Case | 2kg/s to 6 kg/s water mass flow |
|---|---|
| **0 inch** | 8% |
| **6 inch** | 5.7% |
| **12 inch** | 6.3% |
| **18 inch** | 6.45% |

**Figure 3.63:** Table of DT Variation (in percentage terms) with change in mass flow rate

The table in Figure 3.63 represent DT Variation (in percentage terms) with change in mass flow rate as a result of increasing in the mass flow rate the value of temperature decrease about 5% as define in Figure 3.62 and Figure 3.65 this means that the difference between chamber and the maximum nozzle temperature obtained raise Figure 3.61 about 6 to 8 percent this is due to the ideal gas law.

| case | 2 kg/s water mass flow | 6 kg/s water mass flow |
|---|---|---|
| **0 to 6 inch** | 7.9% | 5.2% |
| **0 to 12 inch** | 10.4% | 8.4% |
| **0 to 18 inch** | 12.4% | 10.5% |
| **6 to 12 inch** | 2.6% | 3.3% |
| **6 to 18 inch** | 4.8% | 6.6% |
| **12 to 18 inch** | 2.3% | 2.4% |

**Figure 3.64:** Table of DT Variation (in percentage) with length change

The table in Figure 3.64 represent DT Variation (in percentage terms) with length change as we can see when the length increase the temperature decrease as shown in Figure 3.62 and Figure 3.66, the difference between chamber and the maximum nozzle temperature obtained raise from 2,3% to 12.4% in 2kg/s mass flow rate and about 2.4% to 10.5% in 6kg/s.

| Case | 2kg/s to 6 kg/s water mass flow |
|---|---|
| **0 inch** | 5.57% |
| **6 inch** | 4.30% |
| **12 inch** | 5.08% |
| **18 inch** | 5.16% |

**Figure 3.65:** Table of wall fluid 2 temperature Variation in all cases

| case | 2 kg/s water mass flow | 6 kg/s water mass flow |
|---|---|---|
| **0 to 6 inch** | -5.21\% | -3.93% |
| **0 to 12 inch** | -7.1% | -6.6% |
| **0 to 18 inch** | -8.76% | -8.36% |
| **6 to 12 inch** | -1.95% | -2.75% |
| **6 to 18 inch** | -3.7% | -4.6% |
| **12 to 18 inch** | -1.82% | -1.91% |

**Figure 3.66:** Table of wall fluid 2 temperature Variation in all cases (in percentage) with length change

### 3.4.5.1 Direct comparison between 0 and 18 inches

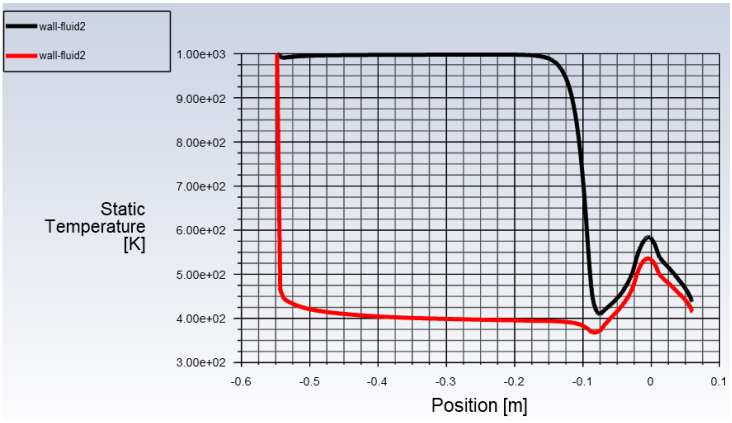


**Figure 3.67:** Axial distribution of static temperature of gas side wall (wall-fluid2) 0 inch and 18 inches cooled length, 6kg/s case

The Figure 3.67 represent axial evolution of static temperature in term of position where the red curve represent gas side (wall fluid2) 18 inches cooled length, the black curve represent gas side (wall fluid2) 0 inch cooled length. The main point of comparing is that :
In 18 inches case the temperature drops quickly from $T_{inlet}$=1000K (position -0.547m) to T=465K (position -0.543m) because the cooling system start with the inlet of combustion chamber ( the effect of the cooling length), Unlike 0 inch case the temperature decrease just before the inlet of the nozzle (position -0.09m), as we can see the wall in combustion chamber can melt and causes thermal failure for the rocket

# 4 CONCLUSION

In this work, we presented a numerical study of compressible flow and wall-fluid conjugate heat transfer, the dynamic and thermal behavior in a water-cooled convergent-divergent nozzle. This investigation tends to emphasize the importance of the cooled inlet length in the cooling process to preserve the integrity of the entire combustion chamber and nozzle wall.

The numerical method used for the study of the fluid flow is the finite volume method based on a second order Roe scheme which is very efficient and widely used in the case of RANS turbulence for the capture of discontinuities in the flow.

The RSM-Omega turbulence model used was found to be very effective mainly with the use of the correction shear flow; this is justified by the excellent agreement of the numerical predictions with experimental data.

From previous transient study (not presented here), it is concluded that it is essential and obligatory to start the cooling before launching the hot gases in the nozzle, because in fact the hot gases develop rapidly from the initial state to the stationary state in a time equal to 10 to 20 microseconds, on the other hand the cooling time takes a very extended time of about 40 to 60 seconds. All cases showed similar behavior in terms of gas-side wall temperature and wall heat flux, with peaks occurring slightly upstream from the throat.

This thesis can be conclude into the following headlines:

One of the most important problems facing rockets is thermal failure (The gases in an engine combustor can reach 3500 K) higher than the melting point of metals and weight.

Regenerative and ablative cooling are two of the most commonly utilized methods for cooling system in rockets.

The hottest part of the rocket (the value of temperature and heat transfer is maximum) is where the mass flux is maximal (just before the throat).

Changes in coolant-inlet length will change the distribution of thermal boundary-layer, hence, the wall temperature distributions. The effect of initial boundary-layer thickness on gas-side wall temperature is larger near the entrance of the nozzle but diminishes downstream in the convergent section. At the throat and in the divergent section, the wall temperature is relatively independent of the initial boundary layer thickness.

It has been known that differences in the thickness of the inlet momentum boundary layer are essentially eradicated by the strong accelerating forces in the subsonic and throat portions of the nozzle. Differences in inlet thermal boundary layer thickness are not erased by this acceleration.

The results prove that the thermal boundary layer history imposed by the use of cooled and uncooled inlet, had an effect on the distribution of wall temperature and heat transfer.

The comparison between the cooled length of 18 inches and the uncooled length of 0 inch shows that the wall temperature difference just at the nozzle entrance is about 35%, diminishes to 6% at the nozzle throat, and this difference decreases more and more as we approach the nozzle outlet.

Based on the findings, it is possible to conclude that the unified approach presented in this study is fully applicable to the class of problems in which high-speed compressible flow and low-speed incompressible flow separated by a solid wall interact via the conjugate convection-conduction process.

# Bibliography


[1] J. G. ST VENANT, C.R.A.S, 17(1843)

[2] O. REYNOLDS, An experimental investigation of the circumstances which determine whether the motion of water shall be direct of sinuous and the law of resistance in parallel channels,Phil. Trans. Roy. Soc. London, 174, pp. 935-982(1883).
"On the dynamical theory of incompressible viscous fluid and the determination of the criterian", Phy. Trans. Roy. Soc. London, 186, pp. 123-164(1895)

[3] A. N. KOLMOGOROV, Equations of turbulent motion of incompressible fluid, Izv. Akad. Nauk SSSR seria fizichiska VI, 56(1942)

[4] P.R. SPALART, Strategies of turbulence modelling and simulations. International Journal of Heat and Fluid Flow 21, pp. 252-263(2000)

[5] HESSELBERG, Die Gesetze der ausgeglichenen atmosphärischen Bewegangen, Beitz-Physik forcien Atmosphäre, vol. 12, pp. 141-160(1925)

[6] G. DEDEBANT et Ph. WEHRLE, sur les équations aux valeurs probables d'un fluide turbulent, C.R.A.S. T. 206, pp. 1790-1791(1938)

[7] VAN MIEGHEN et L. DUFOUR, Thermodynamique de l'atmosphère, Mem. Inst. Roy. Meteor. de Belgique, 30(1948)

[8] A. K. BLACKADAR, The transformation of energy by the large scale eddy stress in the atmosphere, Meteor. papers vol. 1, $n^0$ 4, New York University(1950)

[9] A. FAVRE, Equations statistiques des gaz turbulents, C.R.A.S 246, pp. 2576-2579, 2723-2725, pp. 2839-2842, 3216-3219 (1958)

[10] A FAVRE, Equations des gaz turbulents compressibles, Journal de Mécanique, vol. 4, $n^0$ 3(1965)

[11] D. VONDROMME, Modèle de turbulence à deux équations pour écoulement plan cisaillé à masse volumique variable, Thèse de Docteur-Ingénieur Lille (1980)

[12] P. CHASSAING et H. HA MINH, Physique et Mécanique des fluides réels, Cours de l'E.N.S.A.E (1982)

[13] H. HA MINH, The impact of turbulence modelling on the numerical predictions of flows, Rome 6-10 July (1992)

[14] D. VONDROMME, Turbulence modeling for compressible flows and implementation in Navier-Stokes solvers, V.K.I lecture series, March (1991)

[15] M.W. RUBESIN, A one-equation model of turbulence for use with compressible Navier-Stokes equations, NASA TM X-73-128, (1976)

[16] J.R. VIEGAS, T.J. COAKLEY, Numerical investigation of turbulence models for shock separed boudary layer flows, AIAA paper, No. 77-44, (1977)

[17] G.O. FRESKOS, Etude physique et simulation numérique des écoulements dans les entrées d'air suparsonique, Thèse, Institut National Polytechnique de Toulouse, (1992)

[18] J. BOUSSINESQ, Théorie de l'écoulement tourbillonnant et tumultueux des liquides dans les lits rectilignes à grande section, volume I-II. Gauthier-Villars, (1897).

[19] R.S. AMANO and P. GOEL, Investigation of third-order closure model of turbulence for the computation of incompressible flows in a channel with a backward facing step. J. Fluids Eng., 109:424-428, (1987)

[20] R. FRIEDRICH. Compressible turbulence. In Space Course, Munich, Octobre (1993)

[21] K.HANJALIC, B.E. LAUNDER, A Reynolds stress model of turbulence and its application to thin shear flows. J.F.M (1972)

[22] H. TENNEKES, J.L. LUMLEY, A First course in turbulence. M.I.T. Press. Cambridge, Massachussetts (1972)

[23] D. VONDROMME, Contribution à la modélisation et à la prédiction d'écoulements turbulents à masse volumique variable. Thèse d'Etat de l'Université de Lille (1983)

[24] W.P. JAUNES, B.E. LAUNDER, The prediction of laminarization with a two-equation model of turbulence. J. of Heat and Mass Transfer, Vol.15, PP.301-314 (1972)

[25] J. BOUSSINESQ, Théorie des écoulements tourbillonnaires, CRAS T23, (1887)

[26] T. VON KARMAN, Mechanische anlichkeit und turbulenz, NACA TM. 611 (1930)

[27] P.S. KLéBANOFF, Characteristics of turbulence in a boundary layer with zero pressure gradient,NACA TN. 3178 (1956)

[28] R. MICHEL, C. QUEMARD & R. DURANT, Application d'un schéma longueur de mélange à l'étude de couches limites d'équilibre, Note Technique ONERA. No1. 154 (1969)

[29] E.R. VAN DRIEST, Turbulent boundary layer in compressible fluids. J. Aeronaut. Sci. vol 18, pp. 145-162 (1951)

[30] T. CEBECI, A.M.O. SMITH & S.G. MOSINSKI, Calculations of compressible adiabatic turbulent boundary layer, AIAA Journal. No 8, pp. 1974-1982 (1970)

[31] I.E. ALBER, Similar solutions for a family of separated turbulent boundary-layers. AIAA Paper. 71-203 (1971)

[32] B.S. BALDWIN & H. LOMAX, Thin layer approximation and algebraic model for separated turbulent flows. AIAA Paper. 78-0257 (1978)

[33] D. C. WILCOX, Turbulence Modeling for CFD. DCW Industries, Inc., 5354 Palm Drive, La *Cañada*, Calif., (1993).

[34] P. R. SPALART and S. R. ALLMARAS, A One-Equation Turbulence Model for Aerodynamic Flows. AIAA Paper, 92-0439, (1992).

[35] P. R. SPALART and S. R. ALLMARAS, A One-Equation Turbulence Model for Aerodynamic Flows. La Recherche Aerospatiale, no. 1, pp. 5-21 (1994)

[36] B. S. BALDWIN and T. J. BARTH, A One-Equation Turbulence Transport Model for High Reynolds Number Wall-Bounded Flows. NASA TM- 102847, (1990)

[37] T. CEBECI, Analysis of Turbulent Flows, Elsevier, London, (2004).

[38] W.P. JONES and B.E. LAUNDER, The Prediction of Laminarization with a Two-Equation Model of Turbulence. International Journal of Heat and Mass Transfer, vol. 15, pp. 301-314 (1972).

[39] B. E. LAUNDER and B. I. SHARMA, Application of the Energy Dissipation Model of Turbulence to the Calculation of Flow Near a Spinning Disc. Letters in Heat and Mass Transfer, vol. 1, no. 2, pp. 131-138 (1974).

[40] D. C. WILCOX, "Reassessment of the Scale-Determining Equation for Advanced Turbulence Models", AIAA Journal, Vol. 26, No. 11, pp. 1299-1310 (1988).

[41] F. R. MENTER, Influence of Freestream Values on $k-\omega$ Turbulence Model Predictions. AIAA J. vol. 30, no. 6, pp. 1657-1659. June (1992).

[42] F. R. MENTER, Improved two-equation $k-\omega$ turbulence models for aerodynamic flow, NASA Technical Memorandum 103975(1992).

[43] F. R. MENTER, Zonal two-equation $k-\omega$ turbulence models for aerodynamic flows, in 24th Fluid Dynamics Conference, AIAA (1993).

[44] D. A. JOHNSON and L. S. KING, A Mathematically Simple Turbulence Closure Model for Attached and Separated Turbulent Boundary Layers, AIAA Journal, Vol. 23, pp. 1684-1692(1985).

[45] F. R. MENTER, Performance of Popular Turbulence Models for Attached and Separated Adverse Pressure Gradient Flows, AIAA Journal, Vol. 30, pp. 2066-2072 (1992)

[46] D. M. DRIVER, Reynolds Shear Stress Measurements in a Separated Boundary Layer, AIAA Paper 91-1787,(1991)

[47] P. R. SPALART and C. L. RUMSEY, Effective Inflow Conditions for Turbulence Models in Aerodynamic Calculations, AIAA Journal, Vol. 45, No. 10, pp. 2544 - 2553 (2007).

[48] P. E. SMIRNOV, F. R. MENTER, Sensitization of the SST Turbulence Model to Rotation and Curvature by Applying the Spalart-Shur Correction Term," ASME Journal of Turbomachinery, Vol. 131, 041010, October (2009).

[49] A. HELLSTEN, Some Improvements in Menter's k-omega SST Turbulence Model," AIAA Paper 98-2554, June (1998).

[50] M. MANI, J.A. LADD and W.W. BOWER, Rotation and Curvature Correction Assessment for One- and Two-Equation Turbulence Models, Journal of Aircraft, Vol. 41, No. 2, pp. 268-273 (2004).

[51] A. HELLSTEN and S. LAINE, Extension of the $k-\omega$-SST Turbulence Model for Flows over Rough Surfaces, in AIAA Atmospheric Flight Mechanics Conference, (New Orleans, LA, USA), (1997).

[52] F. R. MENTER, Private communication

[53] D. C. WILCOX, Turbulence Modeling for CFD, 3rd edition, DCW Industries, Inc., La *Cañada* CA, (2006).

[54] R.D. CECORA, B. EISFELD, A. PROBST, S. CRIPPA and R. RADESPIEL, Differential Reynolds Stress Modeling for Aeronautics," AIAA Paper 2012-0465, January (2012).

[55] B. EISFELD, Implementation of Reynolds Stress Models into the DLR-FLOWer Code," Institutsbericht, DLR-IB 124-2004/31, Report of the Institute of Aerodynamics and Flow Technology, Braunschweig, ISSN 1614-7790, (2004).

[56] B. EISFELD and O. BRODERSEN, Advanced Turbulence Modelling and Stress Analysis for the DLR-F6 Configuration", AIAA Paper 2005-4727, June (2005).

[57] B. EISFELD, Computation of Complex Compressible Aerodynamic Flows with a Reynolds Stress Model, Conference on Boundary and Interior Layers, BAIL 2006, Göttingen, Germany, July 2006.

[58] W. HAASE, B. AUPOIX, U. BUNGE, D. (Eds.) SCHWAMBORN, FLOMANIA, A European Initiative on Flow Physics Modelling, Notes on Numerical Fluid Mechanics and Multidisciplinary Design (NNFM), vol. 92, Springer, (2006).

[59] F.R. MENTER, Two-Equation Eddy-Viscosity Turbulence Models for Engineering Applications,AIAA Journal, 32, 1598-1605 (1994).

[60] B.E. LAUNDER, G. J. REECE, W. RODI, Progress in the development of a Reynolds-stress turbulence closure, Journal of Fluid Mechanics, 68, 537-566 (1975).

[61] D. C. WILCOX, Turbulence Modeling for CFD, DCW Industries, La *Cañada*, USA, 2nd ed.,(1998).

[62] C. G. SPEZIALE, S. SARKAR, T.B. GATSKI, Modelling the pressure-strain correlation of turbulence: an invariant dynamical systems approach, Journal of Fluid Mechanics, 227, 245-272 (1991).

[63] J. ROTTA, Statistische Theorie nichthomogener Turbulenz, Zeitschrift *für* Physik, 129, 547-572 (1951).

[64] B. J. DALY, F. H. Harlow, Transport equations of turbulence, Physics of Fluids 13, 2634-2649 (1970).

[65] K. BENSAYAH, A. BENCHATTI, M. AOUISSI, A. BOUNIF, Scalar turbulence model investigation with variable turbulent Prandtl number applies in hot axisymmetric turbulent round jet, Int J Heat Tech. 25: 49-56 (2007).

[66] M. AOUISSI, A. BOUNIF, K. BENSAYAH, Scalar turbulence model investigation with variable turbulent Prandtl number in heated jets and diffusion flames, Heat Mass Transfer, 44:1065-1077, (2008)

[67] W.C. REYNOLDS, Fundamentals of turbulence for turbulence modeling and simulation, AGARD Report No. 755, (1987)

[68] P.A. DURBIN, Turbulence modeling for separated flow, NACA-CR-197352, pp. 97-105, (1994)

[69] J.G. MOORE and J. MOORE, Controlling over-production of turbulence in two-equation models by limiting the anisotropy of the Reynolds normal stresses, ASME Paper FEDSM97-3356, (1997)

[70] J.ZHU and T.H. SHIH, Calculations of turbulent separated flows, NASA TM 106154, (1993).

[71] T.H. SHIH, J.ZHU and J.L. LUMLEY, A realizable Reynolds stress algebraic equation model, NASA TM 105993, (1994)

[72] T.H. SHIH, W.W. LIOU, A. SHABBIR, Z. YANG and J. ZHU, A new $k - \varepsilon$ eddy viscosity model for high Reynolds number turbulent flows-model development and validation, NASA TM 106721 (1994)

[73] S. F. BIRCH and J. M. EGGERS, Free Turbulent Shear Flows, NASA SP-321, 1. 11-40, NASA Langley Research Center, Hampton, VA (1972).

[74] M.V. MORKOVIN, Effect of compressibility on turbulent flows. Mecanique de la Turbulence, edited by A. Favre, p. 367, (1961).

[75] S. SARKAR and L. BALAKRISHNAN, Application of a Reynolds-Stress Turbulence Model to the Compressible Shear Layer, $21^st$ Fluid Dynamics, Plasma Dynamics and Lasers Conference, AIAA Paper No. 1990-1465 (1990).

[76] O. ZEMAN, Dilataion Dissipation: The Concept and Application in Modeling Compressible Mixing Layers, Phys. Fluids, 2(2), pp. 178-188(1990).

[77] T. J. COAKLEY and P. G. HUANG,Turbulence Modeling for High Speed Flows," 30th Aerospace Science Meeting and Exhibit, AIAA Paper No. 92-0436 (1992).

[78] B. AUPOIX, E. DESMET and S. VIALA, Hypersonic Turbulent Boundary Layer Modelling, Symposium on Transitional and Turbulent Compressible Flows, ASME Fluids Engineering Conference (1993).

[79] M. MACLEAN, T. WADHAMS, M. HOLDEN and H. JOHNSON,A Computational Analysis of Ground Test Studies of the HIFiRE-1 Transition Experiment," AIAA Paper 2008-0641, January (2008)

[80] D. C. WILCOX, Progress in Hypersonic Turbulence Modeling, AIAA Paper 91-1785, June (1991).

[81] J. BROWN, Turbulence Model Validation for Hypersonic Flows, AIAA Paper 2002-3308, June (2002).

[82] P. CHASSAING, Turbulence En Mécanique Des Fluides - Analyse Du Phénomène En Vue De Sa Modélisation à L'usage De L'ingénieur. Cépaduès (2000).

[83] ANSYS. Ansys fluent theory guide 12.0: Turbulence models. ANSYS, Inc., January 2009.

[84] L.H.Back, P.E.Massier, H.L.Gier, Convective Heat Transfer in a Convergent-Divergent Nozzle(Revision No.1)JET PROPULSION LABORATORY California, 1965.